Investigating mechanisms of myelin sheath length regulation and plasticity

Franziska Auer

Graduate School of
Systemic Neurosciences

LMU Munich

Dissertation at the
Graduate School of Systemic Neurosciences
Ludwig-Maximilians-Universität München

April 2019

Supervisor
Dr. Tim Czopka
Institute of Neuronal Cell Biology
Technische Universität München

First Reviewer: Dr. Tim Czopka
Second Reviewer: Prof. Dr. Thomas Misgeld
Third Reviewer: Dr. Kelly Monk

Date of Submission: 12.04.2019
Date of Defense: 18.09.2019

ABSTRACT

Myelination of axons is important for proper functioning of the nervous system and breakdown of myelin can cause severe disabilities. By regulating nerve conduction, myelination is also critical for learning and memory processes. Myelination greatly influences conduction properties and remodeling of myelin has been proposed as a potential mechanism to adjust and modulated nervous system function. However, to date it is still unclear if existing myelin is able to remodel and therefore participate in brain plasticity. I used existing zebrafish transgenic lines and generated new constructs to visualize myelinated axons in the CNS and to perform in vivo life imaging. Furthermore, I developed a single cell ablation method with high spatial and temporal precision to selectively demyelinate axon stretches and assess remyelination and remodeling dynamics. Using these tools, I was able to describe the growth dynamics of single myelin sheaths and show that they are independent of neighboring sheaths and time of initiation. Myelin sheath growth can be divided into three different growth phases, an oligodendrocyte intrinsic, highly uniformly growth phase that lasts for about 8 hours, followed by a second variable growth phase, likely regulated by axon intrinsic mechanisms, in which sheath length differences are established. The last growth phase compensates for body growth, and is highly predictable by the length increase of the animal.

By demyelination of short axon stretches I was able to show that myelin segments are able to deviate from their otherwise very stereotypic growth dynamics. Ablation of a myelin sheath resulted in reinitiation of fast sheath growth in the neighboring sheath to remyelinate the gap. A new sheath was formed in the gap and grew which often led to a pushing back of the neighboring sheaths that had invaded the demyelinated territory. Thereby, often re-establishing the pre-ablation pattern, indicating a homeostatic regulation of myelin sheath length along an axon. Similarly, partially myelinated axons regularly restored their pre-ablation pattern after demyelination. Together, these results indicated axonal control of myelin sheath length and node of Ranvier positioning to guide the restoration of pre-ablation patterns. Furthermore, I observed a high number of asymmetrically grown sheath that could

not be explained by physical barriers like neighboring sheaths or axon collaterals, indicating the existence of a molecular growth barrier on the axon. To collect further evidence, I investigated the dynamics of the nodal marker Neurofascin and found that it forms clusters along unmyelinated axons which are predictive for node of Ranvier positions. In order to test if the formation of clusters and the positioning of nodes is axonal activity dependent I established an optogenetic setup for long-term stimulation of freely swimming fish. By manipulating axonal activity by optogenetics I was able to induce myelin sheath remodeling supporting the hypothesis of axonal regulation of node or Ranvier positioning, however, similar effects were observed in control animals.

Together, I was able to describe the dynamics of myelin sheath growth and could show that existing myelin segments can remodel and are therefore able to participate in brain plasticity. Additionally, I collected evidence that node or Ranvier positioning and therefore also myelin sheath length are regulated by axonal mechanisms.

ACKNOWLEDGMENT

I am very grateful for the support and help I got during my PhD. First of all, I would like to thank my supervisor Dr. Tim Czopka for giving me the great opportunity to work in his lab. I greatly appreciate his scientific advice and guidance as well as the constructive discussions and collaboration throughout my PhD. I am also especially grateful to Prof. Dr. Thomas Misgeld for his insightful comments and suggestions during our lab meetings.

I would also like to thank the members of my thesis advisory committee Prof. Dr. Carsten Wotjak and Prof. Dr. Christian Wahl-Schott for their time and support. I would like to thank the GSN not only for the financial support but also for the broad scientific and cultural inspiration and most importantly the amazing support by the GSN team whenever needed. Furthermore, I would like to thank the Gertrud-Reemtsma Stiftung for accepting me as a fellow and the financial support for two years of my PhD. I would also like to thank all members of the Czopka and Misgeld labs, it was a lot of fun to work together. Special thanks to Eleni, Roberta, Stavros and Nic, we had a lot of fun, also outside of the lab. I am also very grateful to Yvonne and Leanne for the mental support and for helping relax my DNA.

Very special thanks also to my friends and family outside the lab. Irena and Cosi, thank you for always being there for me. Saskia, Henne, Jen, Sami, Rasmus and Eva, thanks for your support and the motivation, I am very grateful and happy to know you as my friends. Last but not least, thank you Mama and Papa for always believing in me and supporting me in every imaginable way.

Table of content

LIST OF ABBREVIATIONS

AIS ..... *axon initial segment*
AnkG ..... *AnkyrinG*
AP ..... *action potential*
ATP ..... *adenosine triphosphate*
ChR2 ..... *Channelrhodopsin2*
CI ..... *confidence interval*
CiD ..... *circumferential descending*
CNP ..... *cyclic nucleotide phosphodiesterase*
CNS ..... *central nervous system*
CoPA ..... *commissural primary ascending*
CPG ..... *central pattern generator*
dpa ..... *days post ablation*
dpf ..... *days post fertilization*
dpi ..... *days post initiation*
DRG ..... *dorsal root ganglion neurons*
ECM ..... *extracellular matrix*
FA ..... *fractional anisotropy*
GBC ..... *globular bushy cells*
HDAC ..... *histone deacetylases*
hpd ..... *hours post differentiation*
hpi ..... *hours post initiation*
KO ..... *knock out*
MBP ..... *myelin basic protein*
MCT1 ..... *monocarboxylate transporter 1*
MCT2 ..... *monocarboxylate transporter 2*
MTZ ..... *Metronidazol*
Myrf ..... *myelin regulatory factor*
NF186 ..... *Neurofascin186*
Nrg1 ..... *Neuregulin-1*
NTR ..... *Nitroreductase*
OCM ..... *oligodendrocyte conditioned medium*
OPC ..... *oligodendrocyte precursor cells*
PNS ..... *peripheral nervous system*
RB ..... *Rohon-Beard*

ROI ..... *region of interest*
SBC ..... *spherical bushy cells*
SCoRe ..... *spectral confocal reflectance microscopy*
SD ..... *standard deviation*
TSA ..... *Trichostatin A*
TTX ..... *Tetrodotoxin*

1 INTRODUCTION

Our nervous system is probably one of the most complex organs. It has to compute internal and external inputs, process them and generate voluntary and involuntary actions. The brain, together with the spinal cord, forms the central nervous system (CNS). Besides the central nervous system there is also a peripheral nervous system (PNS).

The CNS consist of two major cell types, neurons and glial cells. The glial cells are comprised of microglia, astrocytes, and oligodendrocytes. It was in 1856, that Rudolf Virchow introduced the term neuroglia to describe the non-neuronal elements in nervous tissue. It was thought that the function of glia is, to keep the nervous system together, hence, their name was derived from the ancient greek word *gloia*, meaning glue (Virchow, 1856). Only at the end of the 19th century it became clear that neuroglia consists of several cell types. In the following years these cells were described in more detail and Ramón y Cajal found that neuroglia contains astrocytes and a 'third element'. Pio del Rio Hortega stated that this third element does not only contain microglia but also another cell type which he later called oligodendroglia. He was able to identify the two cell types with the staining tools he had developed (Sierra et al., 2016); (Pérez-Cerdá et al., 2015).

The substance formed by oligodendrocytes was called myelin as initially it was thought to come from the axon itself and it was considered to be like marrow of long bones and was therefore called myelin (greek: *myelos*, marrow) (Rosenbluth, 1999).

1.1 Structure and function of myelin and subdomains of myelinated axons

Architecture of a myelinated axon in the CNS

The vertebrate central nervous system (CNS) can, macroscopically, be divided in two parts, the gray and the white matter. The gray matter contains mainly cell bodies of neurons, while the white matter consists of axonal tracts. The white matter appears white, due to the high content of myelin lipids. Myelin is a fatty substance formed by oligodendrocytes in the CNS, where one cell can myelinate up to 60 axons (Hildebrand et al., 1993). Oligodendrocytes and their myelin have important functions in maintaining a functional nervous system. The importance of myelin integrity is particularly evident after breakdown of myelin, as this can result in axon damage and eventually neuronal cell death (Franklin and Ffrench-Constant, 2008).

Oligodendrocytes extend thin processes to form myelin sheaths around axons. Myelin sheaths are membranous segments, that wrap around axons multiple times to form a thick fatty insulation on the axon (Sherman and Brophy, 2005). The myelin segments are formed consecutively along axons, only interrupted by short unmyelinated gaps, the nodes of Ranvier. Regions like the soma, dendrites and the axon initial segment (AIS) are spared from myelination (Fig 1.1 A). A myelinated axon consists of several domains: the node or Ranvier, the paranode, the juxtaparanode and the internode (Bunge et al., 1961). Each of these regions has a specific molecular composition (Peles and Salzer, 2000), suggesting different functions (Faivre-Sarrailh and Devaux, 2013). At the myelin sheaths, the membrane is wrapped around the axon and tightly compacted, only at the inner and outer end of the sheath are cytoplasmic regions, called the inner and outer tongue. The extracellular space between the axon and the myelin sheath is called periaxonal space (Simons and Nave, 2015) (Fig 1.1 B).

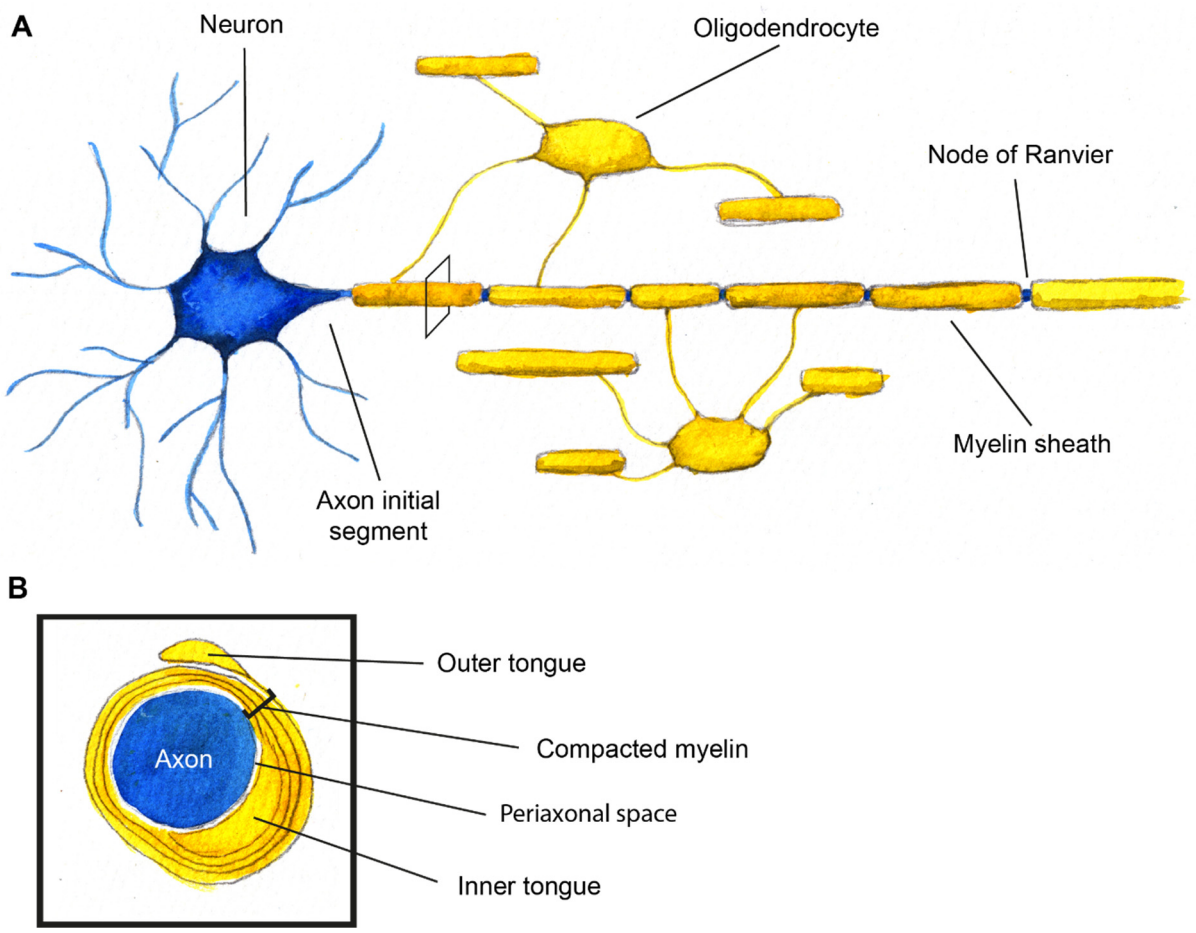

Figure 1.1 Architecture of a myelinated axon in the CNS

(A) Cartoon of a myelinated neuron. Oligodendrocytes (yellow) form myelin sheaths around the axon (blue). The sheaths are interspersed with nodes of Ranvier. One oligodendrocyte forms several sheaths**. (B)** Cartoon of a cross-section through a myelinated axon, showing compact myelin and the inner and outer tongue. Between the myelin sheath and the axon is the periaxonal space.

Architecture of the node of Ranvier

As briefly mentioned above, a myelinated axon consists of several domains (namely the node of Ranvier, the paranode, the juxtaparanode and the internode), with important functions in action potential propagation.

The node of Ranvier is an area highly enriched in specific proteins like voltage-gated sodium channels, Neurofascin186 (NF186) and AnkyrinG (AnkG). The node is flanked on both sides by the paranodal region. Adjacent to the paranodal region is the juxtaparanode (Peles and Salzer, 2000). The node is the region where current can flow and APs are elicited. The nodal area is covered by extracellular matrix (ECM) rich material, which is thought to participate in node formation and to contribute to the formation of a nodal diffusion barrier. Additionally, it is thought to serve as a cationic pool due to the negatively charged sulfated proteoglycans (Bekku et al., 2010). The major sodium channel subtype present at the node is Nav1.6 (Caldwell et al., 2000). During development Nav1.2 is exchanged by Nav1.6. In RGCs, for example, Nav1.2 is expressed when they are unmyelinated and during maturation and myelination, Nav1.2 is exchanged by Nav1.6 (Boiko et al., 2001).

The paranode is the region that is in close contact with the myelin sheath, it is rich in proteins like Caspr, Contactin, and glial Neurofascin155 (Peles and Salzer, 2000). Here, the paranodal loops anchor the myelin sheath to the axonal surface. Furthermore, it functions as a diffusion barrier for nodal proteins. At paranodal junctions, the myelin lamellae form a series of cytoplasmic loops, that are close to the axon, the gap is around 2.5-3nm wide, and form septate like junctions. The paranodal junctions attach the myelin sheath to the axon and thereby separate the nodal part form the internodal axolemma (Rasband and Peles, 2015). Additionally, paranodal interactions likely regulate the density and distribution of nodal components, as KO of the paranodal protein Caspr results in elongated, immature nodes in the optic nerve (Rios et al., 2003).

The juxtaparanode is the region adjacent to the paranode. It contains mainly voltage-gated potassium channels and Caspr2. It is believed to maintain the resting potential and mediate communication between the axon and the glial cell (Poliak and Peles, 2003).

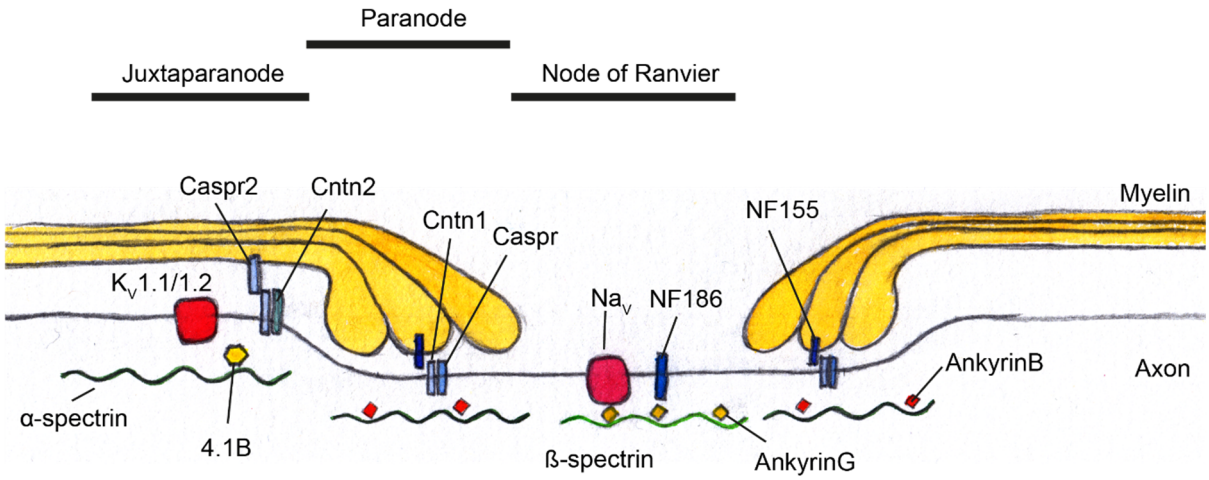

Figure 1.2 Architecture of the node of Ranvier

The node of Ranvier contains high densities of sodium channels (Na_V) that are linked by AnkyrinG to ß-spectrin. Neurofascin 186 (NF186) is as well anchored by AnkyrinG. At the paranode, the paranodal loops anchor the myelin sheath to the axon. Here, proteins like, contactin1 (Cntn1) and Caspr are expressed, as well as α-spectrin and AnkyrinB. Next to the paranode, at the juxtaparanode high numbers of potassium channels (K_V 1.1/1.2) localize. Furthermore, Caspr2, Cntn2, α-spectrin and protein 4.1B can be found at the juxtaparanode. Adapted from (Stathopoulos et al., 2015).

Morphologically a lot about myelinated axons and what they are comprised of is known, however we have not yet unraveled all mechanisms and functional involvement of myelination to nervous system function.

Functions of myelin

Fast saltatory nerve conduction

The first identified function of myelination is to increase nerve conduction speed. Along an unmyelinated axon the conduction speed is directly proportional to the axon diameter. But axon diameter cannot increase indefinitely to secure fast action potential conduction in larger animals, due to spatial constraints. The evolution of myelin in vertebrates circumvented that problem, as with myelination the conduction speed is around 10 times faster without increasing the diameter (Zalc et al., 2008)

The tightly packed myelin is electrically insulating the axon. At the nodes, where it is not myelinated, there is a high concentration of voltage-gated sodium channels, and electric current can flow. The insulation of myelinated axons increases the resistance of the axonal membrane, and as a consequence, the depolarization can spread over a longer distance with a lower potential drop compared to an unmyelinated axon (Fig 1.3 A,B). The depolarization at the following node is high enough for the voltage gated sodium channels to initiate another action potential (AP). The AP ‘jumps’ from one node to the next, hence the name saltatory conduction (Fig 1.3 B). At a myelinated axon the speed of AP conduction can reach up to 100m/s. There are several factors that influence the conduction speed along myelinated axons (Fig 1.3 C). The fiber diameter, for example, is positively correlated with conduction speed (Hursh, 1939). The ratio between the axon diameter and the diameter of the myelinated fiber, the g-ratio, influences conduction speed as well. Mathematical computations show that for a g-ratio around 0.6 the conduction speed is the fastest (RS Smith and ZJ Koles, 1970).

Another factor influencing AP conduction speed, is the myelin sheath length. Here, for a fixed diameter, an optimal sheath length can be calculated, where the conduction speed is the fastest. Deviations from this optimum result in slower conduction (Brill et al., 1997). The same is true for the node length, deviations from the optimal node length result in a slower conduction speed (Arancibia-Cárcamo et al., 2017). Furthermore, ion channel density and

distribution influence the conduction properties along axons (Freeman et al., 2016). Hence, conduction velocity along a myelinated axon can be precisely regulated by adjusting these factors (Seidl, 2014).

Metabolic support

For a long time, it was thought that the only function of myelin is to increase conduction velocity. The obvious consequence of myelination is that myelinated axons are shielded, except for nodal regions, from access to extracellular substrates. Additionally, axons are probably the extreme most example of cellular polarization, where the axon terminal may be several centimeters away from the soma, thus creating the need for extensive axonal transport of proteins and organelles. Therefore, axons show high energy demand, and might require additional sources of energy metabolites (Nave, 2010; Morrison et al., 2013). It was shown, that oligodendrocytes provide these metabolites to the axon (Fünfschilling et al., 2012; Lee et al., 2012b). Indeed, oligodendrocytes express the monocarboxylate transporter 1 (MCT1), a transporter of lactate and pyruvate (Pierre and Pellerin, 2005). MCT1 localizes to the myelin sheath, surrounding the axon (Rinholm et al., 2011). Oligodendrocyte-specific loss of MCT1 causes axon degeneration, supporting the hypothesis, that trophic support by oligodendrocytes is necessary for axonal survival (Lee et al., 2012b). In the current model of oligodenrocytic metabolic support of axons, MCT1 is expressed in the inner layers of the myelin sheath, exporting lactate in to the periaxonal space. From there, axons take up the lactate via MCT2, convert it to pyruvate and use it for ATP production by mitochondria (Fig 1.3 D) (Morrison et al., 2013).

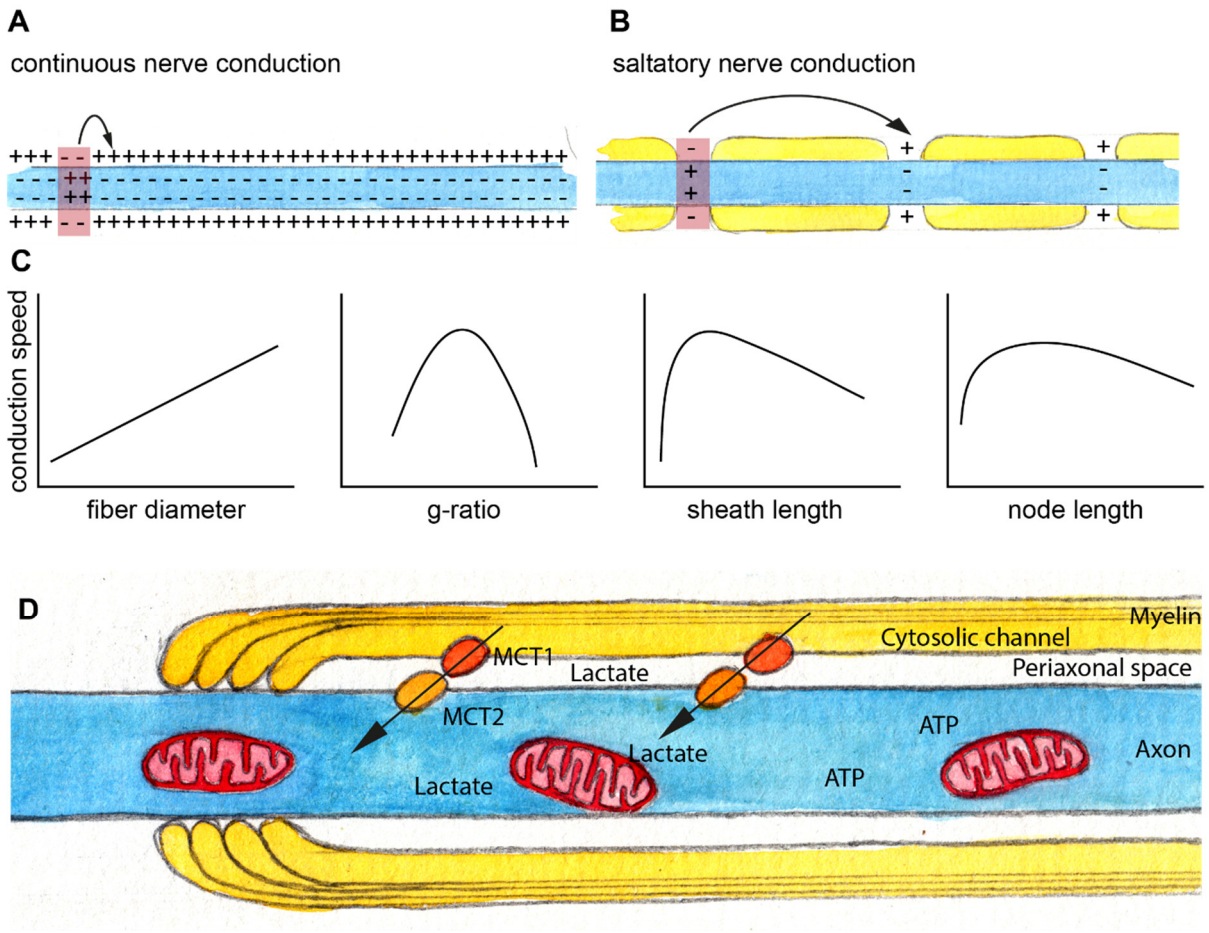

Figure 1.3 Functions of myelin and oligodendrocytes

(A) Schematic of AP conduction along an unmyelinated axon. The AP moves continuously along the axon **(B)** Schematic of AP conduction along a myelinated axon. The depolarization 'jumps' from one node to the next, resulting in a faster conduction **(C)** Theoretical dependence of conduction speed. Correlation between AP conduction speed and fiber diameter, g-ratio, sheath length, and node length. The fiber diameter and the conduction speed have a linear relationship. For the g-ratio, sheath length and node length optimal values can be calculated and deviations from that result in slower conduction speed **(D)** model for metabolic support. Lactate is transported from the oligodendrocyte to the periaxonal space from where it is taken up by the axon and used for ATP production. Adapted from (Morrison et al., 2013)

In conclusion, myelination is crucial to maintain a healthy nervous system by allowing for fast signal transduction and providing metabolic support for the axons.

1.2 Formation of myelin and node of Ranvier

Oligodendrocyte precursor cell differentiation

Oligodendrocytes are generated by differentiation of oligodendrocyte precursor cells (OPC) throughout life (Young et al., 2013). During development, OPCs arise in waves in restricted areas of the CNS from where they migrate to populate the entire CNS (Sun et al., 1998; Miller, 2002; Kessaris et al., 2006). Even in the adult CNS, OPCs account for 5-8 % of all cells (Dawson et al., 2000). They are equally distributed and maintain stable densities, due to self-repulsive mechanisms (Hughes et al., 2013). OPCs are highly motile cells that extend thin processes, with which they scan their environment and they can migrate to areas with a demand for myelination (Fig. 1.4 A)(Kirby et al., 2006; Hughes et al., 2013). Upon differentiation, OPCs form many nascent sheaths (Fig 1.4 B). A high number of these very early nascent sheaths retracts again (Liu et al., 2013), the remaining ones exhibit lateral growth (Fig 1.4 C). Once a cell started to differentiate and form myelin sheaths it has, in the zebrafish, a time window of 5-6h during which it can form new sheaths. Afterwards no more sheaths were added. Sometimes sheaths retracted again, this happened mainly in the first days after differentiation, later only few retractions were observed (Czopka et al., 2013).

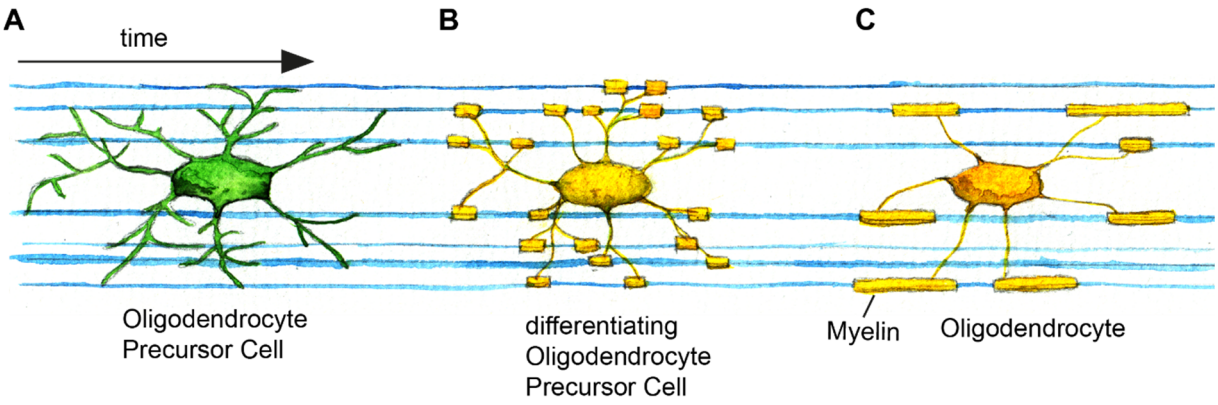

Fig 1.4 Schematic of OPC differentiation

(A) OPC scanning the environment with its processes **(B)** An OPC, that had just differentiated, forms many nascent sheaths on several axons **(C)** Mature oligodendrocyte. Some of the nascent sheaths retracted some were stabilized and grew laterally to increase in length

Myelin sheath growth and compaction

When an OPC starts to differentiate and to form myelin segments, it starts wrapping its processes around axons. The outer edge of the myelin sheath is the growth zone, here it extends in length (Fig 1.5 A). The inner tongue, the cytoplasmic region at the tip of the sheath, wraps around the axon and grows. Simultaneously to wrapping around and increasing myelin thickness, the sheath is also growing laterally and extending in length (Fig 1.5 B). To be able to grow at the inner part of the myelin sheath, newly synthesized membrane components have to be transported there. The membrane components are transported via cytoplasmic channels, that are maintained as long as the sheath is still growing. The majority of these cytoplasmic channels disappears with maturation of the sheath. Also at the edge of the myelin sheath, cytoplasmic channels can be found, that are in close contact with the ensheathed axon. These cytoplasmic channels later become the paranodal loops (Snaidero et al., 2014). Already during growth, myelin sheaths are compacted. The compaction of the myelin sheath starts at the outer layers and progresses to the inside. MBP is important for the compaction, as it interacts with lipid membranes and ensures the adhesion of two lipid bilayers (Harauz et al., 2009). MBP promotes compaction by binding to the cytoplasmic leaflet of two opposing myelin bilayers and bringing them together. Upon binding to membrane MBP self-association is induced (Bakhti et al., 2014).

As compaction starts at the outer layer, compaction of the inner layers must be prevented until the sheath has reached its length and stopped growing. It has been shown, that MBP and CNP have antagonistic functions for the compaction of myelin sheaths. While MBP supports compaction, CNP keeps the cytoplasmic channels open by organizing the actin cytoskeleton in these channels. Myelin sheaths around large caliber axons often maintain cytoplasmic channels, which could be important for the transport of metabolites or to provide a route for plasticity of myelin sheaths (Snaidero et al., 2017).

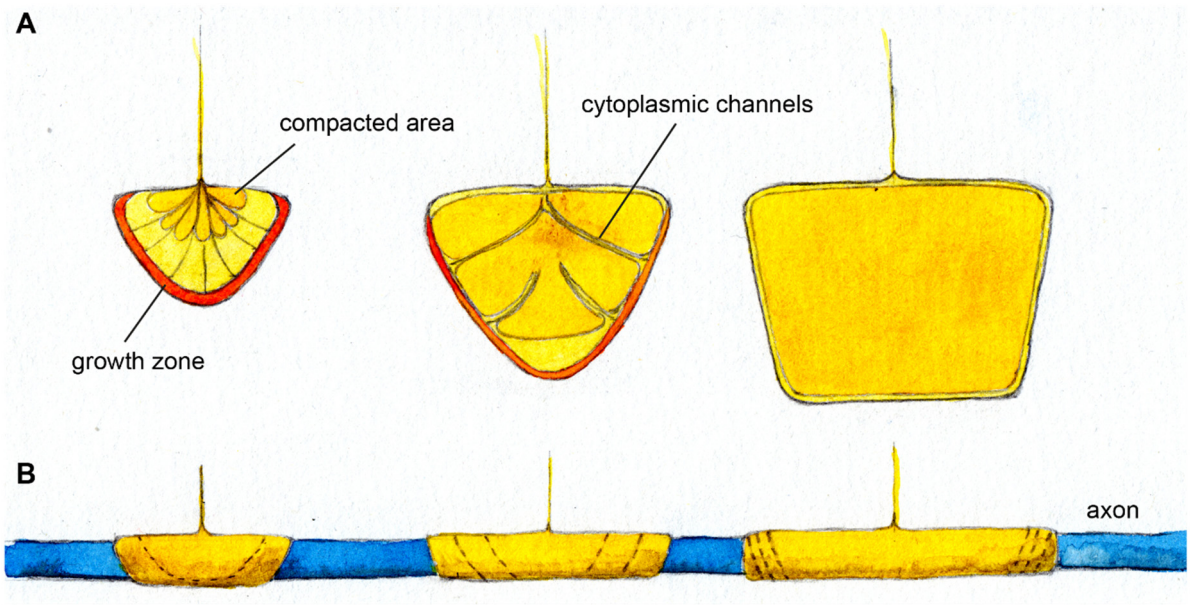

Figure 1.5 Myelin sheath growth and compaction

(A) Schematics of unrolled myelin sheaths during myelin sheath growth. The left example shows a very young sheath, with only little compaction and many cytoplasmic regions. The middle example shows a more mature sheath which has already many compacted parts. The cytoplasmic channels are still open and the sheath is growing. The right example shows a mature sheath. Only at the outer edge cytoplasmic regions can be found, the rest of the sheath is compacted **(B)** The myelin sheaths form (A), shown how they wrap around an axon. The dotted lines indicate the edges of the sheath underneath the outer layer. The sheaths grow in length as well as in thickness. Adapted from (Snaidero et al., 2014)

Formation of the node of Ranvier

Simultaneous to myelin sheath growth node of Ranvier formation takes place. The node has a complex morphology and many different proteins need to cluster at the right position. It is not entirely clear, how nodes of Ranvier are formed in the CNS and many studies report contradictory results, likely due to compensatory mechanisms. However, several intrinsic and extrinsic mechanisms that are involved in node formation have been identified. It is hypothesized, that there are three independent mechanisms that govern the formation of the node. These mechanisms are thought to be complementary as disruption of one can be compensated by the others, but disruption of two results in disrupted node formation. The three mechanisms are: (1) clustering of NF186 by the glia derived extracellular matrix, (2) the formation of paranodal junctions that act as diffusion barriers and (3) the anchoring of sodium channels to the cytoskeleton (Susuki et al., 2013).

The cell adhesion molecule NF186 is clustered by interaction with ECM (Susuki et al., 2013) and is essential for clustering sodium channels at the node (Ghosh et al., 2018). NF186 is anchored to the cytoskeleton by the scaffolding protein AnkG (Salzer, 2003), which is also required for clustering of sodium channels, independent of extrinsic mechanisms. In line with that, mutations of AnkG or AnkG binding motifs result in disrupted nodes and mis-localization of nodal components (Rasband and Peles, 2015). Conversely, deletion of ßIV-spectrin disrupts localization of AnkG and sodium channels (Komada and Soriano, 2002). It has also been shown, that sodium channels, AnkG and NF186 can cluster in culture, when treated with oligodendrocyte conditioned medium (OCM). Suggesting that a secreted factor of oligodendrocytes induces clustering even in the absence of myelin (Kaplan et al., 1997; Freeman et al., 2015). Similarly, AnkG and sodium channel clusters can also be observed *in vivo*, along unmyelinated axons (Freeman et al., 2015).

Paranodal interactions represent a form of extrinsic regulators of node formation. Sodium channel clustering follows the formation of paranodes, and by longitudinal growth these initial clusters are moved along the axon until a neighbor is met to form a node of Ranvier. Axo-glia interactions induce the clustering of sodium channels at the node of Ranvier (Rasband and Peles, 2015). The localization of Caspr2 depends, as well, on axo-glia interactions and the generation of barriers along the axon (Poliak et al., 2001). In contrast, developing nodes of Ranvier are defined by AnkyrinG clustering and seem to be independent of paranodal axo-glial adhesion (Jenkins and Bennett, 2002) and sodium channels can cluster even in the absence of proper paranodal junctions (Ghosh et al., 2018).

Furthermore, the actin cytoskeleton is necessary for proper sodium channel clustering. Disruption of actin disestablishes the ability of oligodendrocytes to induce sodium channel clustering (Kaplan et al., 2001). Similarly, disruption of the cytoskeletal adapter protein 4.1B results in disrupted nodes, showing that anchorage to the cytoskeleton is important for node formation (Brivio et al., 2017).

Together, NF186 clustering by ECM, diffusion barriers formed by paranodal junctions and the anchoring of sodium channels to the cytoskeleton form the node of Ranvier and secure the right molecular composition of the node (Susuki et al., 2013).

1.3 Mechanisms regulating the formation of myelin

Regulation of myelination by OPC differentiation and axon choice

There are different factors that influence myelination in terms of differentiation of OPCs or by regulating the choice of axons to be myelinated. Substantial progress has been made in identifying factors involved in CNS myelin regulation, and several oligodendrocyte intrinsic and extrinsic factors have been identified (Emery, 2010). However, the exact mechanisms by which myelination is regulated remain unknown.

OPC differentiation: As oligodendrocyte intrinsic factors, certain transcription factors, that prevent differentiation, have been identified. Id2, Id4, Hes5 and Sox6 keep OPCs in their undifferentiated state and prevent myelin gene expression. Expression of factors that prevent myelination led to the depression model of oligodendrocyte differentiation and myelination: Only when extracellular signals cause the downregulation of inhibitory factors, differentiation and the expression of myelin genes starts (Emery, 2010). Besides these transcription factors, it has also been shown, that chromatin remodeling plays a significant role. Histone deacetylases (HDACs) regulate oligodendrocyte differentiation and inhibition of HDACs delays differentiation and myelination (Shen et al., 2005). HDACs likely promote myelination by inhibiting factors that would normally block differentiation (Emery, 2010).

Axon choice: One extrinsic, physical factor regulating the axon choice for myelination in the CNS is the axon diameter, but in contrast to the PNS, where diameter is a fixed threshold for myelination, it is less clear in the CNS. In the PNS a diameter of around 1 µm is clear threshold for myelination (Snaidero and Simons, 2014). PNS myelination depends on Neuregulin1 signaling (Garratt et al., 2000)(Nave and Salzer, 2006) while Nrg1 signaling is dispensable for CNS myelination (Brinkmann et al., 2008). Furthermore, in the CNS there is a certain overlap of myelinated and unmyelinated fibers between 0.2µm and 0.8µm axon diameter (Remahl and Hildebrand, 1982; Snaidero and Simons, 2014). The selection of axons to be myelinated seem to involve more complex mechanisms than just axon diameter. Accordingly, axons express ligands like Jagged1 (Wang et al., 1998), PSA-NCAM

(Charles et al., 2000) or JAM2 (Redmond et al., 2016) which inhibit OPC differentiation or myelination. During development PSA-NCAM is expressed on all fibers and then downregulated on the axons that are subsequently getting myelinated (Charles et al., 2000). Neuronal cell bodies and dendrites express JAM2 to prevent their somatodendritic myelination (Redmond et al., 2016).

Furthermore, neuronal activity is a positive signal for myelination. It is speculated, that activity regulates the surface expression of ligands controlling myelination (Itoh et al., 1995) or that there is direct signaling from axons to OPCs. OPCs have been shown to have glutamatergic synapses and they can respond to axonal activity with depolarization (Bergles et al., 2000).

Indeed, it has been shown that optogenetic or chemogenetic manipulation of activity resulted in increased proliferation of OPCs but also increased differentiation into oligodendrocytes. Additionally, thicker myelin and de novo myelination were observed (Gibson et al., 2014; Mitew et al., 2018; Piscopo et al., 2018). But how activity dependent myelination is mediated exactly, is still unknown.

Recent studies performed in zebrafish helped understanding the role of synaptic vesicle release for myelination. Silencing of neurons, by blocking synaptic vesicle release, reduced myelination and myelin sheath length along silenced axons. When all neurons were silenced, the sheath lengths were again similar to control levels, suggesting that oligodendrocytes compare activity along axons and regulate sheath length accordingly (Hines et al., 2015). Additionally, oligodendrocytes produced less myelin sheaths, when synaptic vesicle release was blocked (Mensch et al., 2015). Furthermore, neuron type specific effects of synaptic vesicle release have been reported. In some neurons myelination depended on vesicle release while along others myelination was unaffected by blocking synaptic vesicle release (Koudelka et al., 2016). However, these studies were all done in very young animals and effects of synaptic vesicle release on young sheaths were

investigated. Hence, it remains unclear how sheath length at later developmental stages is influenced by axonal activity and changes in activity.

In another study it was observed, that monocular deprivation increased oligodendrogenesis and led to changes in myelin sheath length along with slower AP conduction in the optic nerve (Etxeberria et al., 2016). However, the shorter sheaths must not be a direct result of the monocular deprivation but they could also be a secondary effect by the increased oligodendrogenesis, as with more cells and sheaths there is less space for each sheath to grow.

Not only increased activity by manipulations influenced myelination, but also physical exercise, like voluntary running, can have positive effects on oligodendrogenesis in the spinal cord (Krityakiarana et al., 2010).

1.4 Distinct myelination patterns

Not only the amount of myelin, but also myelin sheath length or myelination patterns are important for nerve conduction. It remains largely unclear, what regulates sheath length and myelination patterns along axons. Axons can display quite unique myelination patterns (Fig 1.6). One example are the globular bushy cell (GBC) and spherical bushy cell (SBC) axons in the gerbil auditory system. Here, myelin sheath length gets progressively shorter closer to the synapse. This special arrangement secures precise AP conduction, which is crucial for sound localization (Ford et al., 2015). Another special, although very different, myelination pattern are the partially myelinated axons of pyramidal neurons in the cortical layer II/III. These axons exhibit large unmyelinated gaps between myelin sheaths, that are longer than nodes of Ranvier would be. To date, it remains unclear what the function of these patterns could be or if they only represent time-points of ongoing myelination (Tomassy et al., 2014).

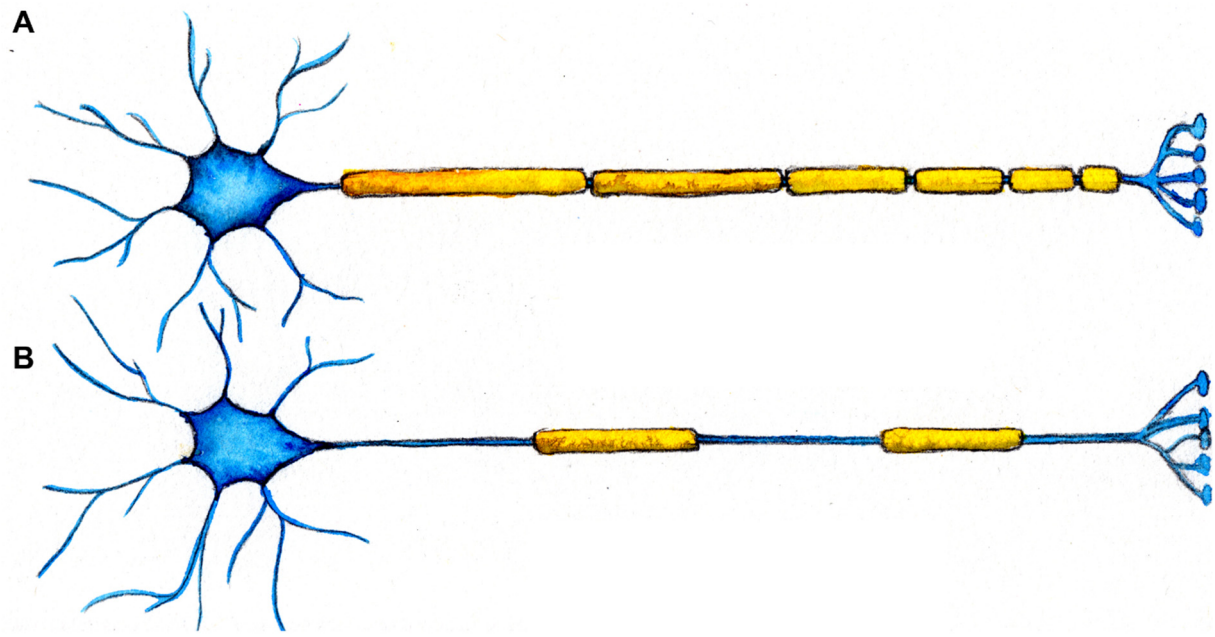

Figure 1.6 Different myelination patterns

(A) Myelination pattern found in the gerbil auditory system (Ford et al., 2015). Myelin sheaths get progressively shorter closer to the synapse **(B)** Partial myelination pattern found in the cortical layer II/III (Tomassy et al., 2014). There are large unmyelinated gaps between myelin sheaths.

Regulation of myelin sheath length

There is not much known about the mechanisms controlling myelin sheath length. One study, were oligodendrocytes isolated form the cortex and the spinal cord were cultured on inert fibers (Lee et al., 2012a), showed that oligodendrocytes from the spinal cord produce longer sheaths than cortical oligodendrocytes. Indicating oligodendrocyte intrinsic, region specific differences in regulating myelin sheath length (Bechler et al., 2015). Recent evidence suggests also influences of axonal activity on myelin sheath length in very early stages of sheath growth. Calcium imaging in developing myelin sheaths showed, that high frequency calcium (Ca) signals led to sheath retractions, while too low Ca^{2+} signals halted sheath growth. Only medium frequencies of Ca^{2+} signals resulted in sheath length elongation. By blocking neuronal activity it was shown that about half of the observed transients are caused by axonal activity (Baraban et al., 2018; Krasnow et al., 2018).

Together, myelination and node of Ranvier position can have very distinct patterns that might have important roles for the proper functioning of these neurons. However, the mechanisms regulating how individual axons are myelinated in terms of myelin coverage and myelin sheath length remains elusive.

1.5 Myelin dynamics

Myelination in the CNS is a dynamic process that takes place at different rates in different regions. White matter tracts are myelination rather quickly and to a large amount while grey matter is myelinated less. The speed of myelination also varies across different regions some are myelinated very quickly while others are myelinated at a slow rate and new myelin can be formed lifelong (Miller et al., 2012). Myelination is not a stereotypic process but there are different degrees of myelination. It has been shown that certain psychiatric disorders come along with changes in white matter. Effects on myelination have also been reported in mice raised in social isolation. Mice that were socially isolated during a critical time-period during their development displayed hypomyelination of the prefrontal cortex. Reintroducing these mice to social contacts could not rescue the phenotype (Makinodan et al., 2012). The hypomyelination phenotype could be mimicked by loss of ErbB3 in oligodendrocytes during a critical period. In line with that, social isolation reduced the expression of the ErbB3 ligand Neuregulin-1 (Nrg1) indicating that the hypomyelination observed after social isolation is mediated via ErbB3/Nrg1 signaling. Furthermore, these mice displayed perturbations in working memory (Makinodan et al., 2012). Similarly, social isolation of adult mice induced myelination changes and led to hypomyelination in the prefrontal cortex (Liu et al., 2012). These findings could represent a link to white matter changes that can be observed in psychiatric disorders.

Furthermore, the development of certain tasks coincides with the developmental myelination of the according brain regions, as well as differences in white matter correlate with the ability in certain tasks, like working memory or musical proficiency (Fields, 2008). There is also evidence, that learning a new motor task in humans induces changes in white matter. MRI scans of subjects that had learned to juggle showed increases in fractional anisotropy (FA), a measure depending on water diffusion and that reflects anatomical changes in white matter like axon caliber or myelination (Beaulieu, 2002), compared to the control group that did not practice the visuo-motor task. These changes persisted, also after

a longer break, in which the task was not practiced (Scholz et al., 2009). Not only learning new motor-tasks, but also cognitive training induced white matter changes, measured by FA (Takeuchi et al., 2010).

However, it is not clear from these studies if the reduced myelination is causal for the observed behavioral phenotype or if it is just correlative. Furthermore, all of these studies reported white matter changes, that were detected by FA, but it remains unclear what these increases in FA mean on a cellular level. It could either be, that new OPCs differentiate or that already present oligodendrocytes remodel their myelin in terms of length or thickness (Zatorre et al., 2012).

There is increasing evidence that myelination and changes in myelination might have functional implications. Studies in mice showed, that the differentiation and localization of NG2 glia can be altered by sensory deprivation of voluntary physical exercise (Simon et al., 2011; Mangin et al., 2012). Furthermore, it was shown, that the proliferation of oligodendrocyte precursor cells depends on the activity of neighboring neurons in the developing rat optic nerve (Barres and Raff, 1993). To proof a causal relation between myelination and behavior McKenzie et al. showed that blocking the formation of new myelin resulted in impaired motor-skill learning. Here, deletion of the Myelin Regulatory Factor (Myrf), a transcription factor that regulates myelin gene expression (Emery et al., 2009)(Bujalka et al., 2013), in mice, impairs the formation of new oligodendrocytes and myelin, without affecting existing oligodendrocytes. Subsequently, these mice performed worse in learning new motor skills like running on a complex wheel (McKenzie et al., 2014). In a high temporal resolution study, it was shown that these performance changes occur already after 2-3h after introduction to the complex wheel. In line with this, after 2.5h resident OPCs started to differentiate , in control mice, resulting in a decrease in OPC number and an increase in oligodendrocytes (Xiao et al., 2016). Together, these studies show that active myelination is important for learning new motor tasks.

Myelin plasticity to modulate circuit function

The observed white matter changes during learning, and the responsiveness to activity make myelination an attractive candidate for how experience can shape the brain. There are several potential ways of how myelin can remodel or change circuit function. Activity changes could lead to de novo myelination of previously unmyelinated axons or to replacement of existing myelin. On the other hand, there could also be changes of already existing myelin in terms of length or thickness. To date it is unclear how big the roles of these different mechanisms, in activity dependent changes in myelination, are (Kaller et al., 2017).

The conduction time along an axon is critical for synaptic plasticity, where timing of AP arrival plays a crucial role. Here, precise timing of conduction could be achieved by activity dependent feedback mechanisms (Fields, 2015). Changes of myelin, after it has been formed, to adaptively change conduction velocity, also after learning, could be an important mechanism of neuronal plasticity. Additionally, many functions of our nervous system rely on brain oscillations. Here, conduction velocity plays an important role as well, as already small changes in conduction velocity have a huge influences on these oscillations (Pajevic et al., 2014). Taken together, myelin remodeling seems to be an ideal candidate to modulate circuit function (Fig 1.7). However, direct evidence that existing myelin can remodel is still lacking. In this thesis, I am addressing this question to unravel if myelin sheaths can plastically remodel and are therefore a candidate to actively modulate circuit function.

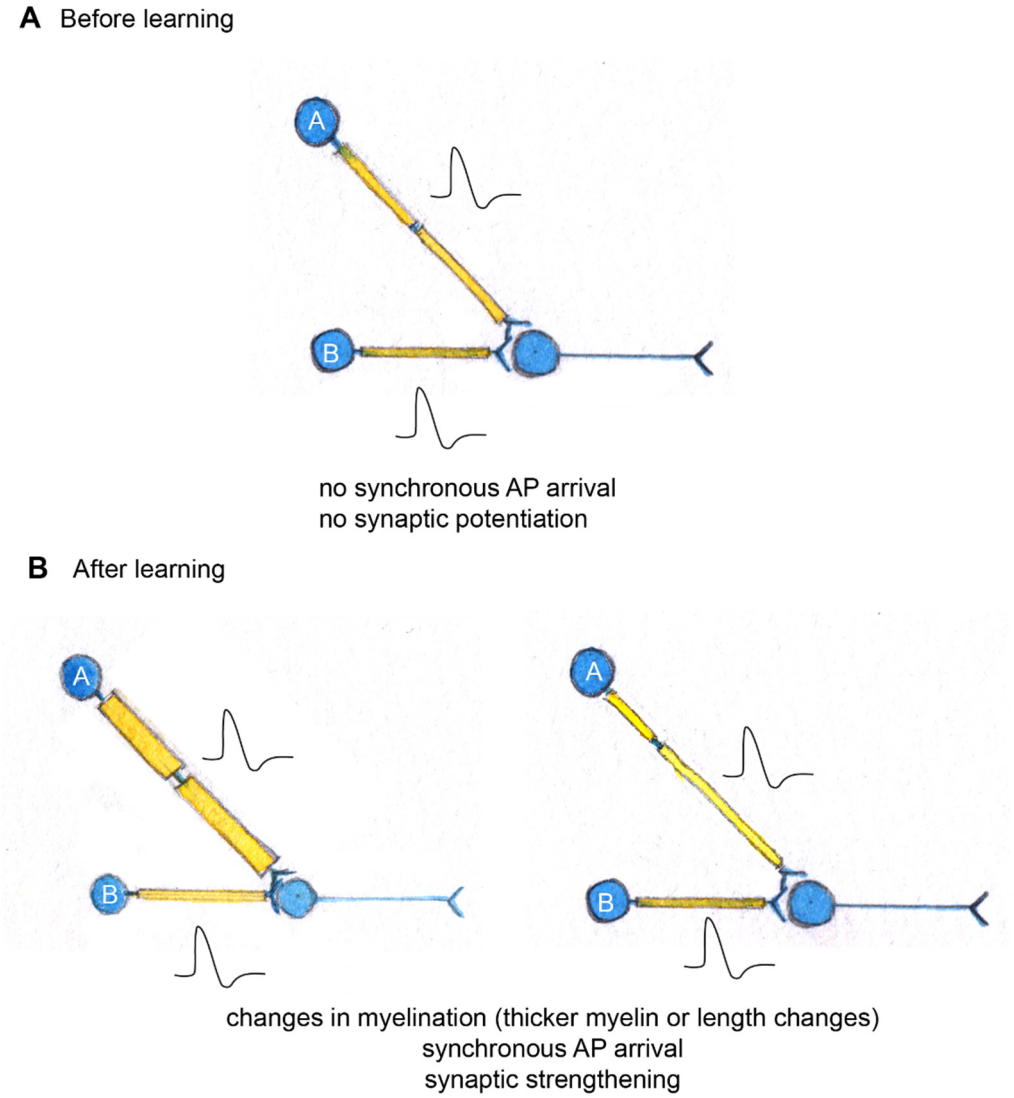

Figure 1.7 Hypothetical model of how learning can be influenced by myelination.

(A) Schematic neuronal circuit with two neurons projecting on one. Due to length differences APs will not arrive simultaneously. Hence there will be not synaptic strengthening in response to coincident firing **(B)** After learning neuron A could have acquired thicker myelin and therefore faster AP conduction to optimized synchronous arrival of AP input from cell A and B. Adapted from (Fields, 2015)

1.6 Aim of the thesis

Myelination influences conduction speed, and changes in action potential transmission can greatly influence nervous system function. One factor that influences conduction is myelin sheath length and the positioning of nodes of Ranvier. Previous studies reported myelin plasticity and showed white matter changes upon training or manipulation of activity, however, none of these studies provided direct evidence for activity-dependent myelin remodeling, rather changes in development were observed. Furthermore, it remains unclear how different myelination patterns and node of Ranvier positioning are mechanistically established and the dynamics of myelin sheath growth remain to be described. Changes in myelination to alter circuit function and modify behavior are an attractive idea, but direct evidence of myelin remodeling is still missing.

In order to address this lack of knowledge I have addressed the following aims during my Ph.D. research:

1. To investigate the dynamics of developmental myelin sheath growth and its potential to remodel that underlie the formation of myelinated axons
2. To investigate the mechanisms that underlie sheath growth dynamics and node of Ranvier positioning

I approached my aims by using zebrafish as a model system and performed in vivo imaging in the spinal cord. I took advantage of several existing zebrafish lines and generated new lines where neurons, oligodendrocytes or oligodendrocyte precursor cells are labeled. To test the ability of myelin sheaths to remodel I established a single cell ablation method with which I could precisely remove single myelin sheaths and observe how neighboring sheaths reacted. Due to the high similarity between zebrafish and mammalian myelin genes zebrafish are a suitable model to study myelination and the optical transparency of the zebrafish larvae make them ideally suited for live imaging studies.

2 MATERIAL AND METHODS

2.1 Cloning

All cloning was done in a collaborative effort between Dr. Tim Czopka, Wenke Barkey, Tobias Hoche and myself.

pME_memCerulean: To generate the middle entry clone pME_memCerulean the coding sequence was PCR amplified from a template plasmid. The primer combination attB1_memC/YFP_F and attB2R_memC/YFP_R was used. The PCR product was then cloned in to a pDONR221 plasmid with a BP-reaction.

pME_tagCFP: To generate the middle entry clone pME_tagCFP the coding sequence was PCR amplified from a template plasmid. The primer combination attB1_tagCFP_F and attB2R_tagCFP_R was used. The PCR product was then cloned in to a pDONR221 plasmid with a BP-reaction.

pME_KillerRed: To generate the middle entry clone pME_KillerRed the coding sequence was PCR amplified from a template plasmid. The primer combination attB1_KillerRed_F and attB2R_KillerRed_R was used. The PCR product was then cloned in to a pDONR221 plasmid with a BP-reaction.

pME_memEYFP: To generate the middle entry clone pME_memEYFP the coding sequence was PCR amplified from a template plasmid. The primer combination attB1_memC/YFP_F and attB2R_memC/YFP_R was used. The PCR product was then cloned in to a pDONR221 plasmid with a BP-reaction.

p3E_EYFP-pA: To generate the 3' entry clone p3E_EYFP-pA the coding sequence was PCR amplified from a template plasmid. The primer combination BamHI_C/YFP_F and EcoRI_C/YFP_R were used. The PCR product was digested with BamHI and EcoRI and was purified using PCR purification kit (Qiagen). The insert was cloned into a pCS2+ plasmid using the BamHI/EcoRI restrictions sites. Subsequently the EYFP-pA sequence was PCR amplified using the primer combination attB2_C/YFP_F and attB3R_pA_R and cloned into pDONR_P2P3R plasmid with a BP-reaction.

p5E_olig1(4.2): To generate the 5' entry clone p5E_olig1(4.2) a 5.4kb gene regulatory sequence upstream of the olig1 gene (Ensembl: ENSDARG00000040948) from genomic zebrafish AB wild-type DNA was amplified using the primer combination olig1_F_SalI and olig1_R_SacII. The PCR product was digested with KpnI, an endogenous restriction site in the olig1 upstream regulatory sequence, and SacII to obtain a 4.2kb insert which was then cloned into p5E_MCS.

pME_Nfasca_nostop: To generate the middle entry clone pME_Nfasca_nostop the coding sequence of the zebrafish Neurofascin gene (Ensembl: ENSDART00000112655.3) was PCR amplified from zebrafish AB wildtype cDNA. The stopcodon was removed from the 3' end using the primer combination attB1_Nfasca_F and attB2R_Nfasca_nostop_R. The PCR product was then cloned into a pDONR221 plasmid with a BP reaction.

pTol2_cntn1b:Nfasca-EYFP: The transgenic expression construct pTol2_cntn1b:Nfasca-EYFP was generated by a multisite LR recombination reaction with p5E_cntn1b (Czopka et al., 2013), the generated plasmids pME_Nfasca-nostop and p3E_EYFP and the Tol2Kit plasmid pDestTol2_pA (Kwan et al., 2007).

pTol2_huC:tagCFP: The transgenic expression construct pTol2_huC:tagCFP was generated by a multisite LR reaction with p5E_huC (Mensch et al., 2015), the generated pME_tagCFP and the Tol2Kit plasmids p3E-pA and pDestTol2_pA (Kwan et al., 2007).

pTol2_mbp:memCerulean: The transgenic expression construct pTol2_mbp:memCerulean was generated by a multisite LR reaction with p5E_mbp (Almeida et al., 2011), the generated entry clone pME_memCerulean and the Tol2Kit plasmids p3E-pA and pDestTol2_pA (Kwan et al., 2007).

pTol2_mbp:KillerRed: The transgenic expression construct pTol2_mbp:KillerRed was generated by a multisite LR reaction with p5E_mbp (Almeida et al., 2011), the generated entry clone pME_KillerRed and the Tol2Kit plasmids p3E-pA and pDestTol2_pA (Kwan et al., 2007).

pTol2_olig1(4.2):memEYFP: The transgenic expression construct pTol2_olig1(4.2):memEYFP was generated by a multisite LR reaction with the generated plasmids p5E_olig1(4.2) and pME_memEYFP and the Tol2Kit plasmids p3E-pA and pDestTol2_pA (Kwan et al., 2007).

pTol2_cntn1b:tagCFP: The transgenic expression construct pTol2_cntn1b:tagCFP was generated by a multisite LR reaction with p5E_cntn1b (Czopka et al., 2013), the generated plasmid pME_tagCFP and the Tol2Kit plasmids p3E-pA and pDestTol2_pA (Kwan et al., 2007).

pTol2_olig1(4.2):tagCFP-NTR: The transgenic expression construct pTol2_olig1(4.2):tagCFP-NTR was generated by a multisite LR recombination reaction with the generate plasmids p5E_olig1(4.2) and pME_tagCFP, and p3E_NTR (Karttunen et al., 2017) and the Tol2Kit plasmid pDestTol2_pA (Kwan et al., 2007).

Primers used

Primer Name	Sequence
attB1_Nfasca_F	GGGGACAAGTTTGTACAAAAAAGCAGGCTGCCACCATGTGGACACAGAGGCGGTG
attB2R_Nfasca_nostop_R	GGGGACCACTTTGTACAAGAAAGCTGGGTCTGCCAAAGAGTAGATGGCATTG
olig1_F_SalI	GAAGTCGACGTATGAAGCCTCTTGGCACAG
olig1_R_SacII	ACCGCGGCTGAAAAAAGATATTCAGAGAACATGG
attB1_memC/YFP_F	GGGGACAAGTTTGTACAAAAAAGCAGGCTGCCACCATGCTGTGCTGC
attB2R_memC/YFP_R	GGGGACCACTTTGTACAAGAAAGCTGGGTCTTACTTGTACAGCTCGTCCATGC
attB1_tagCFP_F	GGGGACAAGTTTGTACAAAAAAGCAGGCTGCCACCATGAGCGGGGG
attB2R_tagCFP_R	GGGGACCACTTTGTACAAGAAAGCTGGGTTTAGCGGTACAGCTCGTCCATG
attB1_KillerRed_F	GGGGACAAGTTTGTACAAAAAAGCAGGCTGCCACCATGGGATCCGAGGGCGGCCCCGCC
attB2R_KillerRed_R	GGGGACCACTTTGTACAAGAAAGCTGGGTCTAATCCTCGTCGCTACCGATGG
BamHI_C/YFP_F	GATGGATCCATGGTGAGCAAGGGCGAG
EcoRI_C/YFP_R	GACGAATTCTTACTTGTACAGCTCGTCCATGC
attB2_C/YFP_F	GGGGACAGCTTTCTTGTACAAAGTGGATATGGTGAGCAAGGGCGAG
attB3R_pA_R	GGGGACAACTTTGTATAATAAAGTTGAAAAAACCTCCCACACCTCCC

2.2 Animals

All experiments were performed according to local regulations as approved by the local regulatory bodies. Zebrafish were kept at 28.5°C with a 14/10-hour light/dark cycle. Embryos were kept in 0.3x Danieau's solution at 28.5°C. The transgenic lines used are listed in Table 2.1.

Table 2.1 Fish lines used

Line	Reference
Tg(mbp:EGFP-caax)ue2	(Almeida et al., 2011)
Tg(mbp:nlsEGFP)	(Karttunen et al., 2017)
Tg(mbp:memCerulean)	generated, see also (Auer et al., 2018)
Tg(mbp:tagRFPt-CAAX)	generated, see also (Auer et al., 2018)
Tg(mbp:KillerRed)	generated, see also (Auer et al., 2018)
Tg(cntn1b:KaltA4)	(Mensch, 2015)
Tg(UAS:GCaMP6s)mpn101	(Thiele et al., 2014)
Tg(olig1:tagCFP-NTR)	generated

Constructs used

Construct	Reference
UAS:ChR2-mCherry	Gift from Baier lab, (Schoonheim et al., 2010)

2.3 mRNA synthesis and injections

Transposase plasmid (Tol2Kit) (Kwan et al., 2007) was linearized with NotI (New England BioLabs), the digest was subsequently purified with a PCR purification kit (Qiagen) according to the protocol. The mRNA synthesis was done with the mMessage machine SP6 kit (Invitrogen) and then purified with an RNA clean up kit (Qiagen). The concentration was measured and the aliquoted transposase mRNA was kept at -80°C until further use.

For the microinjections, the injection needle was calibrated to an injection volume of 0.5nl. Two injections per egg result in a total injection volume of 1nl. To calibrate the needle, the fine tip was broken and test injections into a drop of mineral oil on a stage micrometer were done.

Fertilized eggs were injected at the one cell stage with 1nl of a solution containing plasmid DNA at concentrations between 5 and 20ng/µl and transposase mRNA (Kwan et al., 2007) at concentrations between 25-60ng/µl and 1% PhenolRed (Sigma Aldrich) for visualization.

Generation of new transgenic zebrafish lines

To generate stable transgenic lines injected F0 embryos were raised to adulthood and then outcrossed with wild-type animals. The embryos were screened for germline transmission of the injected transgene under a fluorescent stereo dissecting microscope and raised.

2.4 *in vivo* live imaging

Confocal imaging

Fish were either pre-screened at a fluorescent dissecting microscope (Nikon SMZ18) or they were screened after embedding at the confocal microscope (Leica TCS SP8). Fish were anesthetized with 0.2mg/ml Tricaine in Danieau´s buffer (fish were added in a dish containing the solution), after 5min they were transferred in to a vial with 1% ultrapure low melting point (LMP) agarose (Invitrogen), subsequently removed and mounted in the agarose on a glass coverslip with the head of the fish facing left. If the cell of interest was on the other side of the spinal cord fish were mounted with the head facing right. All images are oriented that the head faces left. The coverslip with the fish was mounted on a glass slide, creating a grease chamber filled with 0.2mg/ml Tricaine in Danieau´s buffer.

Images were acquired either as 8- or 12-bit confocal z-stacks with pixel sizes between 47 and 114nm x/y and a z-spacing of 0.75 - 1µm. 25x 0.95NA and 40x 1.1NA water immersion objectives were used. Higher resolutions were used when the images were used for subsequent deconvolution. Faster time-lapse imaging was done using a 25x 0.95NA water immersion objective with an 8kHz resonant scanner.

After the fish were imaged, they were released again from the agarose and placed in fresh Danieau´s buffer. From 5 days post fertilization (dpf) onwards fish were fed with Sera Micron and Paramecia and kept in a 14/10 light/dark cycle.

Spectral Confocal Reflectance Microscopy

Spectral confocal reflectance microscopy (SCoRe) imaging was used as a method for label free visualization of myelin, as myelinated axons reflect more light than unmyelinated axons and surrounding tissue (Schain et al., 2014). It was used to verify that partially myelinated axons are indeed partially myelinated and that there are no unlabelled oligodendrocytes in our lines. The 488nm, 561nm and 633nm laser lines were used and the reflected light was detected with a 5nm wide filter centred around the laser wavelength.

Calcium imaging

For the calcium imaging a light-sheet microscope was used (Leica SP8 DLS). Fish expressing GCaMP6s were paralyzed by bath application of Mivacurium chloride and, after 5min incubation, laterally embedded in a thin u-shaped glass capillary with 1% LMP agarose. The light-sheet imaging settings were calibrated for each fish individually and two time lapses of each 10min, with a 10min break, were acquired. A 2.5x illumination objective was used together with 2.5mm mirrors and a 10x detection objective.

2.5 2P Laser cell ablations

Mbp:KillerRed expressing cells were ablated using an Olympus FV1000/MPE microscope. The 2Photon laser used was a MaiTai DeepSee HP (Newport/Spectra Physics) together with a 25x 1.05 NA MP (XLPLN25XWMP) water immersion objective. The cells were continuously imaged with confocal scans with a 559nm laser to locate and target the individual KillerRed labelled cells. A line scan was drawn across the soma and the cell was bleached using the MaiTai laser tuned to 770nm (1.75W output) for 500ms.

2.6 Trichostatin A treatment

Trichostatin A (TSA) was used at a final concentration of 15nM. 1.5µl of the 100µM stock solution was diluted in Danieau´s containing 0.2%DMSO. TSA treatment started at 2.5dpf for 24-26h.

2.7 Metronidazol treatment

Metronidazol (MTZ) was used at a final concentration of 10mM. The solution was made fresh the same day (Curado et al., 2008). 0.2%DMSO was added to Danieau´s buffer, then MTZ was added and the solution was stirred until all MTZ was dissolved. 2.5dpf embryos were added for 24-26h.

2.8 Mivacurium chloride treatment

Mivacurium chloride was used at a final concentration of 0.5mg/mL. Fish were added to the solution and incubated for 5 min, they were embedded and subsequently imaged.

2.9 Optogenetics

For testing the optogenetic setup, Channelrhodopsin (ChR2) and GCaMP6s expressing fish were embedded in a glass bottom dish and imaged with a confocal microscope. The blue LED was mounted into the lid of the dish. Baseline recordings were performed, followed by a light stimulation with 0.1 Hz. As the light of the LED was detected in the GCaMP6s channel the background signal was measured as well and subtracted from the GCaMP6s signal of the Channelrhodopsin expressing cell. Calcium traces were analysed with Fiji and Matlab.

For stimulation of freely swimming fish the LED was mounted in the lid of a 12 well plate. The fish were placed in the well in Danieau´s buffer. During the optogenetic treatment fish were kept in the dark at 28.5°C.

Stimulation protocol: The fish were stimulated for 6h per day on two consecutive days. They were stimulated with 4Hz for 15s in 15min intervals.

2.10 Image processing

Images were analysed with Fiji, LasX and Imaris. Deconvolution was done with the Huygens Essentials version 16.10 1p2 (Scientific volume imaging, the Netherlands, __http://svi.nl__).

Fiji was used for registration of the single channels (StackReg) and adjustments of brightness. All measurements were done in Fiji. LasX was used to align channels. Photoshop CS6 was used to adjust the brightness, and Adobe Illustrator CS6 was used to assemble the panels.

2.11 Data analysis

Cell counting

To assess cell numbers, transgenic lines with a fluorescent nuclear tag fused to EGFP were used. For the developmental analysis of oligodendrocytes different fish were imaged at different ages, for the myelin delay experiments the same fish were imaged at different ages. Fish were mounted laterally and the whole depth of the spinal cord was imaged around somite 17. Cells were counted in the whole field of view and then normalized to 100µm length of spinal cord, to obtain the cell density. The transmitted light was imaged as well to measure the somite length to calculated the oligodendrocyte number independent from fish growth.

Sheath length measurements

Myelin sheath length was measured in Fiji using the segmented line tool. Sheath length was either measured with membrane tagged fluorescent protein or with nodal marker. In both cases it was measured in z-stacks, neglecting the third dimension. For the myelin label sheath length was measured from beginning to the end of one myelin sheath, for the node distance the length between two consecutive nodes was measured.

Relative sheath length

To calculate the relative sheath length, the length at the end of the imaging was normalized to one. The values measured at the different days of imaging were divided by the end length.

Reconstructions

Imaris was used to reconstruct myelinated axons. With the filament tracer and the magnetic lasso, the axon was semi-automatically traced and reconstructed in a 3D projection. The same was done for the myelin sheaths.

Prediction of myelin sheath length

For the sheaths in the elongation phase (≥4 days post initiation (dpi)) the relative increase in sheath length equals the relative increase in somite length.

$$\frac{sheath\ length\ x\ dpi}{sheath\ length\ 4\ dpi} = \frac{somite\ length\ x\ dpi}{somite\ length\ 4\ dpi}$$

After transposing the equation, one can calculate the predicted sheath length at any day after 4dpi by knowing the somite lengths at these days.

$$sheath\ length\ x\ dpi = \frac{somite\ length\ x\ dpi}{somite\ length\ 4\ dpi} \times\ sheath\ length\ 4\ dpi$$

Correction for body growth

To correct the sheath length for body growth I divided the sheath length at the given day by the relative increase in body growth. The sheath length and somite length at 4dpi was used as a reference.

$$sheath\ length\ x\ dpi_{corrected}\ = \frac{sheath\ length\ x\ dpi}{\frac{somite\ length\ x\ dpi}{somite\ length\ 4\ dpi}}$$

Relative position on the axon:

To assess the relative positon of myelin sheath along an axon landmarks were used to measure a defined distance before and after ablation. Axon collaterals or somata were used as such landmarks. The relative position on this defined stretch of axon was calculated by using the middle of the respective sheath length. The change in position was then calculated by the difference in the sheath positions before ablation and after remyelination.

For the controls the changes in sheath position during similar time intervals were measured.

Axon diameter:

Axon diameter was measured in light microscopic images. Therefore, the area of 3 axon stretches, around 20µm long, was measured and divided by the exact length of the stretch. The mean of the three values was calculated and used as the axon diameter.

$$diameter_{axon}\ = \frac{area\ _{axon\ stretch}}{length_{axon\ stretch}}$$

Growth rate

The growth rate at any given day is always the length change from the day before to the given day. Growth speed at day x was calculated by subtracting the length at day x minus the length at day x-1.

$$growth\ rate_{xdpi} = length_{xdpi} - length_{x-1dpi}$$

Daily growth rate from day x-y was calculated by subtracting the length at day y minus the length at day x divided by the number of days

$$growth\ rate_{x-ydpi} = \frac{length_{ydpi} - length_{xdpi}}{y - x}$$

Calcium imaging

To analyze the Calcium traces, regions of interest (ROIs) were drawn around the somata of the neurons and the mean intensity was measured with Fiji. The traces were imported in to Matlab and normalized by the first 100 frames. For the Calcium event detection, a threshold of 20% above average was used.

Relative process position

Sheath length was measured and the distance of the sheath end to the process. The ratio of the distance of the left sheath end to the process and the total sheath length was calculated. 0.5 was subtracted from that ratio to calculate the distance of the process from the center. With negative numbers indicating the process being on the left half of the sheath, positive numbers on the right half. The result was multiplied by two, to normalize the scale to go from -1 to 1.

$$relative\ process\ position = \left(\frac{distance_{sheath\ end-process}}{sheath\ length} - 0.5\right) * 2$$

Quantification of ensheathment

To measure the percentage of the axon ensheathed with myelin the length of the axon in the field of view was measured as well as the myelin sheaths on it. The sum of the myelin sheath lengths was divided by the axon length.

$$ensheathment[\%] = \frac{\sum myelin\ sheath\ length}{axon\ length} * 100\%$$

Fluorescent intensity measurements

To measure fluorescent intensities along an axon, a segmented line with 15px width was drawn along the axon. The values were measured, exported into Excel and normalized by the mean fluorescence.

Correlation of cluster and node

To correlate the Nfasca-EYFP clusters before myelination with the node position after myelination the images were aligned by landmarks, to exclude mistakes due to body growth of the fish. Somata of neurons or axon collaterals were used as landmarks. To assess if the cluster and the node are at the same position a box, being as wide as the node, was drawn around the node and if the cluster overlapped with the box it was counted as being at the same position. If the cluster did not overlap with the box it was not counted.

2.12 Statistics

Statistical analysis was done using GraphPad prism. All data were tested for normal distribution using the Kolmogorov-Smirnov normality test, unless the sample size was smaller than 5, in this case the Shapiro-Wilk normality test was used. All data in the running text are presented as mean ± SD independent of normality. In the figures, normally distributed data are presented as mean ± SD, whereas non-normally distributed data are presented as median with the 25% and 75% percentiles. When the data was normally distributed, either paired or unpaired t-test (two variables) or ANOVA (three or more variables) were performed. If data was not normally distributed, either Wilcoxon matched pairs signed rank test or Mann-Whitney test (two variables) or Tukey's multiple analysis (three or more variables) were used. To test for correlation, either the Pearson or Spearman coefficient were calculated. P-values <0.05 are denoted with *, <0.01 with ** and p-values < 0.001 with ***.

2.13 Solutions and Buffers

Danieau's Buffer

Stock solution

Reagent	Quantity for 900ml 30X stock solution
NaCl (Roth)	91.52g
KCl (Roth)	1.41g
MgSO4 (VWR Chemicals)	2.66g
Ca(NO3)2 (Roth)	3.83g
Hepes (Roth)	32.17
Distilled Water	Ad 900ml
Adjust pH to 7.6	

0.3x Danieau´s 10ml 30x Stock solution plus 990ml distilled water

Tricaine

Reagent	Quantity for xM Tricaine solution
Tricaine/MS-222 (PharmaQ, UK)	400mg
Distilled water	100ml
Tris (Alfa Aesar) pH adjusted to 9	2ml
Adjust pH to 7	

Metronidazol

Reagent	Quantity for 10mM Mtz solution
DMSO (Sigma Aldrich)	100µl
0.3x Danieau´s	50ml
Metronidazol (Sigma)	86mg

The Metronidazol solution was made fresh at the day of use.

Trichostatin A

Stock solution:

Reagent	Quantity for 100µM Stock solution
Trichostatin A (Sigma Aldrich)	1mg
DMSO (Sigma Aldrich)	3.308ml

Working solution:

Reagent	Quantity for 15nM solutions
Trichostatin stock solution (100µM)	1.5µl
Danieau´s	5ml
DMSO (Sigma Aldrich)	0.2%

Mivacurium Chloride

100x Stock solution

Reagent	Quantity for 50mg/mL stock solutions
Mivacurium Chloride (Abcam)	25 mg
Distilled water	500µl

Working solution

Reagent	Quantity for 400µl of 0.5mg/mL solution
Mivacurium chloride stock solution (100µM)	3µl
Distilled water	37µl
Danieau´s	360µl

3 RESULTS

3.1 Developmental myelination and myelin sheath growth

3.1.1 Developmental myelination

Conduction velocity along axons is an important factor influencing nervous system function. Myelin sheath length is one factor affecting conduction speed, however, the mechanisms regulating myelin sheath length and node of Ranvier positioning remain unknown. Modulating myelin sheath length could therefore be a mechanism to adjust conduction velocity, but direct evidence for myelin remodeling is still lacking. I aimed to study mechanisms regulating myelin sheath length and node of Ranvier positioning during development and to investigate how dynamic myelin sheaths can be.

The first step was to characterize the time course of myelination in the zebrafish spinal cord, as oligodendrocyte number or density might influence myelin sheath dynamics. Therefore, I assessed the number of myelinating oligodendrocytes in the zebrafish spinal cord at different ages during the first month of development.

I used a zebrafish transgenic line in which all oligodendrocytes express EGFP, under control of myelin basic protein promoter elements Tg(mbp:nls-EGFP), and imaged the fish at different ages. To easily visualize and count the cells, the EGFP was fused to a nuclear tag (Fig 3.1 A) (Karttunen et al., 2017). As myelination in zebrafish shows a gradient from anterior to posterior (Almeida et al., 2011), I counted the cells in a defined area in the middle of the zebrafish spinal cord around somite 17.

I found that in the first two weeks post fertilization, there is a substantial increase in the number of oligodendrocytes per 100µm of spinal cord (2.1 cells/d/100µm). In the third and the fourth week there is still an increase in oligodendrocyte number, but it is lower than in the first two weeks (0.6 cells/d/100µm) (Fig. 3.1 B). During this time, the fish also grow substantially. To quantify the size increase of the zebrafish, I measured the length of one somite in the field of view. Zebrafish grow on average by 3.5% per day (3.5 ± 2.4%/day)

(Fig. 3.1 C). The number of oligodendrocytes per somite, normalized for fish growth, shows an almost linear increase (1.8 ± 1.0 cells/d/somite) (Fig. 3.1 D).

Together, this shows that zebrafish myelination continues at least until 4 weeks of age, with a continuous increase in oligodendrocyte number. The density of oligodendrocytes, on the other hand, seems to reach a plateau after the second week of development.

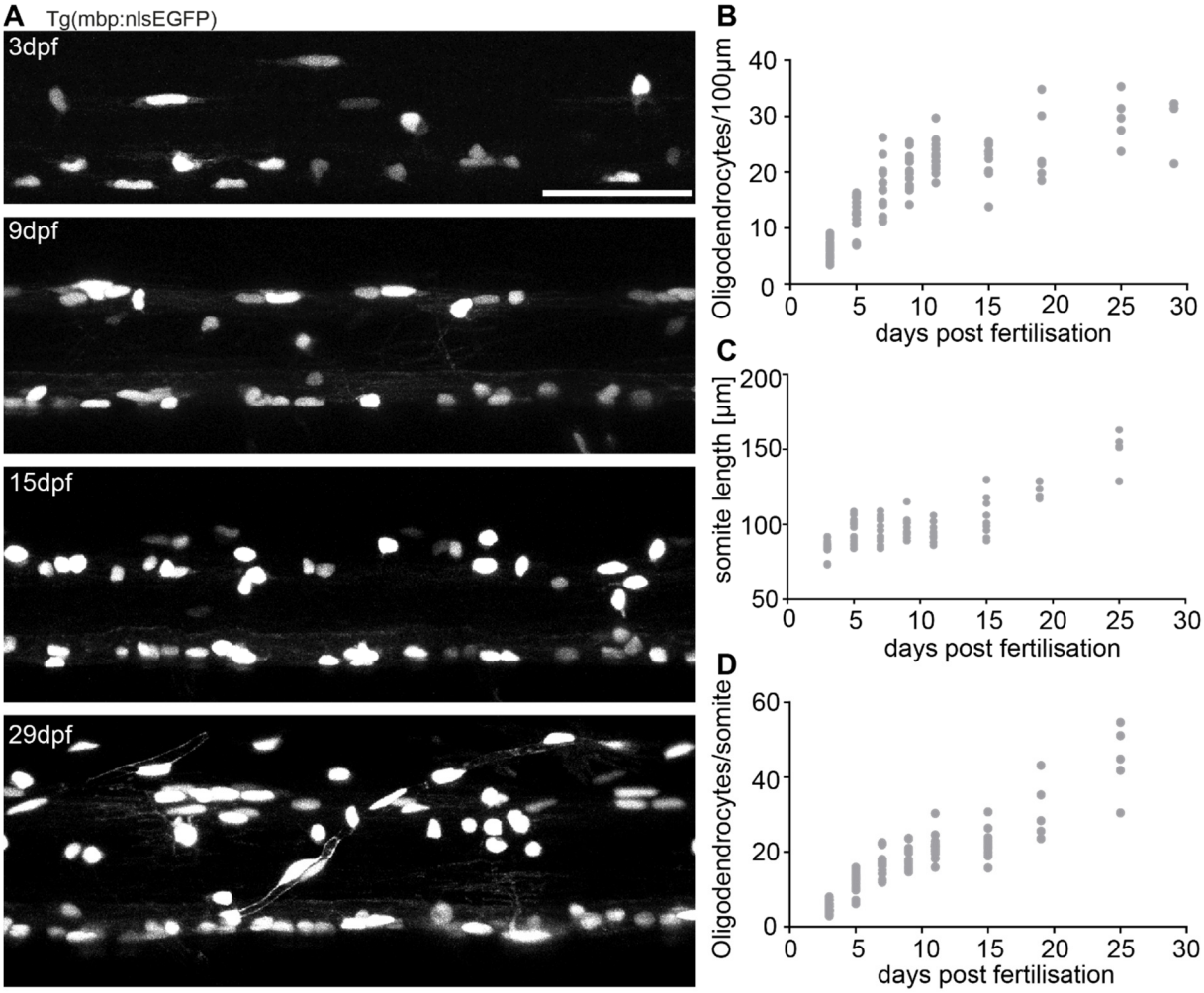

Figure 3.1: Myelination time course in the first month of zebrafish development.

(A) Confocal images of the spinal cord of a Tg(mbp:nlsEGFP) fish. Oligodendrocytes are labelled with EGFP localized to the nucleus. The different timepoints (3, 9, 15, and 29 dpf) show the increase in cell numbers in a defined area of the zebrafish spinal cord at somite 17. **(B-C)** Quantification of oligodendrocyte number over time. **(B)** Oligodendrocyte density, expressed as oligodendrocytes/100µm, shows a steep increase in the first two weeks of zebrafish development. After that the increase in cell numbers is less prominent until it appears to stop at the last two timepoints analyzed. **(C)** The fish growth is measured as length increase of one somite. With ongoing development, the fish increase in length **(D)** Oligodendrocyte number given as cells/somite, shows a continuous increase. Scale bar 50µm

Previous studies, in the mouse frontal cortex and zebrafish spinal cord (Murtie et al., 2007; Almeida et al., 2011), have shown that oligodendrocytes are able to produce myelin sheaths of different lengths. I wanted to verify that finding also for my experimental setup and determine the length range of myelin segments in the zebrafish spinal cord. Hence, I labeled single oligodendrocytes with mbp:tagRFPt-caax in a background in which all myelin was labeled with mbp:memCerulean. The fluorescent proteins are localized to the membrane for better visualization of the sheaths. To get an estimate of the variability of myelin sheaths in the zebrafish at 8dpf, I measured randomly chosen myelin sheaths. I also measured a subset of sheaths, as it was technically often not possible to measure all sheaths, formed by single oligodendrocytes. The sheaths measured at 8dpf were highly variable and ranged between 4 and 71 µm. I found that sheaths formed by a single oligodendrocyte span the whole range of myelin sheath lengths and therefore confirmed the observation that was made in other studies (Murtie et al., 2007; Almeida et al., 2011)

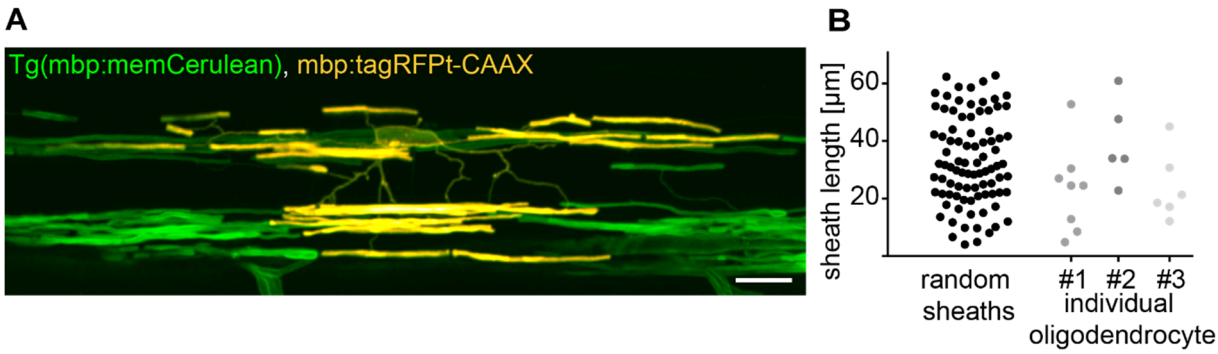

Figure 3.2: Individual oligodendrocytes can form myelin sheaths of different lengths

(A) Confocal image of a single oligodendrocyte (yellow) in a full transgenic mbp line (green). The oligodendrocyte forms myelin sheaths of different lengths. **(B)** Quantification of randomly measured myelin sheaths (black) and a subset of myelin sheaths formed by single oligodendrocytes (gray). The sheaths made by a single cell can span the whole range. Scale bar 10µm. See also (Auer et al., 2018)

3.1.2 Different phases of myelin sheath growth

As one oligodendrocyte is able to produce sheaths of different lengths, this raises the question of how these differences are established. Theoretically, there are two ways of how sheaths with different lengths could be formed. Either the sheaths differ in growth rate, or some grow for longer periods of time than others. To investigate how the different sheath lengths are established, I followed newly differentiated oligodendrocytes over time and assessed the growth pattern of the myelin sheaths. To label the cells, I used olig1 promoter elements, that reliably label oligodendrocyte precursor cells (Fig 3.3 top). Even though with the promoter elements we were using only OPCs are labeled, I was still able to detect the remaining fluorescent protein after differentiation (Fig 3.3 bottom).

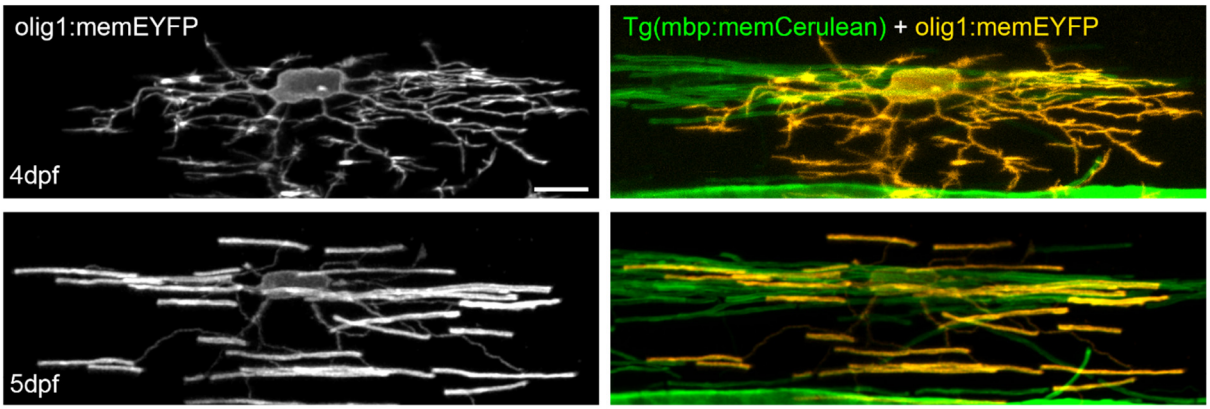

Figure 3.3: Olig1 as a marker for Oligodendrocyte precursor cells

Confocal images of an OPC at two different timepoints, before and after differentiation. The left images show the expression of memEYFP under control of olig1 promoter elements. The right images show olig1:memEYFP expression (yellow) as well as mbp:memCerulean (green) expression. Scale bar 10µm. See also (Auer et al., 2018)

To follow sheath growth over time I performed time-lapse imaging with two different settings. With the first, I aimed to document the very early growth dynamics. I transiently injected olig1:memEYFP into Tg(mbp:memCerulean) and performed time-lapse imaging at 30min intervals of oligodendrocyte precursor cells that were about to differentiate.

Upon differentiation the cells formed many short nascent sheaths, some of which were retracted again (Fig 3.4A, asterisk) while others grew longer over time (Fig 3.4A circle). I measured the sheath lengths at the different timepoints and plotted it versus the time after differentiation. I specified the timepoint of differentiation as the time when the cell had formed several nascent sheaths. In the first hours, up to 8h post differentiation (hpd), all sheaths showed a very similar growth rate (growth rate 0-8hpd 0.70±0.16μm/h) and therefore length, ranging between 5 and 11 μm.

After this timepoint, the individual sheaths grew with very different rates and at the end of the imaging, 19h post differentiation, they had all established very different lengths ranging from 7 to 33 μm (growth rate 8-19hpd 0.70±0.53μm/h, p=0.000653). To verify the observation of similar growth rate between individual sheaths in the first 8h, I calculated the variance of sheath length at the different timepoints and, indeed, it was very low (avg variance 0-8hpd, 1.2±0.72μm^2) until 8h post differentiation; after that there was a significant increase (avg variance 8-19hpd: 18.9±9.46μm^2 p = 0.04373)

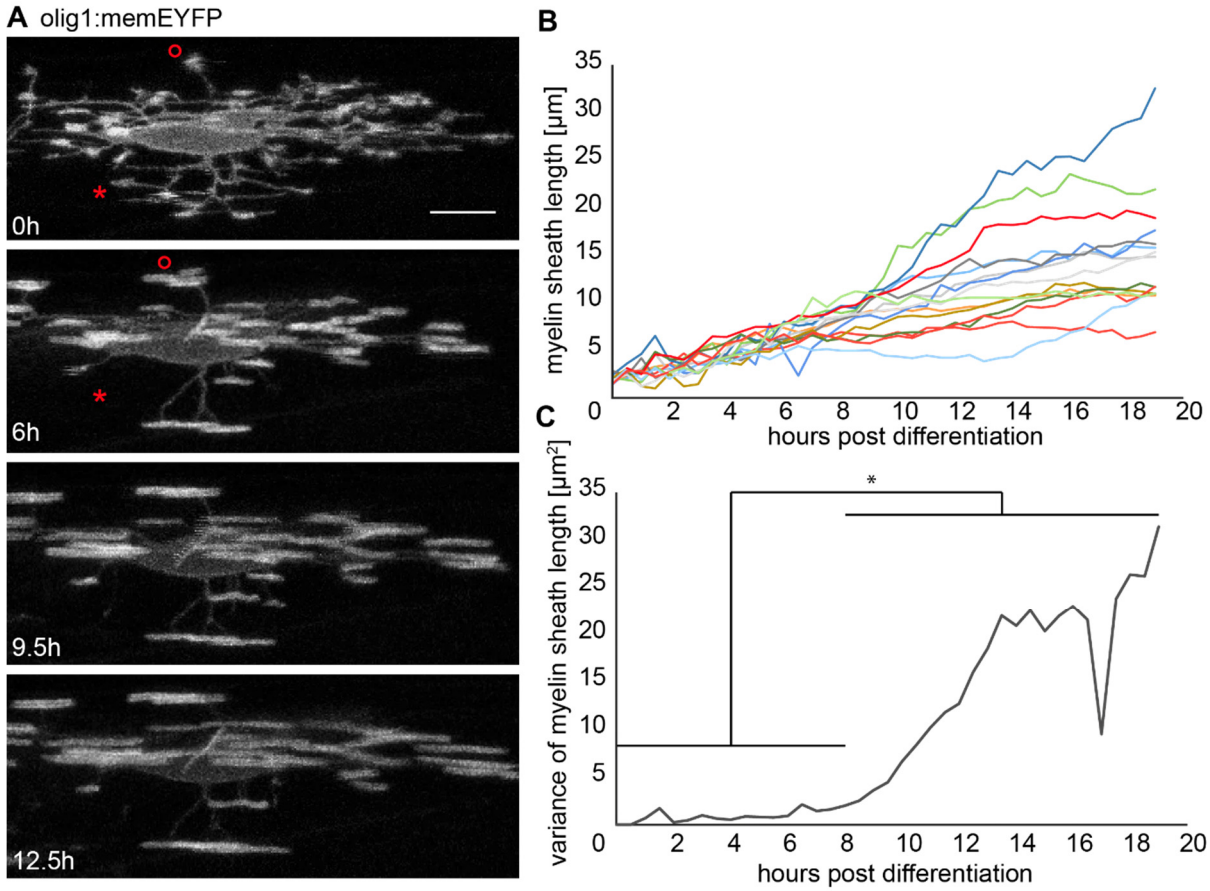

Figure 3.4 Time-lapse of an oligodendrocyte precursor cell differentiating into a myelinating oligodendrocyte

(A) Confocal images of a differentiating OPC at 4 different timepoints (0,6,9.5 and 12.5 hpd). Upon differentiation the cell forms nascent sheaths, some of which are retracted again (*), some sheaths grow longer over time (o) **(B)** measurements of single sheaths over time in the first hours after differentiation. In the first 8hpd the sheaths display a similar growth rate, after that, the sheath length varies more between different sheaths. **(C)** Quantification of the variance of sheath length at different timepoints. Until 8hpd the variance is very low after that it shows a substantial increase. Scale bar 10µm.

To follow the sheaths for longer than one day, I performed time-lapse imaging with different settings. I used the same injection paradigm, olig1:memEYFP injected into Tg(mbp:memCerulean) fish to get mosaic labeling of OPCs. I then imaged the fish once per day in the first days, later I increased the imaging intervals to every second day to reduce the stress for the fish. I screened the fish for OPCs, that had just differentiated and where I could see short myelin segments formed, and followed these segments over time.

I found that in the beginning, the first 2-3 days after differentiation, the myelin segments were growing relatively fast compared to their growth after 3-4days post initiation (dpi) (growth rate 1-3dpi: 9.3 ± 4.2 µm/day; n = 77/13 sheaths/animals) (Fig 3.5 A,B). From 4 dpi

onwards, they were all growing slowly and their length increase was barely detectable (growth rate 4-10dpi: 1.6 ± 1.7µm/day; n = 74/12 sheaths/animals, p<0.001). As the OPC marker was injected into a transgenic line where all oligodendrocytes, and therefore also myelin, are labelled, I could also assess the environment of the sheaths, regarding how many neighboring sheaths they had. When the sheaths are growing along an axon and they reach a neighboring sheath they will form a node and stop growing. Neighboring sheaths could therefore act as a physical barrier of sheath growth. Some sheaths had no neighboring sheath, others had just one (Fig 3.5B) and some sheaths were surrounded by two neighboring sheaths (Fig3.5A). Strikingly, even when there was no neighboring sheath, and therefore no physical barrier, the sheaths slowed down their growth rate and seemingly stopped growing (Fig 3.5B).

When I measured the length of the sheaths and plotted it versus the days post initiation (dpi) it also showed that the sheaths were growing fast in the first few days and after that they slowed down and showed only little length increase. Moreover, in the fast growth period (the first 3 days) the sheaths all grew at very different rates.

A significant portion of their length was achieved in the first 3 days, as after that time the growth curves run almost parallel (Fig 3.5C). To verify that the growth dynamics and sheath lengths are indeed independent from neighboring myelin segments, I analyzed the sheath length at the end of analysis of all three groups (namely, sheaths with no neighboring sheath, sheaths with one neighbor, and sheaths with two neighbors). The sheath lengths for all three groups are not significantly different from each other (33.6 ± 10.8 versus 41.9 ± 17.9 versus 36.4 ± 19, n = 16/14/16 sheaths, p=0.3) (Fig 3.5D). To analyze the growth dynamics of the three different groups, I normalized the sheath growth to the end length and averaged the sheaths with zero, one, or two neighbors respectively. The curves almost perfectly overlapped (Fig 3.5E) and the sheaths had reached the majority of their end-length at 3dpi (83% ± 17% versus 78% ±15% versus 72% ± 15%, n = 12, 13, 14/39 sheaths, p = 0.2) for an 8±1 day analysis. All sheaths displayed the same growth behavior: a fast initial

sheath growth then a slowing of the growth rate, independent of them having zero, one, or two neighboring sheaths.

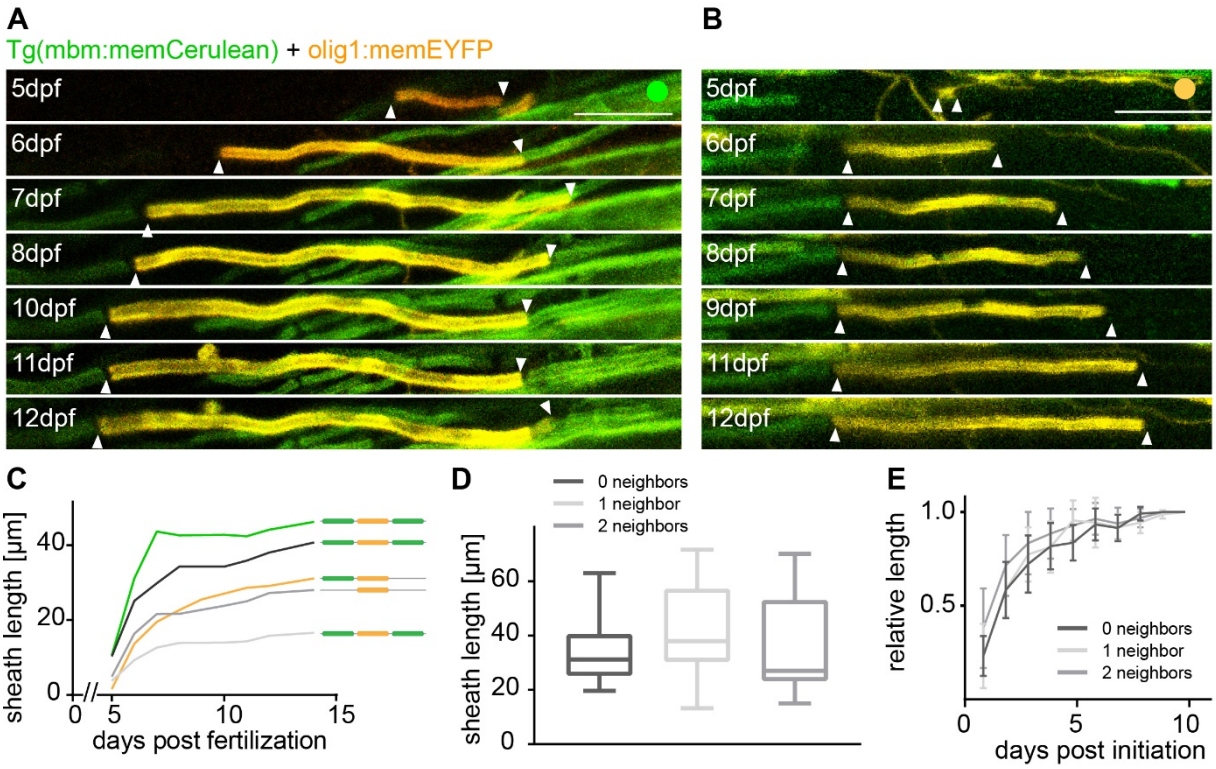

Figure 3.5 Myelin sheath growth over time

(A,B) Confocal images of newly generated sheaths followed for a week. **(A)** The newly formed sheath reaches a neighboring sheath on both sides at 8dpf **(B)** The newly formed sheath reaches another neighboring sheath only on one side, nevertheless it substantially slows down its growth **(C)** Growth curves of single sheaths, generated at 5dpf and followed until 14dpf. All sheaths show a similar growth pattern, a fast, initial sheath growth followed by a slower extension phase. The cartoon indicates if the sheath had zero, one, or two neighboring sheaths at the end of the imaging period **(D)** Comparison of end length of the sheaths with zero, one, or two neighboring sheaths. The end length between the three groups is not significantly different **(E)** Averaged and normalized growth curves of sheaths with zero, one, or two neighboring sheaths show that the sheaths show all the same growth behavior. Scale bar 10µm. See also (Auer et al., 2018)

As shown before, the overall density of oligodendrocytes in the spinal cord reached a plateau after the 2nd week of development (5dpf: 12.7 ± 2.8 versus 15dpf: 21.5 ± 3.1 cells/100µm, $p < 0.001$). I wondered, if there is a difference in sheath length and growth dynamics of sheaths that are initiated at later timepoints, when oligodendrocyte density had reached a plateau. Early generated sheaths are formed when there are few myelin sheaths present and many permissive axons. Sheaths generated during the plateau phase might have less space to grow due to more surrounding myelin.

To investigate if oligodendrocyte density influences sheath growth and length, I imaged newly differentiated sheaths at different timepoints of zebrafish development. I started the imaging at 5dpf and 14dpf, respectively, and continued imaging the sheaths in both groups for 9-10 days and assessed their length at the end of the analysis. Sheaths formed at 5dpf and 14dpf showed both huge variabilities in terms of length, but had overall the same end length (37.2 ±13 vs. 34.2±11.1, p-value 0.596) (Fig 3.6A). To analyze differences in the growth dynamics of early and late generated sheaths I plotted the growth curves of single sheaths (Fig 3.6B) as well as the averaged growth curves for both groups (Fig.3.6B'). There was no difference between the two groups observed, showing that oligodendrocyte density influences neither sheath growth nor sheath length.

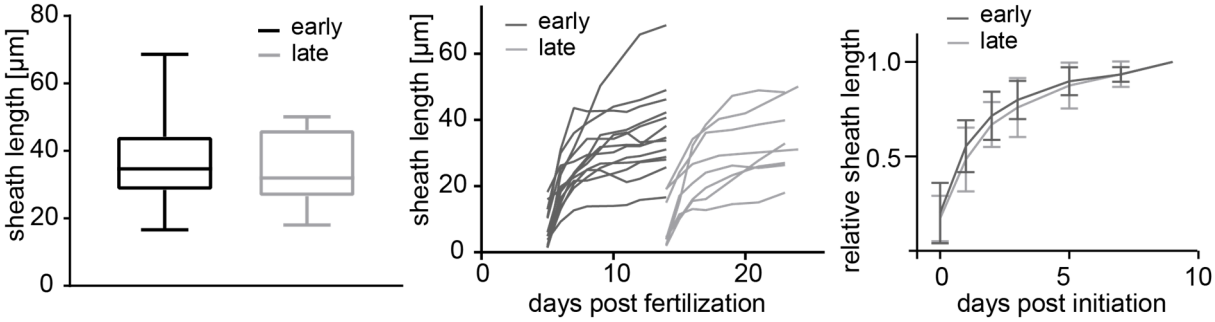

Figure 3.6 Comparison of early and late generated sheaths during zebrafish development

(A) Quantification of the sheath length of sheaths initiated at two different timepoints during development (5 and 14dpf). Sheath length, after 9-10 days of growth, does not differ between cells generated at 5dpf, when there is a fast addition of new oligodendrocytes, and 14dpf, when only few new oligodendrocytes are added. **(B)** Growth curves of single sheaths generated at 5 and 14dpf, respectively. Almost all sheaths show the same dynamics, a fast initial growth followed by a slower growth phase **(C)** Quantification of the averaged and normalized growth curves. The growth curves for both groups overlap, there is no difference in growth behavior between early and late generated sheaths. See also (Auer et al., 2018)

To proof, that it is indeed the growth rate that differs between the sheaths and that determines its length, I analysed the daily growth rates in the first 10 days of sheath growth. I calculated the growth rate on day x as the length at day x minus the length at the day before. In the first three days the growth rate is very variable and high (growth rate 1-3dpi: 9.3 ± 4.2µm/day; n = 77/13 sheaths/animals), after that there is less variability in growth rate and the it is overall significantly slower (growth rate 4-10dpi: 1.6 ± 1.7 µm/day; n = 74/12 sheaths/animals, $p<0.001$) (Fig 3.7 A).

As the highest variability in growth rates was observed in the first 3 days of sheath growth, I correlated the sheath growth during these first days with the sheath length at 8dpf (r=0.87, n = 16 sheaths, p<0.001) (Fig 3.7B). I found a high correlation between the two values supporting the hypothesis that sheath length is determined in the first 3 days after initiation by differences in growth rate.

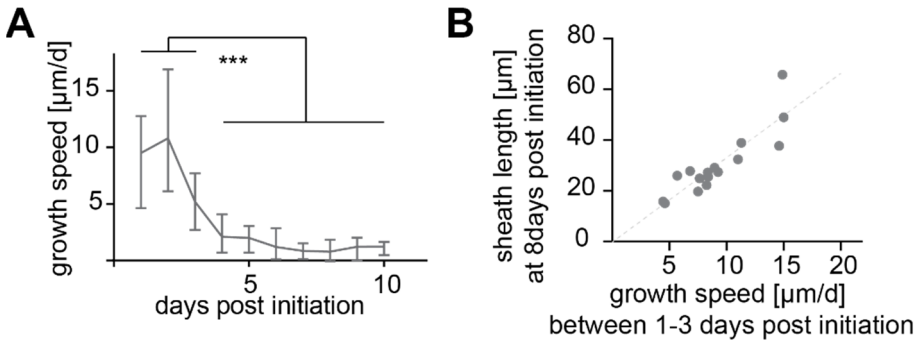

Figure 3.7 Quantification of growth speeds of myelin sheaths

(A) Quantification of growth rates of myelin sheaths in the first 10 days after initiation. In the first three days the sheaths show highly variable but fast sheath growth. After that, sheath growth slows down and becomes more uniformly. **(B)** The growth rate in the fast growth phase correlates with the sheath length at 8 days post initiation supporting the hypothesis that sheath length differences are established in the fast sheath growth phase. *** p < 0.001. See also (Auer et al., 2018)

I wondered, if sheath length differences are already established in the first three days by the fast growth phase, why the sheaths continue to grow slowly after the three days of fast growth. The slow growth phase could be due to the body growth of the fish; as previously mentioned, the fish do grow substantially during the long imaging periods. From 4dpf to 28 dpf they almost double in length (Fig 3.8A). To measure the length increase or growth of the fish I measured the length of one somite on the respective days (Fig 3.8B). To do this, I simultaneously acquired images of the somites by collecting the transmitted light with the confocal microscope.

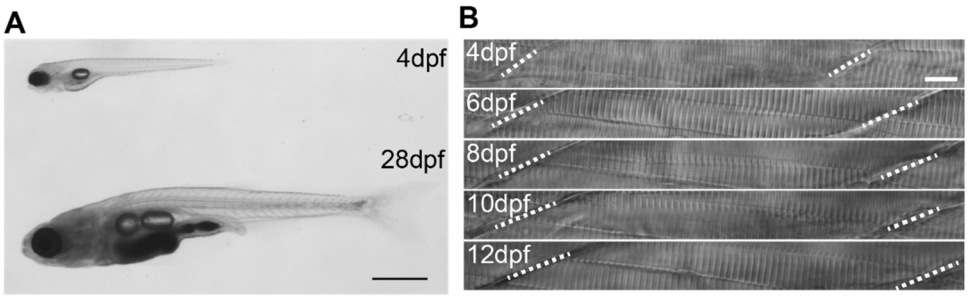

Figure 3.8: Fish growth over time

(A) Pictures of larval zebrafish. The top image shows a larval zebrafish at 4 days post fertilization. The bottom image shows a zebrafish larva at 28 dpf. Zebrafish show a substantial increase in body size in the first month of development. Scale bar 1mm. **(B)** Transmitted light images were simultaneously acquired. The end of the somite is indicated by the white dotted lines. To measure the growth of the fish, the length of the somite was measured at different timepoints. Scale par 10µm. See also (Auer et al., 2018)

To test if the slow growth phase does correlate with the growth of the fish, I measured the somite length and calculated the relative length by normalizing it to the end length, i.e. the length at 10 days after initiation of the respective sheath. I then plotted the relative somite length together with the relative sheath length, also normalized to the length at 10 days after initiation, revealing that the curves overlap after 3-4 days post sheath initiation (Fig 3.9A). To further verify that the slow growth phase is due to the fish's body growth, I calculated the relative differences between the somite length and the respective sheath length for the different days. In the first two days there is large difference between the two relative lengths, but from three days post initiation onwards there is no measurable difference (Fig 3.9B).

I could further separate the sheath growth into a fast growth phase from 0-3 (dpi) followed by a slower elongation phase from 4 days onwards. As the elongation phase perfectly overlaps with the body growth of the fish it probably compensates for it. To test the hypothesis, that the elongation compensates for fish growth, I calculated predictions for the sheath lengths in the elongation phase. Therefore, I calculated the relative fish growth, now normalized to the length at day 4 post initiation, which is the first day of the elongation phase. I then multiplied the relative size at a certain day with the sheath length at day 4 post initiation. I calculated the predictions for sheaths at two different timepoints, 6 and 10dpi, and correlated them with the measured value at the respective day (Fig 3.9C). For both

days the measured and the predicted value correlated with a high correlation coefficient (6dpf: r = 0.95, 10dpf r= 0.98, p<0.001 n=13 and 10). Together this shows that as soon as a new sheath has reached the elongation phase its behavior becomes highly predictable based on the body growth of the fish.

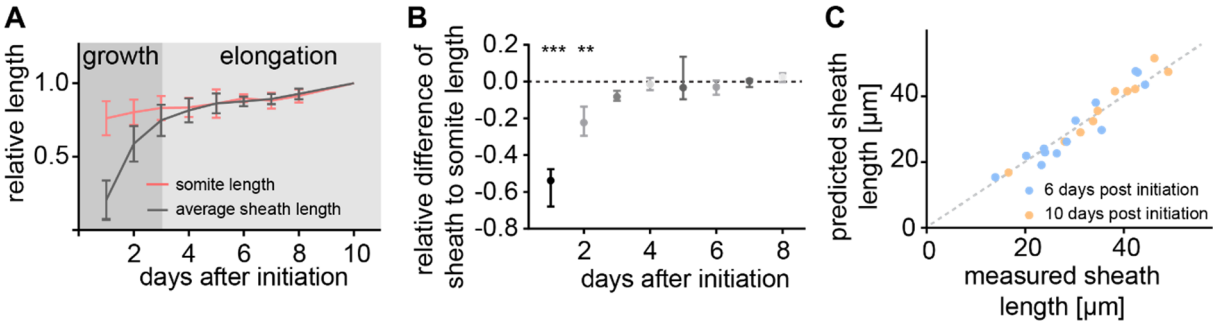

Figure 3.9: Myelin sheath growth consist of an elongation phase to compensate for body growth

(A) The growth curves of myelin sheaths (gray) and the somite length (red) do overlap after the third day post initiation when normalized to end length. Myelin sheath growth shows a growth phase and an elongation phase. **(B)** The difference between the relative somite length and the relative sheath length is significant in the first two days, after that its indistinguishable from zero. **(C)** Sheath length in the elongation phase is highly predictable by knowing the somite length of the fish. Predicted values highly correlate with measured values at two different timepoints after sheath initiation, 6 and 10dpi. ** p < 0.01, *** p < 0.001 See also (Auer et al., 2018)

Together, I could show that myelin sheath length consists of three different growth phases that are independent of physical barriers like neighboring sheaths. In the first early growth phase, that lasts for about 8h the sheaths all grew very uniformly with a very low variability. In the second fast growth phase, that lasts about 3 days, the sheaths all show a high variability and very different growth rates. This second phase also determines the differences in sheath length. In the last growth phase, which is rather passive, the sheaths are elongating only to compensate for body growth. In this third growth phase the sheath length becomes therefore highly predictable by the body growth of the fish.

3.1.3 Axonal myelination patterns

In the previous section I could show that myelin sheaths have different growth rates that determine sheath length differences. This raises the question, of how these different growth phases are regulated. As one cell can make sheaths of different lengths, it is unlikely to be oligodendrocyte intrinsic. Another option could be axonal regulation of myelin sheath length. In line with that, earlier studies reported a correlation between axon diameter and myelin sheath length (Murray and Blakemore, 1980; Ibrahim et al., 1995).

To assess how sheath length varies along an axon, I measured the length of consecutive sheaths along different axons. As it is not possible to measure this in the full transgenic mbp lines due to the high density of labeled myelin, I labeled the nodes of Ranvier and measured nodal distance. I labeled the nodes by transient injections of Nfasca-EYFP, a fusion protein of the transmembrane nodal protein Neurofascin and EYFP, under control of contactin 1b promoter elements (cntn1b) (Czopka et al., 2013). Cntn1b is a neuronal promoter used for labeling large caliber axons. To better follow the axons along their length, I co-expressed another cytoplasmic fluorescent protein, also driven by cntn1b promoter elements. The two constructs were co-injected into full transgenic mbp lines. As injections of these constructs give a random expression pattern, I screened the fish for myelinated neurons that express both markers.

I assessed the localization of the marker and was able to show that Nfasca-EYFP labels unmyelinated stretches of axons (Fig 3.10 A) and when the axon is fully myelinated it eventually localizes only to the nodes of Ranvier. (Fig 3.10 B).

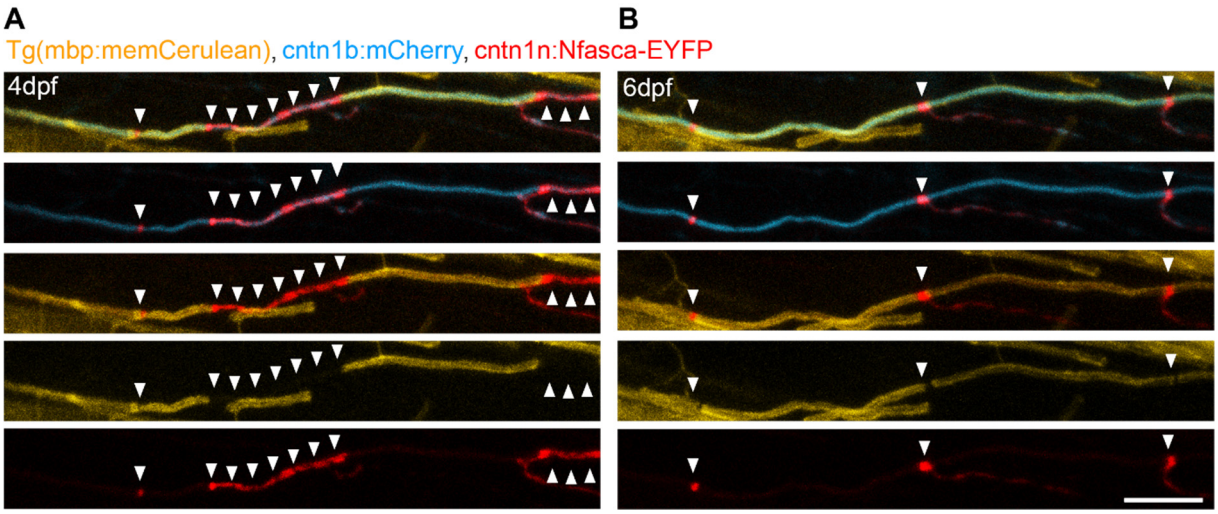

Figure 3.10: Expression of Neurofascin tagged with YFP to label unmyelinated axon stretches

(A,B) Confocal images of an axon co-expressing mCherry and Nfasca-EYFP at two different timepoints (4 and 6 dpf) **(A)** Nfasca expression (red) in a neuron (cyan) with larger unmyelinated stretches. Nfasca is localized to the unmyelinated regions and nodes (white arrows). When there is a myelin sheath (yellow) there is no Nfasca signal. **(B)** At 6dpf the neuron is fully myelinated and the only red signal is localized at the nodes of Ranvier. Scale bar 10µm. See also (Auer et al., 2018)

Using this method, I was able to follow neurons for almost 0.5mm along their length. Figure 3.11A shows a fully myelinated neuron labelled with mCherry (depicted in cyan). The white arrows indicate Nfasca signal (depicted in red) and the location of the nodes. I measured the distance between consecutive nodes, an indicator of myelin sheath length, along several axons, from different neuron types.

I found that the myelin segments on fully myelinated axons showed a high variability and ranged between 6 and 87 µm (37.7 ± 16.8 µm n=143/15/15 sheaths/axons/animals) (Fig 3.11 B). Nevertheless, there were also differences between different neurons. Some axons had overall shorter myelin segments than others (Fig. 3.11 B). Multiple comparison of the sheath length of the different axons showed that 7/15 axons had significantly different sheath lengths. I could not detect any correlation with the neuronal type - different interneurons like Commissural primary ascending (CoPA), Circumferential descending (CiD) and other interneurons were analyzed - indicating that sheath length along an axon seems to be a feature of every individual axon (e.g. #1 and #4 are the same type).

As mentioned before, it was proposed that axon diameter influences myelin sheath length (Murray and Blakemore, 1980; Ibrahim et al., 1995). In my experiments I could not detect a correlation between average myelin sheath length and axon diameter (r = -0.02; p = 0.95. Fig 3.11 C). All axons measured had a similar diameter (0.9 ± 0.1 µm)

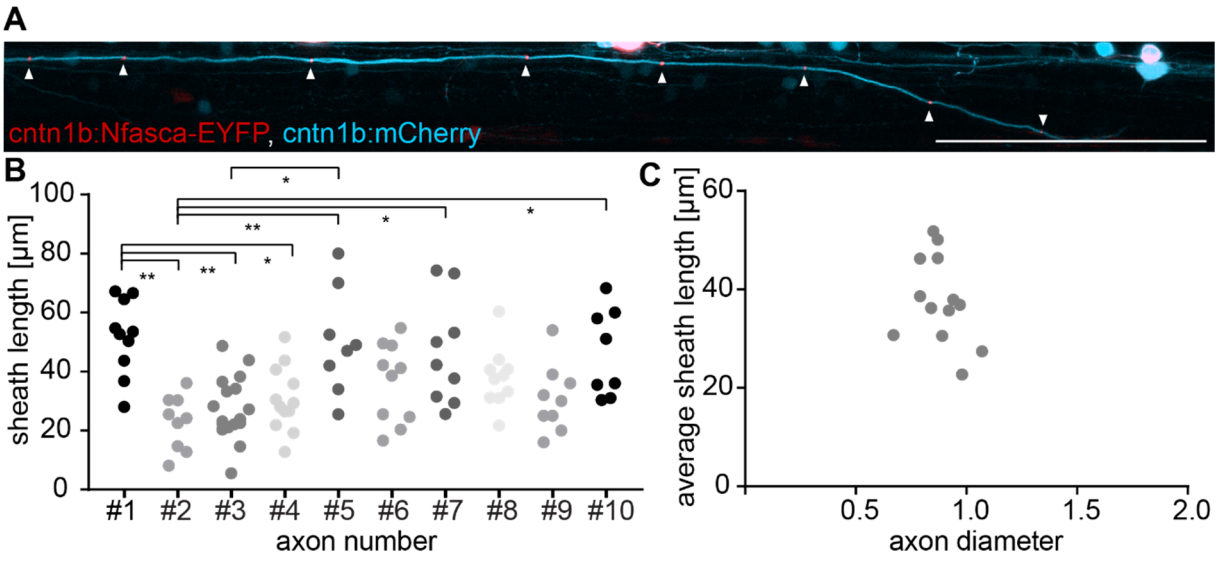

Figure 3.11 Myelin sheath length along individual axons

(A) Confocal image of a neuron expressing mCherry and Nfasca-EYFP. The white arrows point to the Nfasca signal, that labels the nodes of Ranvier. **(B)** Quantification of myelin sheath length along individual axons. Myelin sheath length differs between different axons but it spans wide ranges of the total myelin sheath lengths measured **(C)** Quantification of average sheath length and the respective axon diameter. There is no correlation between sheath length and axon diameter. Scale bar 100µm. * $p < 0.05$, ** $p < 0.01$ See also (Auer et al., 2018)

It was recently shown that besides fully myelinated axons, there are also axons in cortical layers in the mouse with a partial myelination profile (Tomassy et al., 2014). As this was no longitudinal study, these patterns could also be snapshots of an axon that is slowly being myelinated. To see, if I could also find partially myelinated axons in the zebrafish spinal cord and to follow them over time, I injected a DNA construct encoding an axon marker in transgenic lines with all myelin labeled (Tg(mbp:memCerulean)).

I did find partially myelinated axons and followed them for several days from 6dpf onwards. In some cases, (3/6), the axons did get more ensheathments over time (Fig 3.12A blue) but in other cases, (3/6) the axons maintained a stable number of myelin sheaths during the time window of observation (Fig 3.12A red). From this investigation it is clear that some

axons eventually do get fully myelinated while others maintain their partial myelination status, at least until the end of the analysis. (Fig. 3.12B).

As the myelin segments on these partially myelinated axons often did not have physical barriers like neighboring sheaths, I also measured their length, to assess if the absence of physical barriers has a positive influence on sheath length. The sheath lengths on these axons were highly variable, but they were not longer than the myelin sheaths on fully myelinated axons, confirming previous observations during sheath growth analysis. Although there was no physical barrier stopping them from growing (these experiments were done in the full transgenic line), the sheaths did not grow longer than the ones on fully myelinated axons (9 – 68 µm, 23.9 ± 14.9, n = 11/11 axons/animals) (Fig 3.12C).

To rule out incomplete labeling of our full transgenic lines, I performed Spectral Confocal Reflectance Microscopy (SCoRe) (Schain et al., 2014) of partially myelinated axons. In SCoRe imaging the light reflected by the tissue is collected, and as myelinated axons reflect more light than unmyelinated axons and surrounding tissue, this is a suitable tool for label free visualization of myelinated axons. Whenever I could detect a SCoRe signal there was also EGFP signal, confirming that the labeling was complete and that unmyelinated axon stretches are indeed unmyelinated (Fig 3.12D).

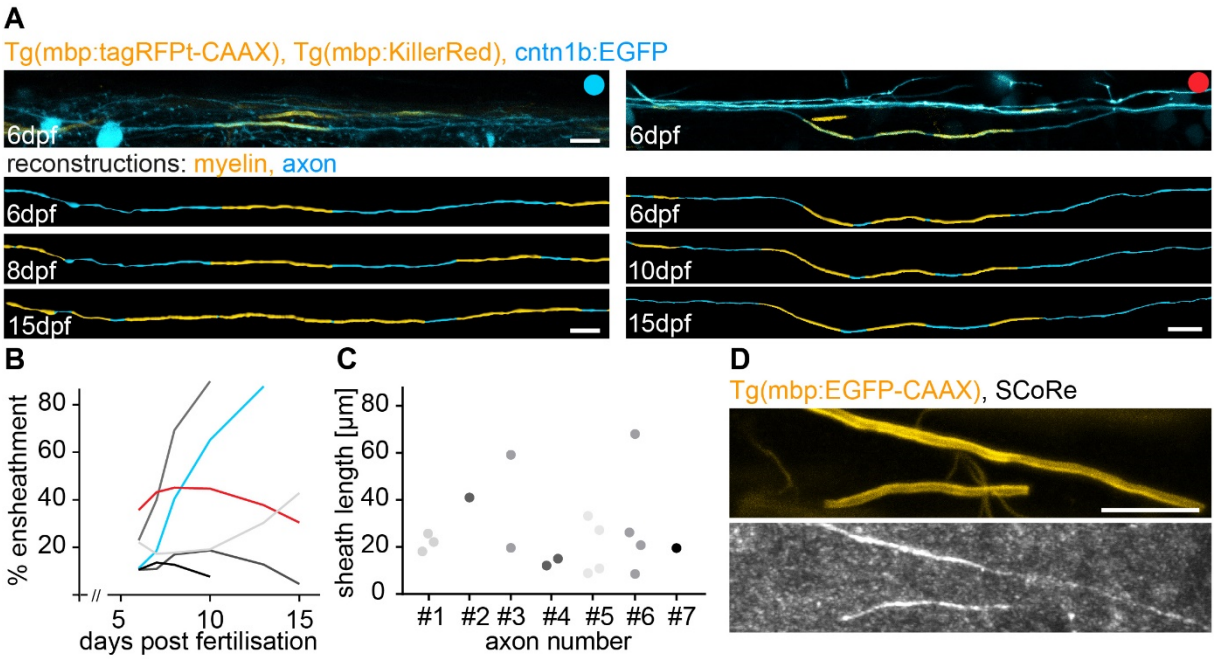

Figure 3.12 Partial myelination patterns in the zebrafish spinal cord.

(A) Confocal images and reconstructions of partially myelinated axons. The reconstructions show the myelination over time. The left example shows an axon that gets increasingly myelinated (blue). The right example shows an axon that maintains its partial myelination pattern (red) **(B)** Quantification of myelin coverage over time. Some axons (3/6) get increasingly myelinated while others maintain their partial myelination pattern **(C)** Quantification of myelin sheath length along partially myelinated axons. Sheaths formed on partially myelinated axons have similar lengths than sheaths on fully myelinated axons **(D)** Confocal image and SCoRe image of a full transgenic mbp line (Tg(mbp:EGFP-caax)). All myelin sheaths are labelled with EGFP and detected with SCoRe, confirming full labeling of the used transgenic lines. Scale bar 10µm. See also (Auer et al., 2018)

To follow axon myelination patterns over time, I co-expressed mCherry and the fusion protein Nfasca-EYFP in neurons. I was able to image axons for up to 450µm of length (Fig 3.13 A) and to assess the nodal position with the EYFP signal. I followed the axons over time and imaged them in regular intervals. When the images are aligned to a landmark, here the soma of another neuron between myelin sheath #6 and #7, one can see that the nodes do not keep the same position but they move slowly along the axon, reflecting the body growth of the fish and therefore sheath elongation (Fig 3.13B). To quantify and better compare axon myelination patterns I plotted the sheath length versus the sheath number along the axon (Fig 3.13C).

I observed very specific myelination patterns for the neurons and, as the sheaths were still growing in the beginning, the patterns changed over time (Fig 3.13 C, shades of gray). At

later timepoints, when all sheaths are in the elongation phase, I corrected the single sheaths for body growth. The newly obtained pattern looks much more stable over time (Fig3.13 D). I did this for several neurons and found that all neurons had a unique myelination pattern; but what they all had in common is, that once the pattern is established, it is remarkably stable over time when it is corrected for body growth of the fish (Fig 3.13 E-E'''). Sometimes I observed two nodes merging to become one node, indicating sheath retractions, as it was previously reported (Czopka et al., 2013). These retractions temporarily disrupted the pattern (Fig. 3.13 E', sheath #8) but once the sheath fully retracted the pattern was stable again.

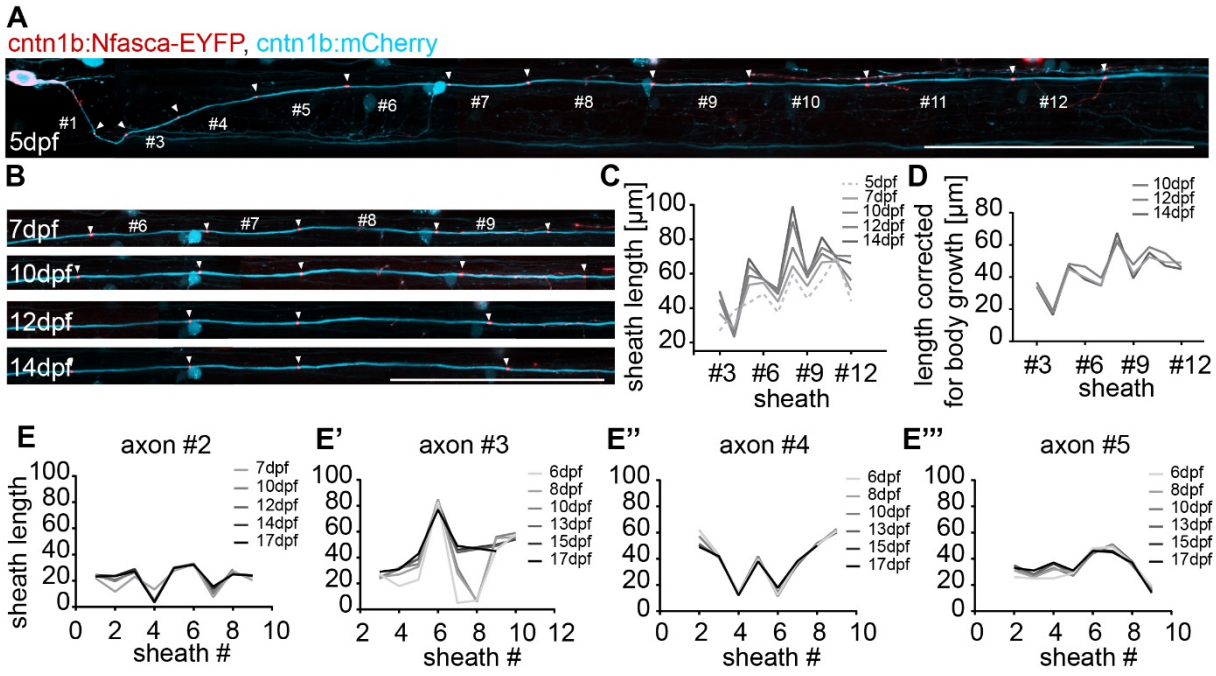

Figure 3.13 Timeline of axonal myelination patterns

(A,B) Confocal images of a neuron labelled with cntn1b:mCherry and cntn1b:Nfasca-EYFP. The white arrows point to the EYFP signal and therefore to the node position. **(A)** Confocal image of a labelled CoPA neuron, showing the first ~450µm of the axon at 5dpf. **(B)** Timeline of the same neuron from 7-14dpf showing a subset of sheaths. Images are aligned to the soma between sheaths #6 and #7. Sheath growth of single sheaths can be observed by the nodes moving. **(C)** Graph showing myelin sheath length plotted against sheath number. The neuron shows a very specific myelination pattern, that changes over time. **(D)** Graph showing sheath length corrected for body growth plotted versus sheath number. The pattern is stable over time. **(E-E''')** Myelination patterns from different neurons, corrected for body growth. The patterns are stable over time. **(E')** Sometimes sheaths retract, resulting in a temporarily disruption of the pattern. All axons analyzed had a unique myelination pattern. Scale bar 100µm. See also (Auer et al., 2018)

When I followed the axons over time, I observed that different neurons showed different myelination dynamics. Some axons got myelinated very fast, while others maintained long unmyelinated axon stretches. To investigate if these differences are specific for different neuronal types, I chose three different types that are easy to distinguish by their morphology and assessed their myelination dynamics. I investigated the myelination dynamics of two interneurons, Commissural Primary Ascending (CoPA) and Circumferential Descending (CiD), as well as the sensory Rohon-Beard (RB) neuron. CoPA neurons receive sensory input from RB cells (Gleason et al., 2003) and project to CiD neurons (Pietri et al., 2009). Their soma lies in the dorsal part of the spinal cord. CoPA axons cross the midline in the ventral spinal cord and project to the contralateral anterior spinal cord (Fig 3.14A). CiD neurons receive, besides input from CoPAs, also supraspinal input from Mauthner cells and they project to motor neurons (Ritter et al., 2001). The somata of these neurons are located between the ventral and dorsal spinal cord and their axon projects to the posterior spinal cord, with one bifurcation projecting to the anterior (Fig 3.14B). RB neurons are sensory neurons that sense touch and elicit, via CoPA and CiDs, an escape response (Ritter et al., 2001; Douglass et al., 2008). RB cells are located in the dorsal spinal cord (Fig 3.14C) and they are, during the course of development, replaced by Dorsal Root Ganglion (DRG) neurons (Williams et al., 2000) (Svoboda et al., 2001).

To assess the myelination dynamics of these three different neuronal types, I injected cntn1b:Nfasca-EYFP together with another cytoplasmic fluorescent protein under control of cntn1b promoter elements in a full transgenic mbp line (Tg(mbp:memCerulean)). I used the Nfasca-EYFP label and the myelin label as a double control for assessing myelinated parts of the axon. I screened the fish at 4dpf for expression of the two neuronal markers in the respective neurons. I imaged the neurons at 4,6 and 8dpf and measured the percentage of axon, in the field of view, that was covered with myelin.

I plotted the percentage of ensheathment versus the days post fertilization and found that CoPA neurons were all myelinated very fast. Already at 4dpf all of them were covered to at

least 50% with myelin, and by 8dpf almost all were fully covered with myelin (Fig 3.14 D). For the CiD neurons, I observed a very diverse pattern. At 4dpf almost all of them were covered by less than 50% with myelin. The individual neurons were myelinated at different rates, and at 8dpf most of them were covered between 50 and 85% with myelin (Fig 3.14 E). RB were never ensheathed by more than 10% with myelin. Often the sheaths that had formed were transient and retracted again (Fig 3.14 F). I also measured the diameter of the analyzed axons and found that at 8dpf CoPAs have a larger diameter then RB axons. CiD axons are more variable in their diameter (CoPA: 0.81 ± 0.06µm CiD: 0.69 ± 0.11µm RB: 0.64 ± 0.07, $p = 0.020$ Overall, I found that the axon diameter correlates with the amount of myelin formed along the axon ($r = 0.678$, $p = 0.0095$) (Fig 3.14 G).

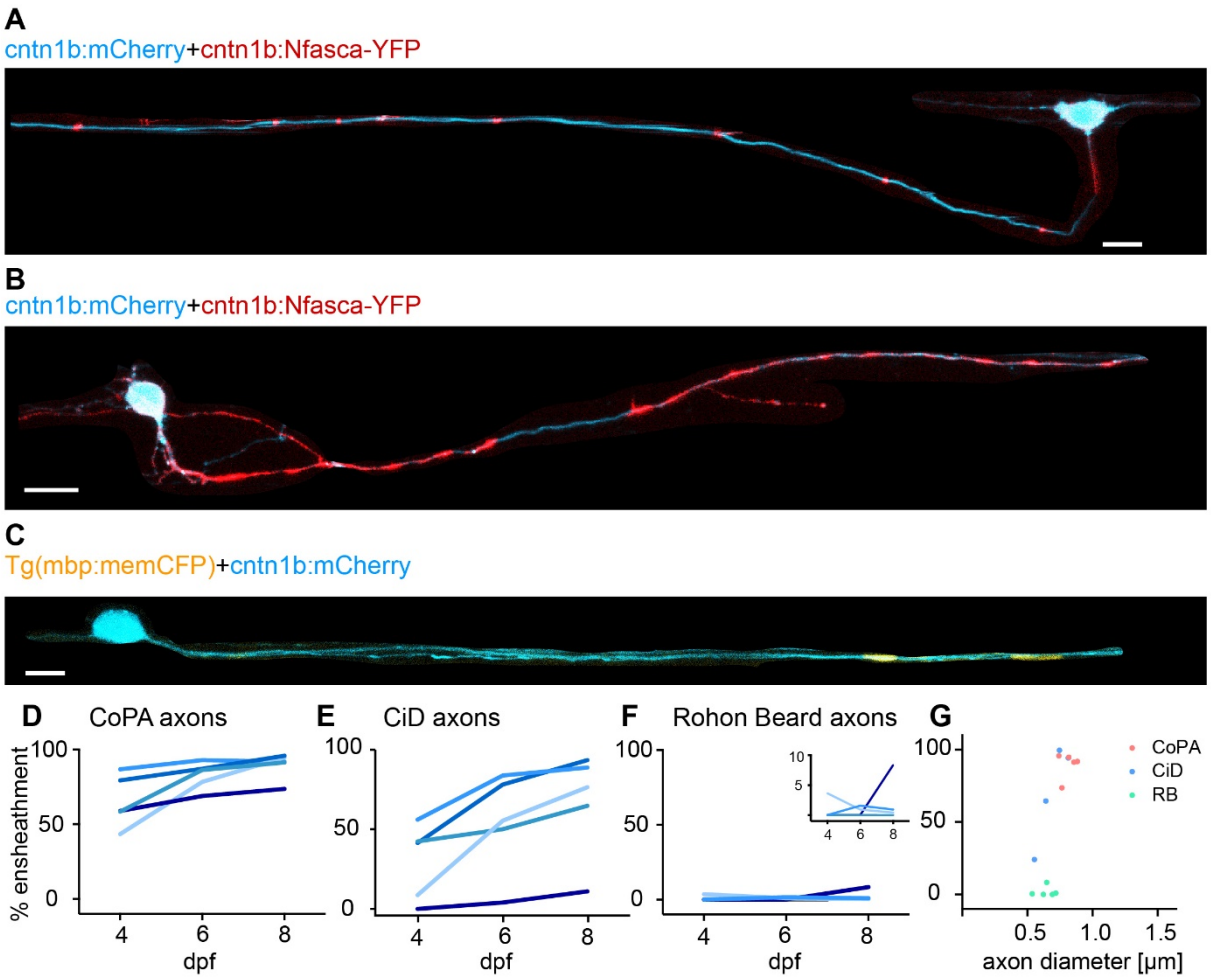

Figure 3.14 Myelination profiles of different neuronal types

(A-C) Cropped confocal images of different neuronal types in the zebrafish spinal cord **(A)** CoPA neuron with typical morphology **(B)** CiD neuron **(C)** Rohon-Beard neuron **(D-F)** Quantification of percent ensheathment at 4,6 and 8dpf. **(D)** CoPA axon analysis. CoPA axons show almost full myelination by 8dpf **(E)** CiD axon analysis. CiD axons are myelinated at different rates. Some are myelinated very fast, while others have only few ensheathments at 8dpf **(F)** RB axon analysis. RB axons had only few and short ensheathments that were often transient. **(G)** Correlation of ensheathment and axon diameter. There is a correlation between axon diameter and ensheathment. Scale bars 10µm

As mentioned before, activity is one regulator of myelination. To assess if the spontaneous activity correlates with the amount of ensheathment, I performed calcium imaging. I therefore used Tg(cntn1b:KaltA4) crossed with Tg(UAS:GCaMP6s) fish to obtain mosaic labeling of neurons labeled with GCaMP6s. To obtain z-stacks with a fast imaging rate I used a lightsheet microscope for the calcium imaging. As the anesthetic used for confocal imaging (Tricaine) blocks neuronal voltage gated sodium channels (Attili and Hughes, 2014), I paralyzed the fish for the calcium imaging with Mivacurium chloride, to prevent

movement artefacts without affecting neuronal signaling, and imaged at a frequency of 0.5Hz. For each fish I took two movies of each 10min with a 10min break in between. The fish were imaged between 4 and 5dpf.

I analyzed the somatic Calcium events for CoPA, CiD and RB neurons (Fig 3.15 A,B). I found that the amount of spontaneous Calcium transients greatly differed between the three different types. CoPAs were mostly silent (6/7) and the one cell that showed calcium events had only two transients during 20min of imaging. Almost all of the analyzed CiD neurons were active (5/6) and they had a highly variable number of Calcium transients (0-37 Ca^{2+} transients/20min). From the analyzed RB neurons, about half of them were active with the number of Ca^{2+} transients ranging between 0 and 15 per 20min (CoPA: 0.013 ± 0.035/min CiD: 1.017 ± 0.834/min RB: 0.124 ± 0.195/min, $p = 0.0049$). To assess if spontaneous activity influences the amount of ensheathment, I correlated the amount of Calcium transients with the % ensheathment measured in the above-mentioned experiment (Fig 3.15 C). There was no correlation detected ($r=-0.5$, $p>0.999$), as the most silent neurons (CoPA) were the ones with highest amount of ensheathment. The CiD neurons varied greatly in terms of activity and ensheathment, but as the data was obtained from independent experiments I could not assess if activity correlates with ensheathment for the CiD neurons.

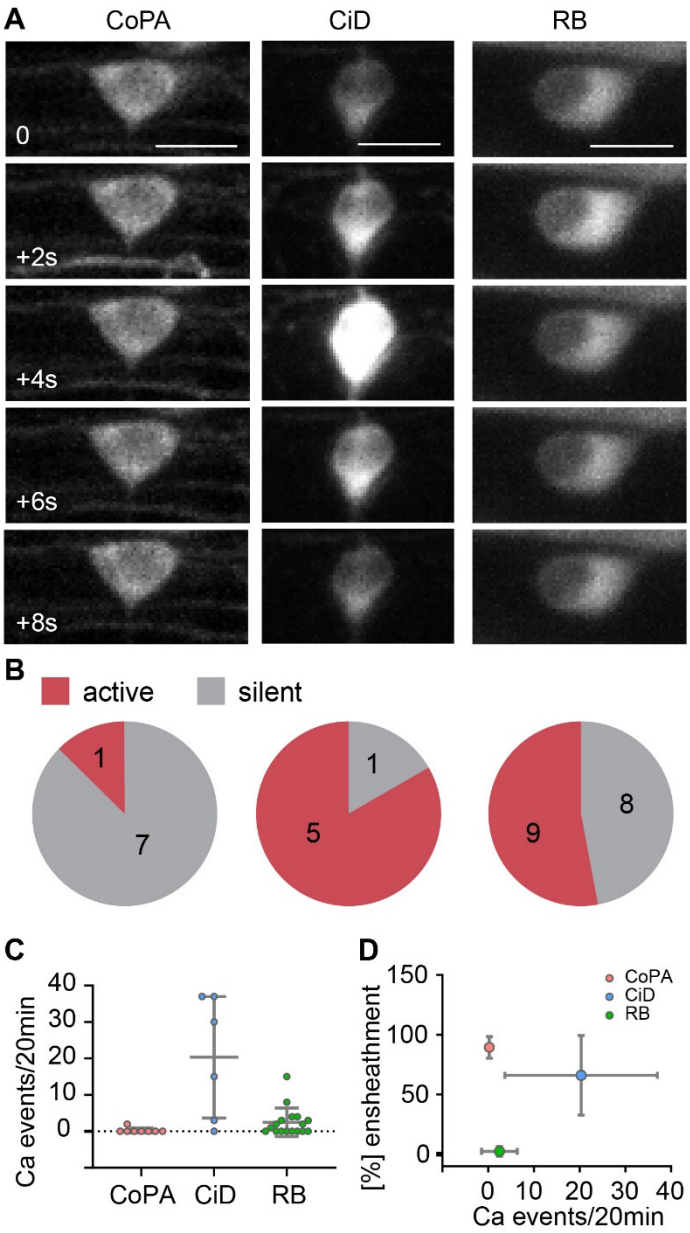

Figure 3.15 Analysis of calcium imaging in CoPA, CiD and RB neurons

(A) Examples images of GCaMP6s from CoPA, CiD and RB **(B)** Quantification of neurons with the number of cells active and silent **(C)** Quantification of calcium events per 20 min in the three neuronal types. CoPAs show almost no Ca^{2+} transients; CiDs show a high variability in terms of Ca^{2+} events; RBs also show some variability, but overall fewer compared to CiDs. **(D)** Correlation of ensheathment with activity. The amount of Ca^{2+} events does not correlate with the amount of ensheathment. Mean ± SD Scale bar 10µm

Together, I could show that there are different myelination patterns in the zebrafish spinal cord. Besides fully myelinated axons also partial myelination patterns exist and are maintained for more than a week. Myelination patterns and node of Ranvier positioning seem to be independent of the neuronal type, however regarding the amount of ensheathment there are parallels between neurons of the same type. The amount of ensheathment does not only depend on the neuron type but also correlates with the axon diameter. Spontaneous activity, on the other hand, did not show a correlation with the amount of ensheathment between different neuronal types.

3.2 Myelin sheath length plasticity following oligodendrocyte ablation

3.2.1 Remodeling of myelin sheath patterns

As mentioned before, evidence for remodeling of existing myelin sheaths is still lacking. To test if myelin sheaths, once they have reached their elongation phase, are still able to actively grow and remodel their length, I aimed to remove neighboring myelin segments, in order to expose permissive axon and investigate if sheaths can reinitiate sheath growth and will invade the demyelinated territory.

I established an ablation method with which I can precisely ablate single oligodendrocytes, which allows for the precise removal of its sheaths along the axons. To ablate single cells with high spatial and temporal precision, I expressed the photosensitizer KillerRed (Bulina et al., 2006; Teh et al., 2010) in oligodendrocytes. KillerRed is a red fluorescent protein that produces reactive oxygen species upon illumination with green light (540-580nm). I injected the newly synthesized construct mbp:KillerRed in Tg(mbp:EGFP-caax) fish to label single cells with KillerRed in a background were all myelin is labelled. I first tried to bleach the cells with green light (Teh et al., 2010), but the efficiency of cell ablation was very low so we decided to combine KillerRed expression with 2Photon laser bleaching. To ablate labeled cells, I targeted the 2Photon laser to the cell soma and scanned with a horizontal line through the center of the soma. The 2Photon laser, set to 770nm, bleached the cell for 500ms. The bleaching of KillerRed led to ROS production which eventually killed the cell and led to the fragmentation of the soma and the myelin sheaths (Fig 3.16A).

Using this method, I was able to ablate single oligodendrocytes without harming the surrounding cells. Only the targeted KillerRed labeled cells died and their myelin sheaths disintegrated, leaving demyelinated axon stretches behind. KillerRed negative cells are not affected and their myelin sheaths remain intact (Fig 3.16 B).

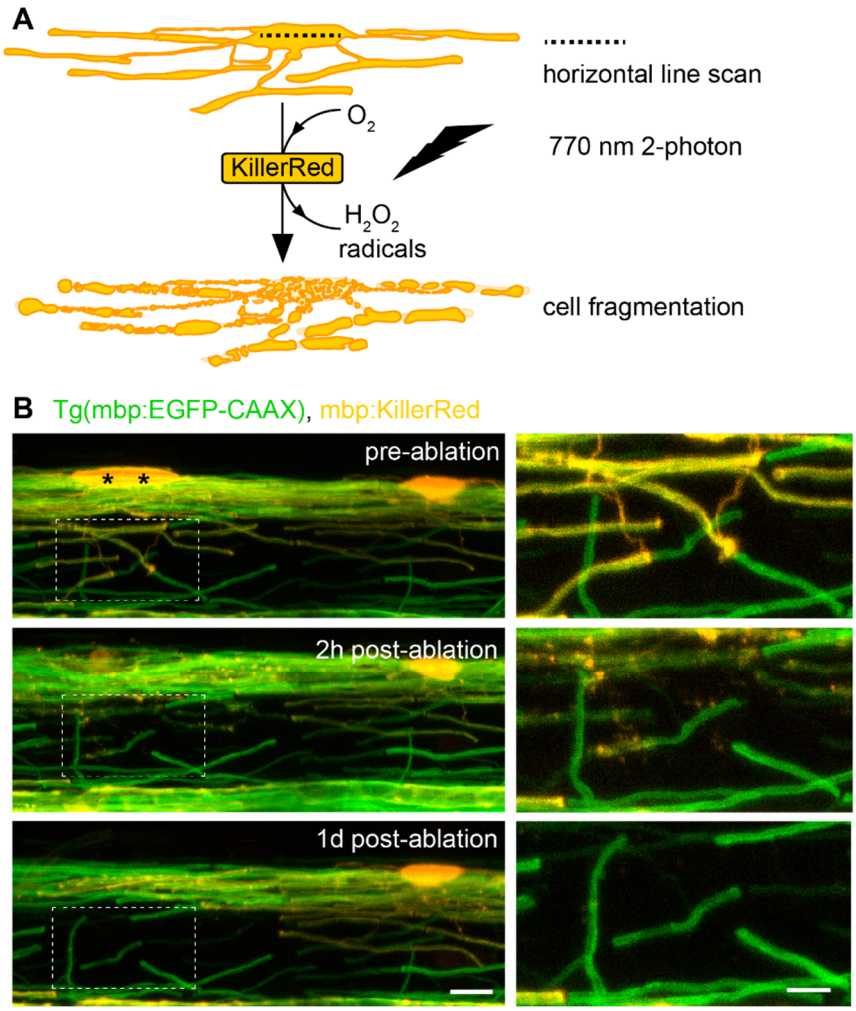

Figure 3.16 Oligodendrocyte ablation using KillerRed

(A) Schematic of the KillerRed ablation method. A horizontal scanning line is drawn through the oligodendrocyte soma. Upon bleaching KillerRed produced ROS that led to cell fragmentation **(B)**[1] Confocal images of a KillerRed mediated cell ablation. The images show two KillerRed labelled cells (yellow) in a transgenic line with all myelin labelled with EGFP (green) before, directly after and one day after the ablation. The asterisks label the two targeted cells. After the cells were bleached with the 2-Photon laser they fragment and by 1 day post ablation the myelin sheaths are removed. The surrounding segments remain unaffected. Scale bar 10µm. See also (Auer et al., 2018)

To test how dynamic myelin sheaths can be upon manipulation, I developed an experimental setup where I removed single sheaths along a fully myelinated axon and followed the demyelinated gap and the neighboring sheaths over time. Therefore, I injected mbp:KillerRed in Tg(mbp:EGFP-caax) fish and screened the fish to find single KillerRed

[1] Images were taken by my colleague Stavros Vagionitis

positive cells that formed a myelin sheath between two KillerRed negative sheaths (Fig 3.17A).

I will discuss the series of events with a specific example in detail, which is illustrated in Figure 3.17. I started the imaging at 4dpf. As I did not know when the sheaths were initiated I followed them until 8dpf to ensure that they were in their elongation phase, when their growth behavior is predictable. At 8dpf I performed the cell ablation of the KillerRed labeled oligodendrocyte and its sheaths and then followed the demyelinated gap for several days after the ablation. I observed that the neighboring sheath invaded the demyelinated territory and that a new myelin sheath was formed. The new myelin sheath was growing longer even though it already had reached the neighboring sheaths resulting in a pushing back of the adjacent sheaths. At the end of the imaging, the new myelin sheath had grown to a similar length as the ablated sheath, restoring the pre-ablation myelination pattern (Fig 3.17B). For better analysis of the growth dynamics of the neighboring sheaths I plotted the growth curve of the left neighboring sheath #1 – I only analyzed the dynamics of #1 in this case as the other neighboring sheath #3 was only born at the day of the ablation and hence not in the predictive growth phase (Fig 3.17 C gray line). As sheath #1 was born before 4dpf I knew that it was in its elongation phase and therefore in its predictive phase. It showed its normal slow growth behavior typical for the elongation phase but upon ablation of sheath #2 it changed its behavior and showed a rapid increase in length. After this short rapid increase in length it slowed down again and even shrunk a bit. I compared the measured growth curve with the predicted growth curve and saw that upon ablation it clearly deviates from the predicted length but later it approaches again similar values (Fig 3.17 C dotted line). As the newly formed sheath seemed to grow longer than normal and also pushed back the neighboring sheath I also analyzed its dynamics compared to the prediction. I plotted the prediction for the ablated sheath (Fig 3.17 D orange curves) as well as the growth curve and the respective prediction for the new myelin sheath (Fig 3.17 D gray lines). For the new myelin sheath, to be in the predictive elongation phase, I calculated the prediction from 4dpi onwards. The growth curves supported what I could observe with the confocal images: the

newly formed sheath grows for longer and does not seem to reach its elongation phase. It reaches a length similar to the prediction of the ablated sheath.

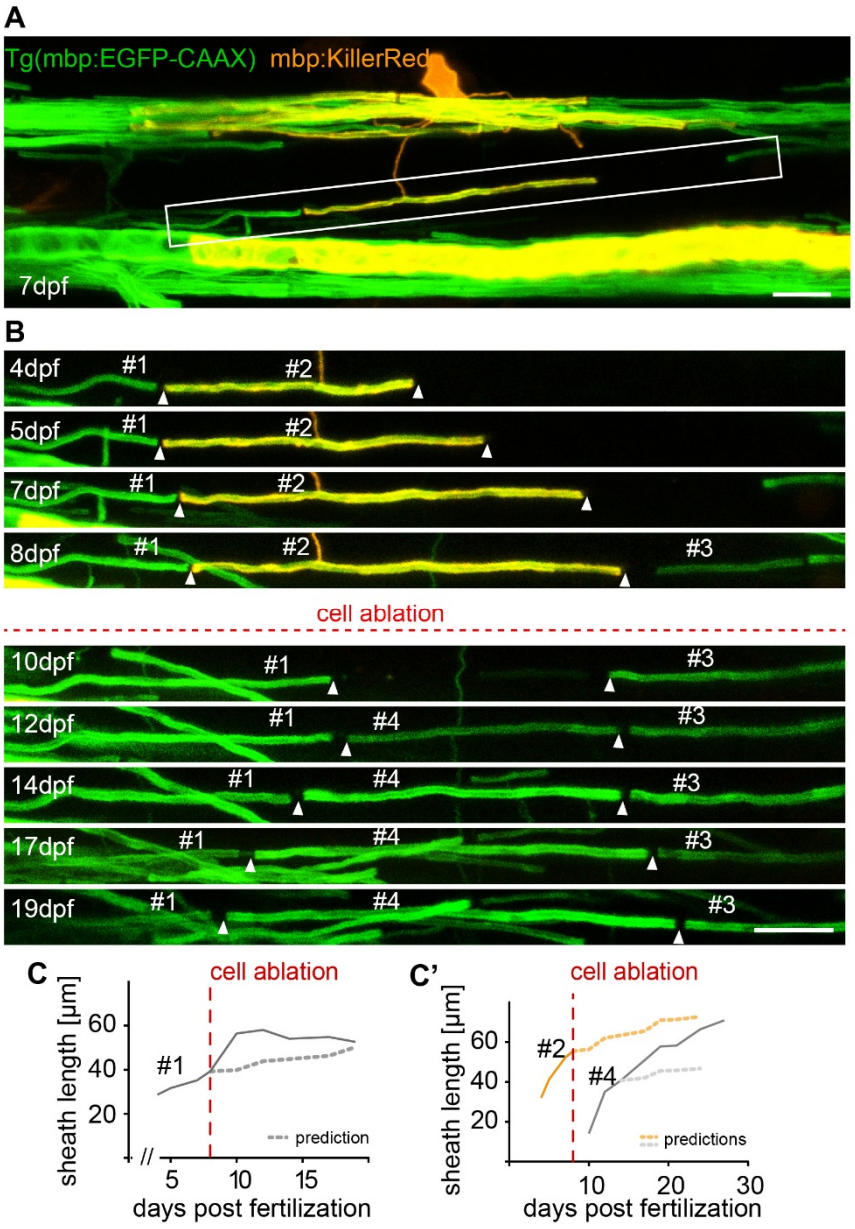

Figure 3.17 Remodeling after sheath ablation

(A,B) Confocal images of a full transgenic Tg(mbp:EGFP-caax) line injected with mbp:KillerRed **(A)** Overview of a KillerRed labelled oligodendrocyte in the zebrafish spinal cord at 7dpf. **(B)** Close up of the white box and timeline of the myelin sheath. The imaging started at 4dpf. At 8dpf the KillerRed labelled oligodendrocyte was ablated and its myelin sheaths disappeared leaving an unmyelinated gap at 10dpf. At 12dpf a new sheath was formed in the gap and the axon was fully remyelinated. The newly formed sheath did not stop growing although it had reached the neighboring sheaths. The neighboring sheaths shrink and at 19dpf the myelination pattern looks similar to the pattern before ablation. **(C)** Growth curve of the neighboring sheath #1 (gray line) together with the predicted growth curve (dotted gray line). After the ablation the measured sheath length deviates from the predicted length, but a few days later the measured and predicted lengths approach similar values **(D)** Growth curve of the ablated sheath (orange) and the remyelinating sheath (gray) together with their respective predictions (dotted lines). The new sheath deviates from its prediction, it is growing longer and thereby reaching a length similar to the prediction of the ablated sheath. Scale bar 10µm. See also (Auer et al., 2018)

To better analyze the deviating dynamics of the neighboring segments, I calculated their deviation from the respective predicted value and plotted it versus the days post ablation (Fig. 3.18). To visualize how significant the deviations are, I also calculated the difference of the measured value and the predicted value for myelin sheaths without ablation during the same days. I used the 8th day post fertilization as a reference day and calculated the 95% confidence interval (CI) of the deviations. In the beginning the interval is very small indicating a good prediction, later is becomes wider indicating less precise predictions. I plotted the deviations from the different ablation cases together with the 95% CI. One can see that directly after the ablation the predictions and the measured value clearly deviate from each other (in the case of 4/5 sheaths). The neighboring sheaths grow at faster rates than predicted (4.5 ± 3.0 versus 0.6 ± 0.5 mm/day at 1–3 days post ablation (dpa), p = 0.04, n = 5/4 sheaths/animals). This was only a very short-term effect, as 3 days later the sheaths slowed down again and some even shrunk. For some sheaths, when I was able to follow them for long enough, I could even observe them reaching lengths similar to what would be predicted.

As mature oligodendrocytes do not produce new myelin sheaths, a new oligodendrocyte precursor cell needs to differentiate to remyelinate the demyelinated axons (Czopka et al., 2013). The new myelin segments only reach their predictive behavior after 4 days of growth, hence, I could only analyze the growth from 4dpi onwards. I observed that the sheaths were also growing at faster rates than predicted. They prolonged their active growth phase and reached the elongation phase later (2.3 ± 0.9 versus 0.6 ± 0.1 µm/day growth from 4 to 5 dpi for up to 15 days, p = 0.04, n = 4/3 sheaths/animals).

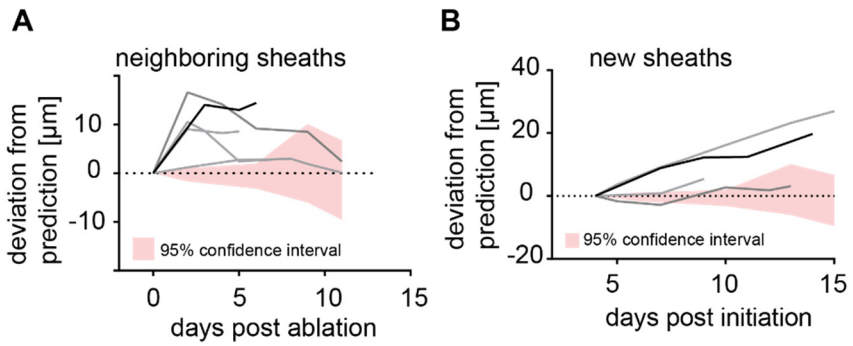

Figure 3.18 Quantification of the deviations from the predictions

(A) Quantification of the deviation of neighboring sheaths from their predicted dynamics. 4/5 sheaths substantially deviate from their predictions after the ablation. In the first 5 days post ablation all sheaths are longer than the predictions and outside of the 95% confidence interval (pink area). A few days after the ablation the sheaths shrink again and reach their predicted values **(B)** Quantification of the deviation of the remyelinating sheaths from their predicted dynamics. 3/4 sheaths grow longer than predicted and their lengths are outside of the 95% confidence interval (pink area). See also (Auer et al., 2018)

There was a typical series of events I could observe after cell ablations. In the first 1-2 days after the ablation the neighboring sheaths reinitiated fast sheath growth and invaded the demyelinated territory. I was able to observe this behavior in 13/17 cases. In the remaining four cases the neighboring sheaths did not invade the demyelinated territory (Fig 3.19A). 2-4 days post ablation I observed that a new myelin sheath was formed to remyelinate the demyelinated gap. A new oligodendrocyte precursor cell had differentiated to form a myelin sheath in the demyelinated area. In the remaining three cases I could not observe a new sheath being formed, as the neighbors grew so fast that they had already remyelinated the gap before a new sheath could be formed (Fig 3.19 B). From 5 days post ablation onwards I could observe, in 80% of the cases, a pushing back of the neighboring sheaths by the newly formed myelin sheaths. In 6 out of the 8 cases the newly formed sheath pushed back neighbors that had grown in to the demyelinated gap, in the remaining 2 cases the new myelin sheath pushed neighbors back that had not invaded the demyelinated territory. In some cases, I could even observe a reestablishment of the pre-ablation pattern after the neighbors had grown into the gap and the newly formed sheath pushed them back again.

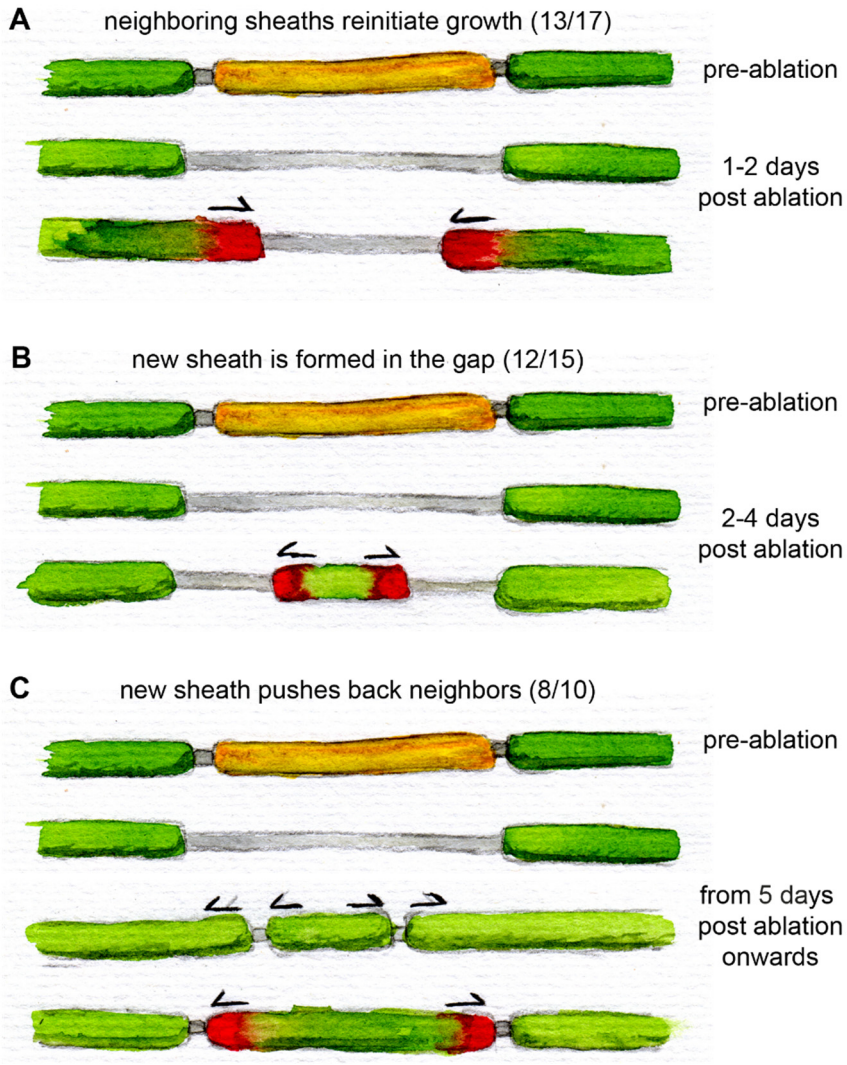

Figure 3.19 Summary of the remodeling events

(A) Schematic of the events in the first 1-2days post ablation. The ablated sheath is removed and leaves an unmyelinated gap. Following that the neighboring sheaths reinitiate fast growth and invade the demyelinated territory (red parts of the sheath show active growth)**. (B)** Schematic of the events 2-4 days post ablation. Following the removal of the ablated sheath, a new sheath is formed and remyelinates the demyelinated axon stretch. **(C)** Schematic of the events from 5 days post ablation onwards. After the invasion of the neighboring myelin segments and the formation of a new myelin sheath, the new sheath continues to grow and pushes the neighbors back.

Together, I was able to show that, upon manipulation, the normally very predictive and stable myelin sheaths are able to remodel and deviate from their predicted pattern of growth. In some cases, I could even observe a reestablishment of the pre-ablation pattern indicating homeostatic myelin sheath length regulation.

3.2.2 Restoration of partial myelination patterns

As I could observe a reestablishment of the pre-ablation pattern, I wondered if there is something like a ‘memory’ of where the sheaths had been.

To test if there is something on the axon marking the territory where a myelin sheath has been, I performed oligodendrocyte ablation to demyelinate only partially myelinated axons. Due to the partial myelination, the newly formed sheath would have large stretches of an in general permissive axon to remyelinate it. To do this, I injected an axon marker, cntn1b:EGFP, into Tg(mbp:tagRFP-t-caax), Tg(mbp:KillerRed) lines. I used the combinations of these lines to facilitate ablation of an oligodendrocyte that forms sheaths on a partially myelinated axon. I used the KillerRed line together with the mbp:tagRFPt-caax line to have a membrane tagged fluorescent protein, which helps visualizing the myelin sheaths.

I performed the ablation of the oligodendrocytes with the same technique as mentioned before. Upon ablation, the oligodendrocytes died leaving a demyelinated axon behind. A few days later, a new oligodendrocyte differentiated and new myelin sheaths were formed on the demyelinated axon. By aligning the images to landmarks, like the somata of neighboring neurons, I found that the new sheaths were formed at similar positions to where the ablated sheaths had been. For the analysis of the partially myelinated axons and their de- and remyelination I reconstructed the axon and the sheaths formed on it, using the Imaris software, as the labeling was often too dense to follow the axon with its sheaths. In some cases, I found additional myelin sheaths formed indicating that the axon was slowly getting myelinated (Fig 3.20B).

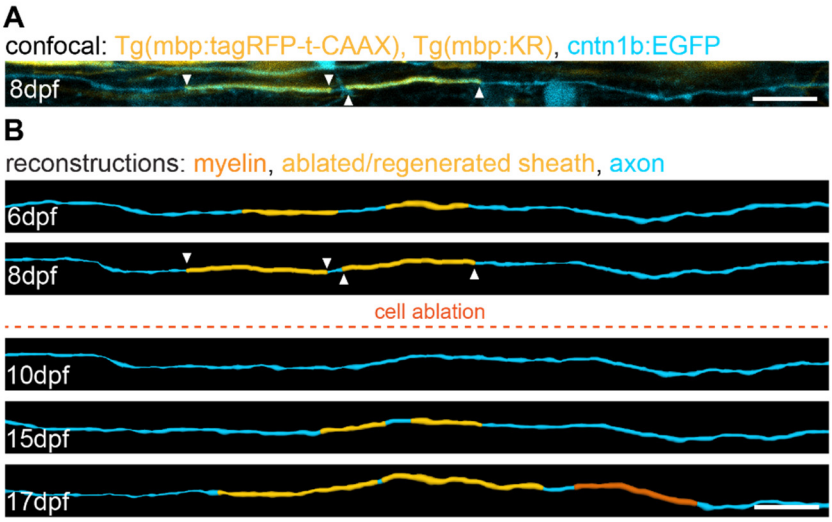

Figure 3.20 Partial myelination patterns are restored upon ablation

(A) Confocal image of a partially myelinated axon at 8dpf. The white arrows point to the beginning and end, respectively, of the two myelin sheaths **(B)** Reconstructions of the axon from (A) with the timeline from 6dpf to 17dpf. Cell ablation was performed at 8dpf. Upon cell ablation the axon is demyelinated. At 15dpf two new sheaths are formed at similar positions to where the ablated sheaths were. At 17dpf the sheaths had reached lengths similar to the ablated sheaths. A third new sheath was formed (darker orange). Scale bar 10µm. See also (Auer et al., 2018)

To quantify if the position of the newly formed sheath is indeed at the position where the old sheath was I measured the length of the axon stretch between two clearly distinguishable landmarks, like collaterals or somata of other neurons and calculated the relative position of the sheath before ablation. To avoid influences of the fish growth I used landmarks, like somata of other neurons or axon collaterals, to determine the sheath position on the axon. To precisely determine the sheath position, independent of sheath length, I always used the position of the center of the sheath.

When the new sheath was formed I did the same measurements using the same landmarks for the respective neurons. In order to obtain the difference in sheath position I calculated the difference of the relative positions before and after ablation. To compare the relative changes in sheath positioning, I measured the relative positions of myelin sheaths without ablation with the same time difference between the two measurements.

I found that there was no difference in the changes of sheath position between control myelin sheaths and between the ablation and remyelination group (-2.8% ± 1.6% deviation,

n = 5/4 sheaths/axons versus -1.2% ± 1.4% n = 4/2 sheaths/axons in control, p = 0.15, Fig. 3.21A). I also quantified the length of the ablated and the newly formed sheath. To exclude the influence of fish growth, I corrected the sheath length for body growth. The average sheath length before ablation was 18.5 ± 5.3 µm and after remyelination, corrected for body growth, it was 18.3 ± 5.4 (p = 0.96, n = 4/3 sheaths/animals, Fig. 3.21 B)

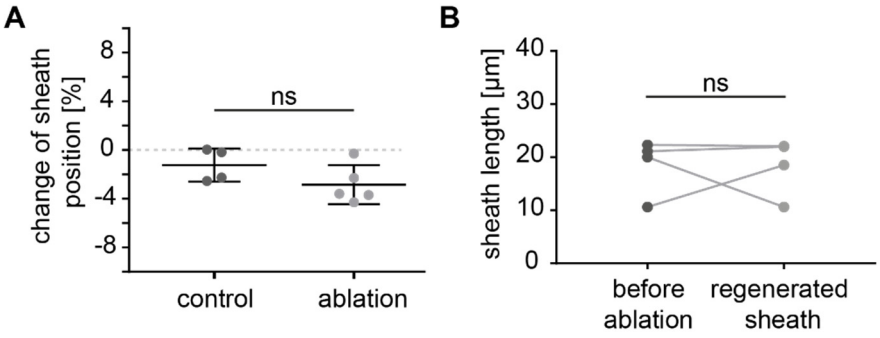

Figure 3.19 Quantification of the remyelination of partially myelinated axons

(A) Quantification of the relative change in position of control sheaths and sheaths before and after ablation. No difference could be detected in the sheath positioning between control and ablation. **(B)** Quantification of the length of myelin sheaths before and after ablation. The regenerated myelin sheaths were corrected for body growth to exclude differences due to fish growth between de- and remyelination. There was no difference in sheath length before and after ablation. See also (Auer et al., 2018)

Together, I could show that myelin sheaths exhibit very stereotypic growth dynamics, with a fast sheath growth in the first 3 days that determines length differences and a slow elongation phase that compensates for body growth. These growth dynamics are independent of neighboring myelin sheaths and timepoint of sheath initiation. Upon manipulation, like ablation of neighboring myelin segments, sheaths can deviate from their predictive growth and remodel their length. Furthermore, myelination patterns along fully, as well as along partially myelinated axons, are regularly restored upon sheath removal, indicating axonal regulation of node of Ranvier positioning.

3.3 Axonal mechanisms influencing node of Ranvier position

Node of Ranvier positioning is an important factor influencing conduction speed, however, how the positioning is regulated is not known yet. My previous results indicate axonal influences on node of Ranvier positioning and myelination patterns, as I regularly observed reestablishment of myelination patterns along axons. I therefore aimed to further investigate how axonal mechanisms might influence node of Ranvier positioning.

3.3.1 Asymmetric lateral sheath growth

During the imaging, I often observed that the feeding process of the myelin sheaths - the point of sheath growth initiation (Snaidero and Simons, 2014) - was not located in the center of the sheath, therefore indicating asymmetric lateral extension (Fig 3.22 A, white box). In some of the sheaths that I had followed over time, I observed asymmetric growth as well. The sheaths seemed to stop growing into one direction while they were still growing into the other (Fig 3.22B). To quantify the amount of asymmetrically grown myelin segments I analyzed the relative process position of myelin sheaths. To exclude asymmetric growth due to neighboring sheaths, I included only myelin sheaths without any neighboring myelin segments. I measured sheaths in full transgenic mbp lines to ensure that the sheaths, indeed, had no neighboring sheaths. I measured the feeding process position with regard to the sheath length. I calculated the relative process position with -1 and 1 being at the end of the sheath while 0 marks the middle of the sheath (Fig 3.22 C), and plotted the relative process position versus the myelin sheath length. I defined sheaths to be symmetric, when their process position did not deviate from the center by more than 5% in each direction. About 80% of all sheaths I measured had their process outside of this 10% region around the respective center of the sheath (34/42 in 16 animals) and were therefore counted as asymmetrically grown. I could not detect any bias towards the sheath length, as long and short sheaths were equally asymmetric ($r = 0.01$ $p = 0.942$) (Fig 3.22D).

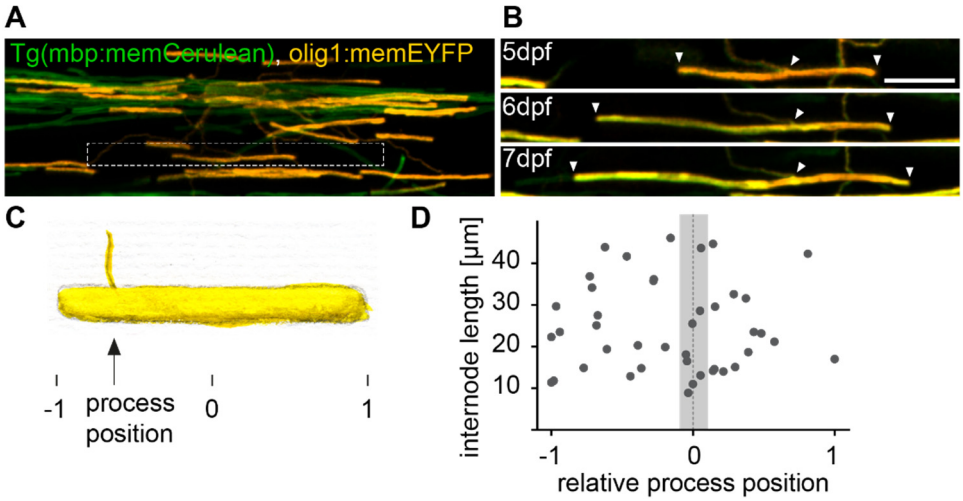

Figure 3.22 Asymmetric lateral sheath growth

(A) Confocal image of a myelinating oligodendrocyte (yellow) in a full transgenic mbp line (green). The white box shows an asymmetrically grown myelin sheath. **(B)** Confocal images of the timeline of the asymmetrically grown sheath. At 5dpf it is still symmetric from then on it grows more to the left than to the right, ending up with an asymmetrically positioned feeding process. The white arrows point to the ends of the sheath and to the feeding process. **(C)** Scheme of how the relative process position was analyzed. The myelin sheath length was set to be from -1 to 1 with 0 being the center of the sheath **(D)** Quantification of the relative process position. Most of the processes are outside of a 10% area (gray area) around the center of the sheath. Scale bar 10µm. See also (Auer et al., 2018)

In the previous experiment I only analyzed myelin segments without neighbors, to exclude them acting as physical barriers, but other potential physical barriers exist. Some axons have collateral sprouts that could act as growth barriers. To see if they can account for the asymmetric growth, I assessed the frequency of axon collaterals at nodes of Ranvier. To count the number of nodes that had formed due to a collateral, I injected the cntn1b:Nfasca-EYFP construct together with an axon label, cntn1b:mCherry. Next I screened the fish for fully myelinated neurons expressing both markers. I counted the number of nodes that had formed at the position of a collateral and the number of nodes that had formed without a collateral (Fig 3.23 A). I found that only about a quarter of nodes had formed at positions of collaterals (28.5% n=45/158 nodes on 15 axons, Fig. 3.23 B). I never observed a collateral on a fully myelinated axon without a node indicating that collaterals are one axonal determinant of node position (0/12 nodes, n = 6/6 axons/animals).

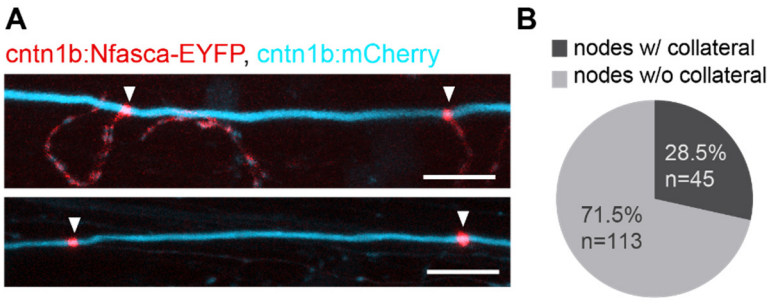

Figure 3.23 axon collaterals determine node position

(A) Confocal images of mCherry (cyan) labeled neurons co-expressing Nfasca-EYFP (red). The arrows point to the nodes. The upper image shows nodes that are at the position of axon collaterals, the lower image shows nodes without axon collaterals. **(B)** Quantification of nodes with and without collaterals. The majority of nodes does not form at positions of collaterals. Scale bar 10µm. See also (Auer et al., 2018)

As only about a quarter of all nodes analyzed had axon collaterals, they cannot alone account for the high number (80%) of the observed asymmetric sheath growth. I could show that axon collaterals are indeed one axonal determinant of node position, but there must be another growth barrier to explain the high number of asymmetrically grown sheaths.

3.3.2 Pre-myelination clustering of the nodal protein Neurofascin

The fact that myelin sheaths stop growing and show asymmetric growth even without the presence of neighboring sheaths or other physical growth barriers raised the question if axonal signals could act as molecular growth barriers.

As previously mentioned, I observed very different myelination patterns along different types of neurons. When I imaged the neurons while there were still unmyelinated stretches present, I often observed that Nfasca-EYFP was not homogeneously expressed along the unmyelinated parts of the axon. Nfasca-EYFP accumulated and formed clusters along unmyelinated axons. It has been shown in vitro that certain nodal proteins like voltage-gated sodium channels and AnkyrinG can form functional clusters in unmyelinated axons, if treated with oligodendrocyte conditioned medium (Freeman et al., 2015). I investigated if Nfasca-EYFP also shows different localization along neuronal types with different myelination dynamics.

Therefore, I co-labelled the respective neuronal types with Nfasca-EYFP and mCherry in full transgenic mbp lines. I imaged the neurons from 3dpf onwards, as most of the neurons are not fully myelinated by that age, and there are still unmyelinated stretches. I followed the neurons for up to 7dpf to assess Nfasca-EYFP localization before and after the axons got myelinated.

Along CoPAs as well as CiDs I observed that Nfasca formed clusters with higher signal intensities, but there was always a faint Nfasca signal detectable between clusters, when the axons remained unmyelinated. When myelin sheaths were formed Nfasca was fully excluded from the ensheathed axon segment (arrows, Fig 24 A).

Along RB axons I also found some ensheathments, but here, unlike the other neurons, the Nfasca-EYFP signal was still localized underneath the myelin segment (Fig 3.24 B). Whenever I found ensheathments on Nfasca-EYFP labelled RB neurons, the Nfasca signal was never excluded from the myelinated parts. Another difference compared to CoPAs and

CiDs was that along RB axons Nfasca did not form clusters, it was rather homogeneously distributed.

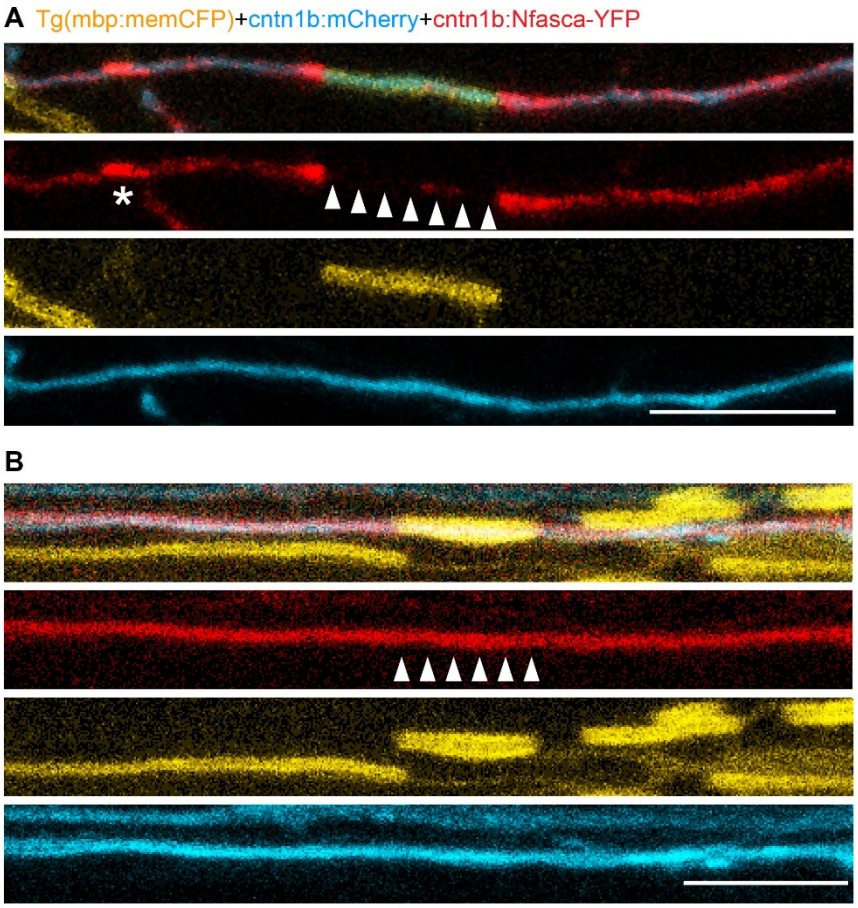

Figure 3.24 Nfasca localization differs along different neuronal types

(A) Confocal images of a CiD with an ensheathment, Nfasca is excluded from underneath the myelin sheath (arrows). Along the unmyelinated parts it shows clustering (asterisk) **(B)** Confocal images of a RB neuron with an ensheathment, Nfasca is not excluded from underneath the myelin segment (arrows) nor does it form clusters at the unmyelinated parts.

To better investigate the clustering dynamics of Nfasca, I used the same experimental setup as described above, co-labeling of neurons with Nfasca-EYFP and another fluorescent protein in full transgenic mbp lines, and took high resolution images of unmyelinated axons and partially myelinated axons (Fig 3.25A). To exclude that the clusters are due to axonal swellings, I compared the relative fluorescence of Nfasca-EYFP with the localization of the cytoplasmic fluorescent protein. I plotted the relative fluorescence intensity of both to assess the homogeneity of expression.

For CoPA and CiD axons, axons that regularly get myelinated, I found that while the cytoplasmic fluorescent protein was expressed homogeneously, Nfasca-EYFP showed areas with high fluorescence and parts with very low amounts of fluorescent protein (Fig 3.25B). At myelinated segments (Fig 3.25 A, yellow bars) there was no Nfasca-EYFP signal. There was no correlation between the two different protein localizations, excluding accumulation due to physical constraints like swellings. In RB axons Nfasca showed, as well as the cytoplasmic labeling, a homogeneous expression along the length of the axon (Fig 3.25 C,D).

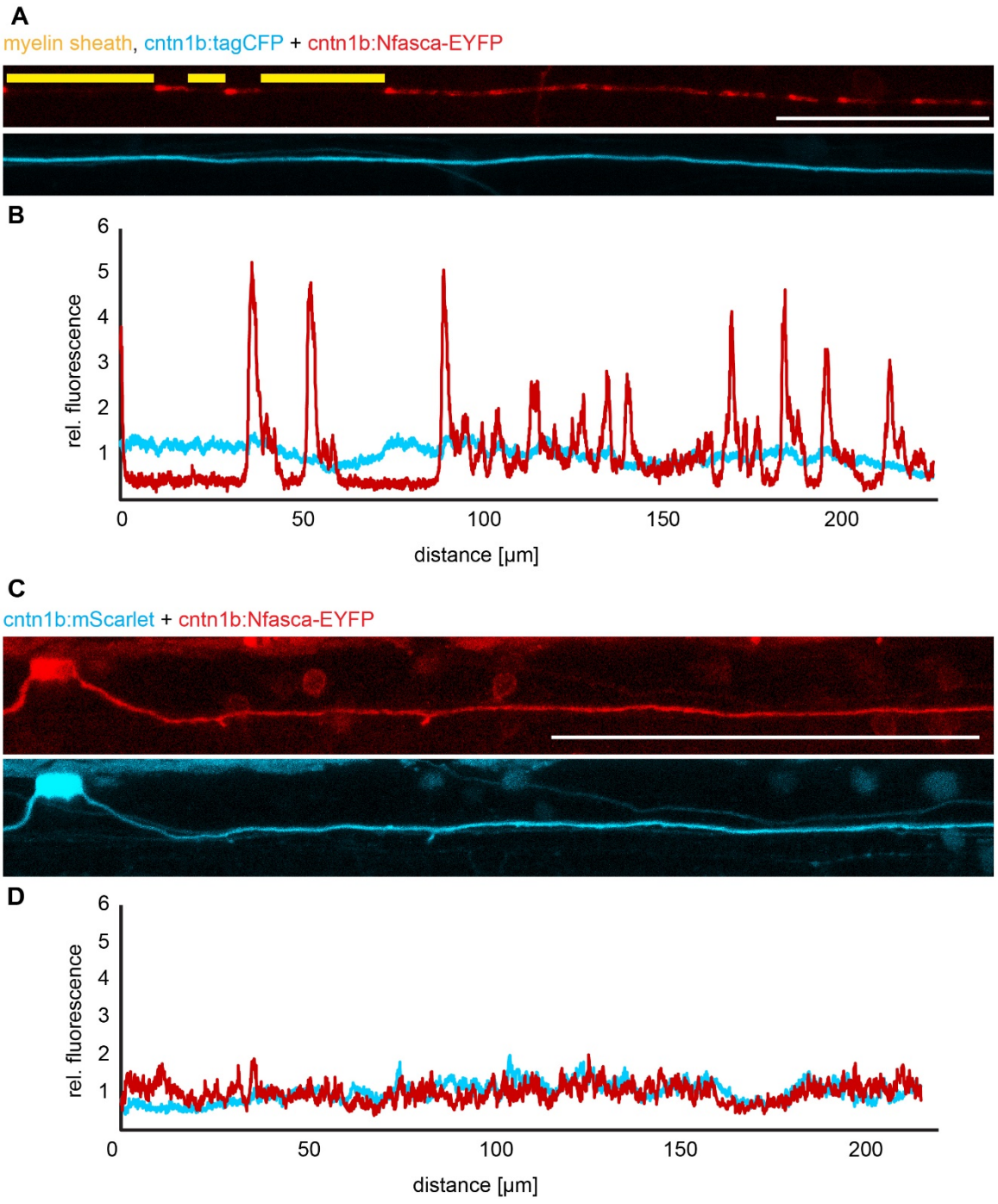

Figure 3.25 Neurofascin clusters along some but not all unmyelinated axons

(A) Confocal images of a partially unmyelinated CoPA axon labelled with Nfasca-EYFP and tagCFP. The Nfasca signal shows clustering while the tagCFP signal is distributed homogeneously. The yellow bars indicate where myelin sheaths are formed **(B)** Graph showing the relative fluorescent intensity of Nfasca-EYFP and tagCFP along the axon from (A). Nfasca-EYFP shows a very inhomogeneous distribution while tagCFP is distributed homogeneously **(C)** Confocal image of an unmyelinated RB axon labelled with Nfasca-EYFP and mScarlet. Both markers show homogeneous distribution **(D)** Graph showing the relative fluorescent intensity along the axon. Nfasca-EYFP does not show any clustering.

I wondered if these clusters are involved in nodal positioning and if they are stable over time in an unmylinated axon, and could therefore resemble prenodes, which have been described earlier (Kaplan et al., 1997; Freeman et al., 2015).

To assess the stability of Nfasca-EYFP clusters, I followed unmyelinated axons, labelled with Nfasca-EYFP and tagCFP, over time. I started the imaging at 3dpf. Often there were no clusters detectable at these early timepoints (Fig 3.26 3dpf) but at 4dpf Nfasca-EYFP clusters started to form. In the beginning they were just slightly brighter than the surrounding but with time they became more pronounced. To assess stability, I aligned the images of the different timepoints. I found that the clusters were remarkably stable over time in neurons that remained unmyelinated. Most of the clusters stayed at the same position (moving only due to body growth), and only few clusters appeared or disappeared during the imaging (asterisk Fig 3.26).

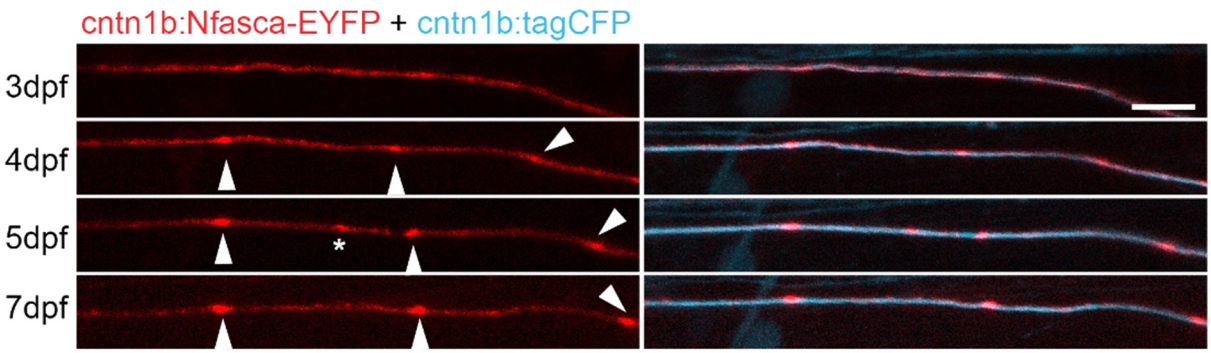

Figure 3.26 Nfasca clusters are stable over time

Confocal images of an unmyelinated axon stretch over time from 3 to 7dpf. The left images show the Nfasca-EYFP channel, the right images the merged images of Nfasca-EYFP (red) with the axon label tagCFP (cyan). The Nfasca-EYFP clusters are formed around 4dpf. Most of the clusters are stable (arrows) and only few clusters appear or disappear (asterisk).

I found that Nfasca-EYFP shows different dynamics along different neuronal types. Along axons that are usually substantially myelinated, like CoPAs and CiDs, Nfasca-EYFP shows clustering along unmyelinated parts and it is excluded from myelinated parts of the axon. On the other hand, in RB axons that are normally unmyelinated or show only rare, short ensheathments, Nfasca-EYFP does not show a clustering behavior, nor is it excluded form myelinated parts.

3.3.3 Correlation of Neurofascin clusters and node position

The fact that myelin sheaths stop growing even in the absence of neighboring sheaths and the presence of Nfasca-EYFP clusters raised the question if Nfasca could act as a molecular growth barrier. Another finding supporting the hypothesis of Nfasca acting as a growth barrier, and therefore node position determinant, is that I only found clusters in neurons that are regularly getting myelinated to a significant proportion. To investigate if sheaths stop growing when they reach a Nfasca cluster, I co-labelled axons with Nfasca-EYFP and another cytoplasmic marker in full transgenic mbp lines. I used the second cytoplasmic axon label to ensure that I analyzed the clusters on one axon and that the myelin sheaths are formed on the respective axon. I started imaging at 3dpf, an age where most of the axons are not yet fully ensheathed and continued it until the axons were myelinated. I analyzed the cluster – node correlation retrospectively. Therefore, I assessed the position of the node in the fully myelinated axon and tested if there was a Nfasca cluster at the same position before the neuron was myelinated (Fig 3.27). For the analysis of the cluster and node position I defined three different cases. I analyzed if there was a pre-myelination cluster at the node position, if there was a heminode or if there was no sign of a cluster prior to myelination. The heminode was put in a separate category as there is already an ensheathment on one side, but the sheath that formed the heminode had stopped growing here. To assess if node position and cluster are at the same place, I analyzed the images pre and post myelination, and measured if they are at the same position. As fish grow during that time, I aligned the images at landmarks to exclude false results due to body growth of the fish. I found that for the majority (75%) of the analyzed nodes there was either a cluster or a heminode at the same place. Only in 25% percent there was no indication of a cluster (Fig 3.27).

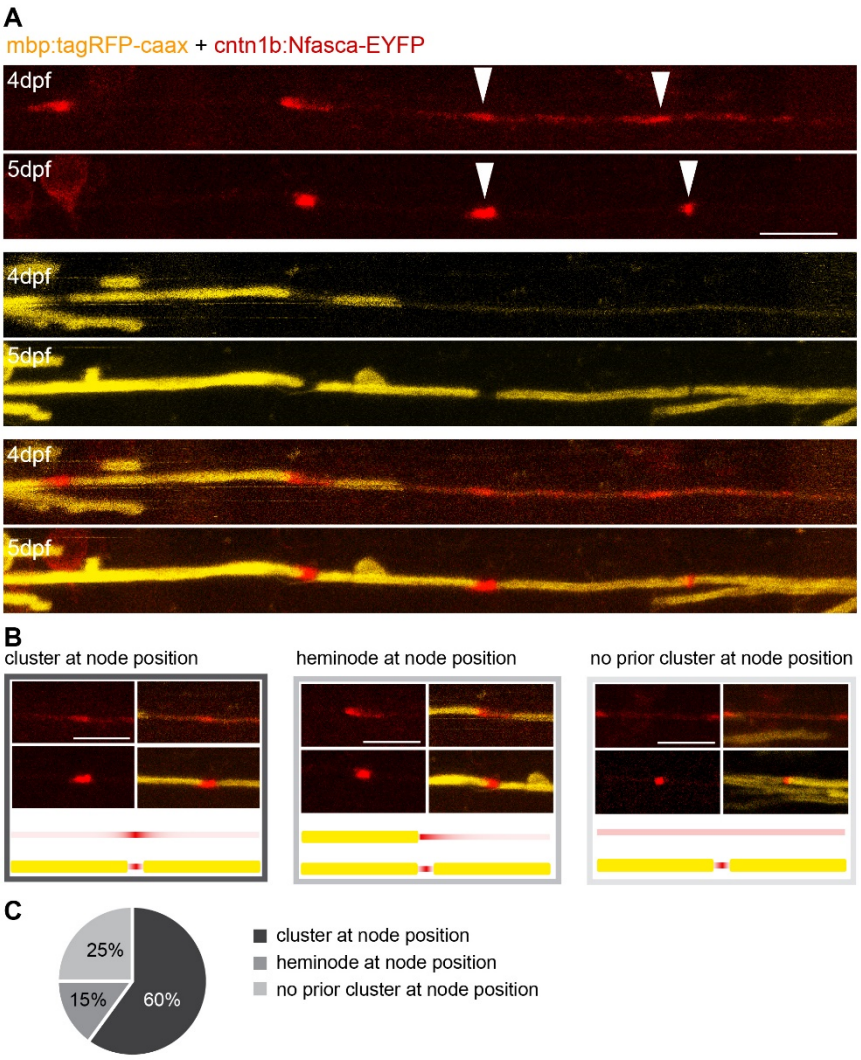

Figure 3.27 Quantification of Neurofascin cluster and node position

(A) Confocal images of a partially myelinated neuron that is getting myelinated. The Nfasca clusters that are present at 4dpf (white arrows) are at the same position as the nodes at 5dpf (white arrows) when the neuron is fully myelinated **(B)** Confocal images and graphical representation of the three different analysis categories. Either there was a cluster at the node position, there was a heminode at the node position of there was no prior clustering at the node position. **(C)** Quantification of the node position. The majority of nodes showed pre-myelination clustering of Nfasca-EYFP or a heminode at node positon.

When I assessed the cluster – node correlation, I often imaged neurons that did not have clusters at 3dpf and at the next day they were fully myelinated. Many axons were myelinated very quickly before clusters could emerge which could be due to the Nfasca clustering and myelination happen simultaneously. To disentangle these two processes and to prolong the time for clusters to be formed I aimed to delay myelination. In another set of experiments, I aimed to prevent myelination to investigate if clusters also form in the absence of myelination.

To ablate the OPCs and therefore prevent myelination, I used a Nitroreductase (NTR) mediated cell ablation. Here, NTR reduces the non-toxic prodrug Metronidazole (MTZ) into a DNA cross-linking reagent. NTR is expressed in the cells of interest and MTZ is bath applied to the fish. Only the cells expressing NTR are ablated while the surrounding tissue remains unaffected (Curado et al., 2007).

I used a transgenic line where NTR fused to tagCFP is expressed in OPCs (Tg(olig1:tagCFP-NTR)) to visually confirm the expression of NTR in the cells. I started the treatment around 2.5dpf, as the first oligodendrocyte precursor cells appear around 48hpf and the first myelin at 60hpf (Brösamle and Halpern, 2002).

First, I wanted to quantify the reduction of oligodendrocytes with the NTR mediated OPC ablation. Therefore, I crossed mbp:nlsEGFP fish with olig1:tagCFP-NTR fish to count the number of oligodendrocytes, when OPCs are ablated, during development (Fig 3.28 A). I incubated the fish for 24h either with 10mM MTZ in 0.2%DMSO or, the control fish, only with 0.2%DMSO in Danieau´s buffer. After the incubation I imaged the fish between 3 and 9dpf and counted the number of oligodendrocytes in both groups. Similar to the oligodendrocyte numbers during development, I imaged the fish around somite 17 but here I performed longitudinal studies and imaged the same fish at different ages (Fig 3.28 B).

At 3dpf there was no difference in cell number between ablated and control fish, but for the following timepoints, the oligodendrocyte number in the ablated fish only slightly increased until 6dpf. After that no more cells were added. In the control fish, new cells were constantly added, as shown before (cells added from 6-9dpf: 4.3 ± 0.7 vs. 0.2 ± 0.4, $p = 0.0286$ n=4 animals). Upon OPC ablation, myelination seems to stop around 6dpf with no new oligodendrocytes being generated. The myelination is not fully prevented, but there is a significant reduction in oligodendrocytes, at least until 9dpf in the ablated fish (cell number at 9dpf 23.5 ± 2.3 vs. 11.1 ± 1.5, $p = 0.0286$ n=4 animals) (Fig 3.28 C).

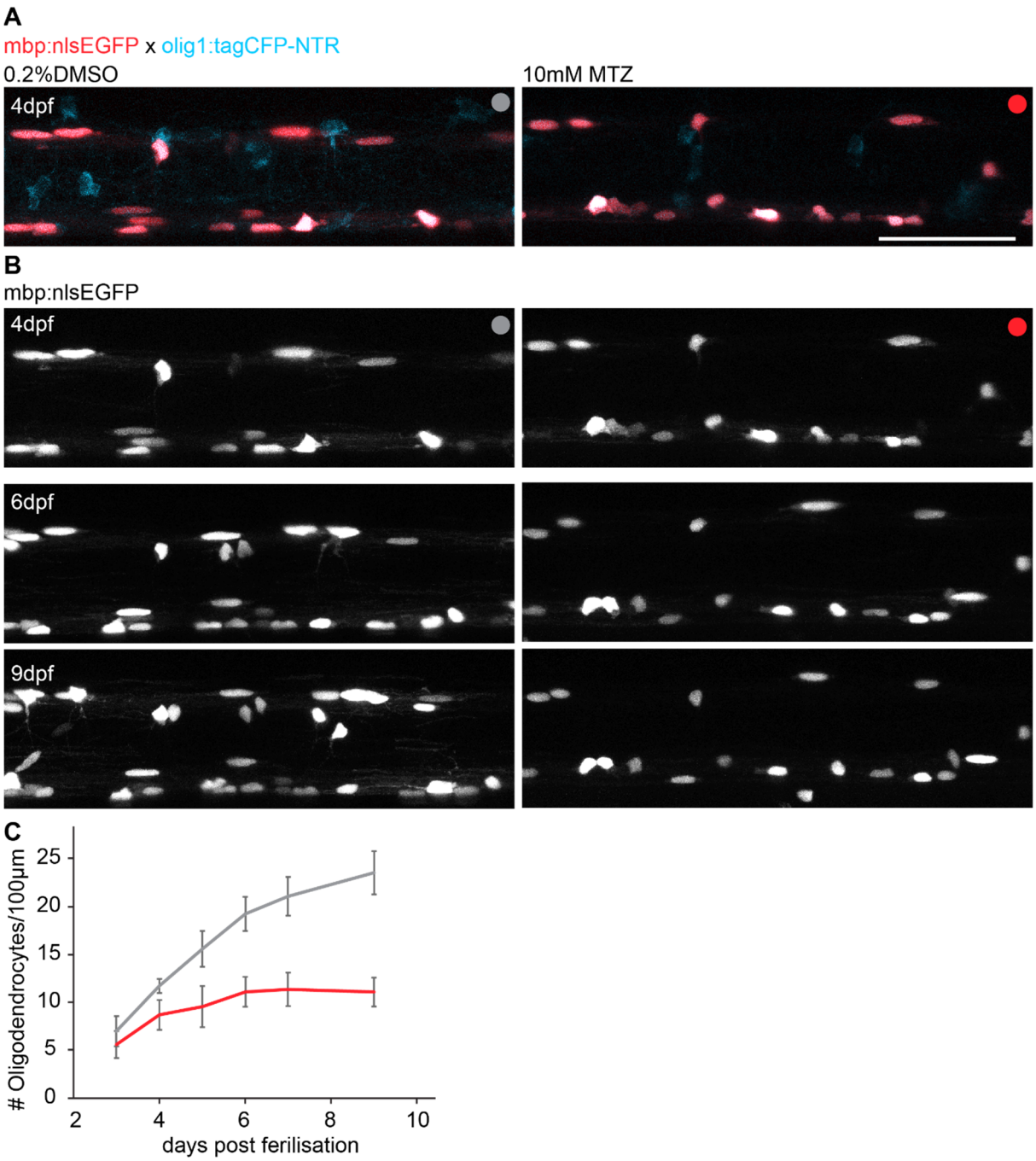

Fig 3.28 NTR mediated ablation of OPCs reduces the number of oligodendrocytes

(A) Confocal image of mbp:nlsEGFP (red) x olig1:tagCFP-NTR(cyan) control and MTZ treated animals at 4dpf **(B)** Confocal images of mbp:nlsEGFP from control and MTZ treated animals at 4,6 and 9dpf **(C)** Quantification of oligodendrocyte number per 100µm spinal cord. There is a reduction of EGFP labelled oligodendrocytes in the MTZ treated animals.

For the second manipulation, I did not ablate OPCs but aimed to inhibit their differentiation.

It has been shown before that treating zebrafish with the HDAC inhibitor Trichostatin A

(TSA) drastically reduces the number of oligodendrocytes in the spinal cord (Takada and Appel, 2010; Early et al., 2018).

As I wanted to delay myelination by a few days, I first titrated the optimum concentration to reduce the number of oligodendrocytes without impacting the development of the fish. I tried different concentrations between 5 and 100nM and assed the health appearance of the fish. Up to 10nM the fish looked overall healthy and all of them had inflated the swim bladder by 5dpf. The fish treated with 20nM still appeared healthy but only around 50% inflated their swim bladder. I chose to use 15nM TSA to increase the effect of the myelination delay without impacting the health of the fish too much. Again, I first quantified the severity of the myelination delay. Therefore, I treated mbp:nlsEGFP fish with 15nM TSA in 0.2% DMSO for 24-26h starting around 2.5dpf. The control fish were incubated with 0.2% DMSO. I imaged the same fish from both groups at 3,4 and 6dpf around somite 17 and counted the nlsEGFP labelled cells in the spinal cord (Fig 3.29A).

I found that there is overall just a slight, not significant, reduction in oligodendrocyte number between the control and the TSA treated groups (cell numbers at 6dpf: 22.2 ± 3.7 versus 20.1 ± 2.1, $p = 0.292$) (Fig 3.29B). When looking at the cell number of single fish, it appeared quite variable, some fish responded to the treatment with a substantial reduction of oligodendrocytes, while others had cell numbers similar to controls.

I also observed in these experiments, that the nlsEGFP signal of the cells in the TSA treated animals was dimmer than in the controls. I needed 3-4x the laser power of the controls to get similarly bright images in the TSA treated animals (Fig 3.29A).

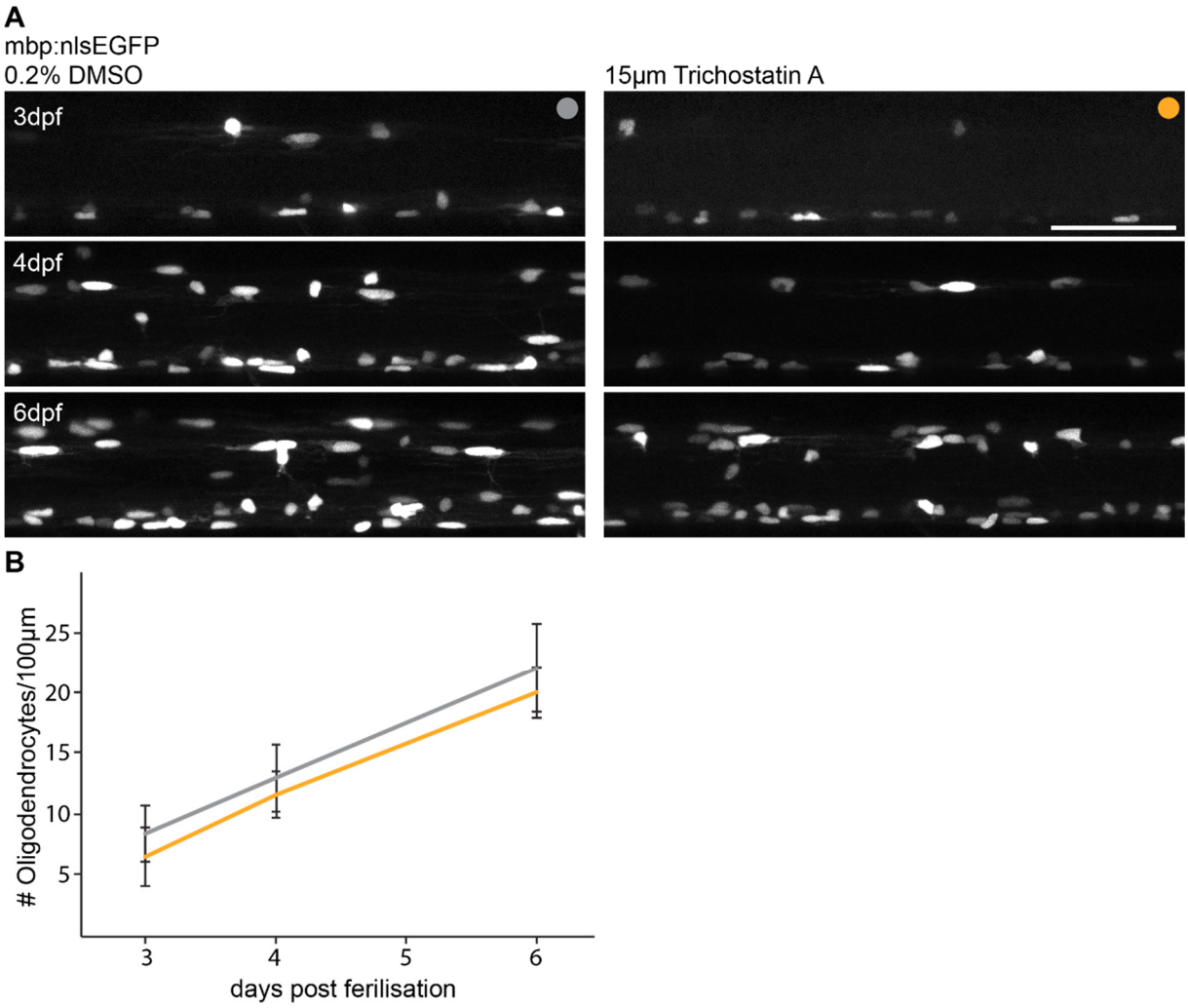

Fig 3.29 Inhibiting OPC differentiation with TSA only slightly reduces the number of oligodendrocytes

(A) Confocal images of mbp:nlsEGFP fish treated either with 0.2% DMSO (control group) or with 15nM TSA in 0.2%DMSO. The cells in the TSA treated animals appear dimmer than in the control animals **(B)** Quantification of the oligodendrocyte number in control and treated animals. There is a slight reduction in oligodendrocyte number in the TSA treated animals compared to the control, but this reduction is not significant.

Although I could not fully prevent the formation of myelin, I used both of the above described methods, to prolong the time in which the imaged axons are unmyelinated. To analyze the cluster-correlation with the NTR mediated cell ablation I crossed Tg(mbp:tagRFPt-caax) fish with Tg(olig1:tagCFP-NTR) fish and injected cntn1b:Nfasca-EYFP as well as cntn1b:tagCFP. Although the same fluorescent protein was used to label OPCs and axons, they were distinguishable by their morphology. The fish were then treated with MTZ as described above.

Although the overall delay in myelination was not significant with the TSA treatment, I also used this method, as in some fish it substantially decreased the number of oligodendrocytes. Here I injected the same constructs, cntn1b:Nfasca-EYFP and cntn1b:tagCFP, in Tg(mbp:tagRFPt-caax) fish. I started the treatment around 2.5dpf with 15nM TSA.

For both treatments I screened the fish at 3dpf for Nfasca-EYFP and tagCFP positive neurons. The neurons were then imaged from 3dpf onwards, until the axon was myelinated. I assessed the cluster-node correlation, for each delay method separately, as explained before. I found that, also with a delay or reduction of myelination, the majority of nodes were formed at positions where either a Nfasca cluster or a Nfasca heminode had been before myelination (Fig 3.30).

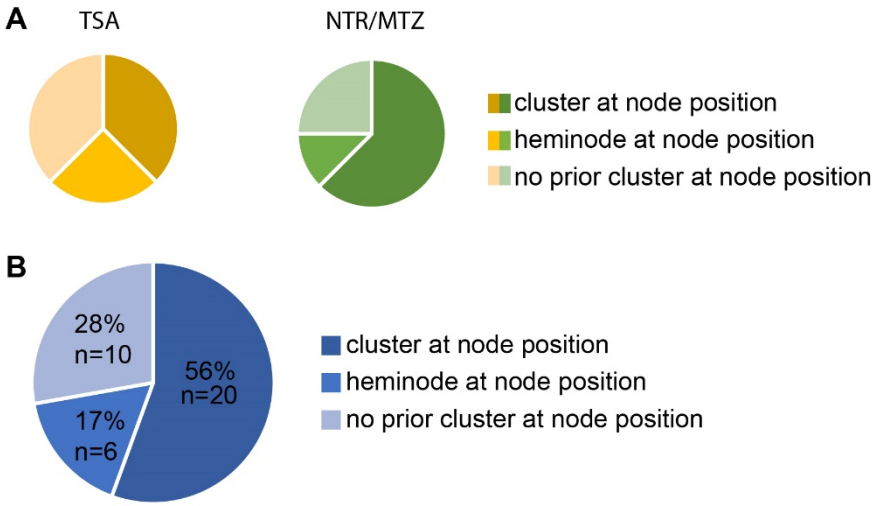

Fig 3.30 Quantification of cluster-node correlation with and without myelination delay

(A) Quantification of the cluster-node correlation with pharmacological treatments to delay myelination (TSA, NTR/MTZ). With both of the methods, to delay or reduce myelination, the majority of nodes analyzed had a Nfasca cluster or Nfasca heminode at the same position **(B)** Quantification of all nodes, with and without delay of myelination. The majority of nodes had pre-myelination Nfasca clusters or heminodes.

Together, I could show that pre-myelination Nfasca cluster position and post-myelination node of Ranvier position highly correlate. Even in fish with pharmacologically induced reduction or delay of myelination, this correlation persists.

3.3.4 Optogenetic manipulation of myelin sheath length

By correlating Nfasca cluster position with node of Ranvier position, I was able to show that cluster position seems to be predictive for node position. As these clusters can also form already days before the axon stretch gets myelinated they seem to be intrinsically regulated by the axon. It has been shown in culture, that prenodes can be functional in terms of AP propagation (Freeman et al., 2015). It could therefore be, that axon intrinsic properties like activity regulate the positioning of prenodes or Nfasca clusters. If activity is indeed a regulator of cluster position, manipulating activity may induce changes in node position.

To test this hypothesis, I designed an experimental setup in which I can hyper activate single neurons and follow the node positioning. For this experiment I chose to use CoPA neurons, for two reasons: they all show fast myelination dynamics and are relatively quickly fully myelinated and they are spontaneously very silent, which should maximize possible effects due to hyper activation.

To test if the ChR2 stimulation works in my setup, I tested my settings with embedded fish and expressed GCaMP6s to measure Calcium transient. Therefore, I crossed Tg(cntn1b:KaltA4) fish with Tg(UAS:GCaMP6s) fish and injected UAS:ChR2-mCherry. I then screened for expression of ChR2-mCherry in CoPAs or nearby RB neurons, and CoPAs expressing GCaMP6s (Fig 3.31 A).

The fish was embedded in a glass bottom dish, and the LED was mounted in the lid. I took time-lapse movies of GCaMP6s during light stimulation. To see if there are Calcium responses upon light stimulation I subtracted the background, as the light from the LED was detectable in the GCamp channel, and normalized the curve (Fig 3.31 B).

I could detect Calcium rises in response to ChR2 activation, confirming that my setup can be used for the planned experiment.

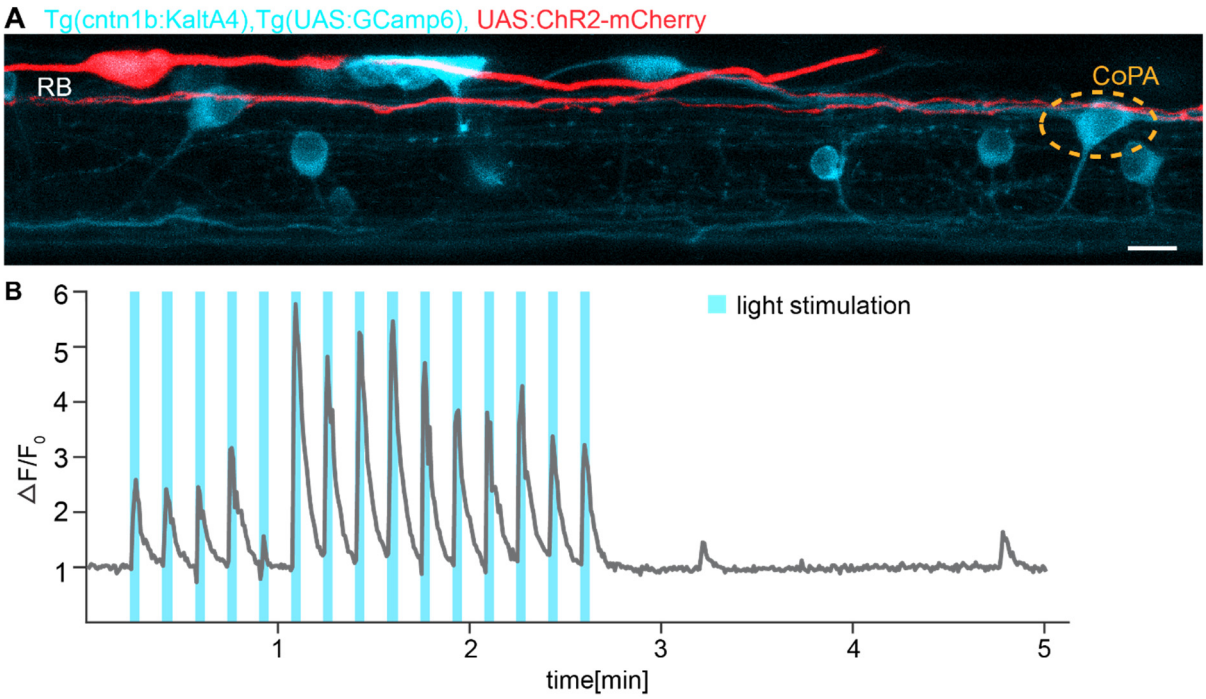

Figure 3.31 Calcium increases in response to optogenetic stimulation

(A) Confocal image of a ChR2+ RB neuron and a GCaMP6s+ CoPA **(B)** Calcium trace of the CoPA labelled in (A) during and after optogenetic stimulation. Stimulating the RB cell with blue light elicits a Ca^{2+} response in the CoPA neuron

To test if stimulating and therefore hyper activating the neuron can induce sheath remodeling I developed a long-term stimulation setup.

I used Tg(cntn1b:KaltA4) fish injected with UAS:ChR2-mCherry, cntn1b:tagCFP and cntn1b:Nfasca-EYFP. I screened the fish for co-expression of all these markers in CoPA neurons. In case I found a CoPA co-expressing Nfasca-EYFP and tagCFP and a nearby RB expressing ChR2-mCherry I included these cells as well. I started the imaging at 4dpf and followed the axons until 8dpf to know which sheaths have reached their elongation phase and are therefore in their predictable growth phase. At 8 and 9dpf the fish were stimulated with the optogenetic stimulation protocol. During the stimulation, the fish were freely swimming and kept in a small well, to secure equal illumination, with the LED mounted into the lid. As it was shown that low frequency stimulation like 1Hz and 8Hz has effects on myelination (Piscopo et al., 2018) I chose to use 4Hz as a stimulation frequency. To minimize the stress for the fish due to the bright blue light, the stimulation was on for 15s in

15min intervals, for 6h per day. I continued to image the axon until 14dpf. For control experiments I used fish that did not express ChR2-Cherry and treated them in the same way. I then analyzed the sheath length with the Nfasca marker, to assess if node position does remodel. To better visualize the effects, I calculated the deviations from the predicted growth of each sheath.

I found that sheaths do remodel upon light stimulation as I saw deviations from their predicted growth pattern. I will explain the example #1 in more detail (Fig 3.32 A,A'). Fig. 3.32 A shows the confocal images of the node marker and the axon marker at timepoints before and after stimulation. The images are aligned to the node in the middle to easily see the remodeling sheath/node on the left (#6) and the regular growing one on the right (#7). Sheath #6 shows shortening after the stimulation and a rapid elongation in the following days. Sheath #7 does not show remodeling induced by optogenetic light stimulation.

The graphs in A' and B summarize the dynamics of myelin sheaths along axons that express ChR2, the graph in C shows the myelin sheath dynamics in a ChR2- fish during and after light stimulation. I saw similar remodeling effects in the control animals, likely due to the stimulation with bright blue light. When treating the animals, I could observe that during the treatment the fish show increased swimming behavior, which also resembles increased activity in the neurons. It was not possible to disentangle the ChR2 mediated effects from the bright light stimulation effects. Future experiments with ChrimsonR, another light sensitive channel that is activated by red light, and also more light sensitive (Klapoetke et al., 2014), should circumvent that problem and minimize the side effect caused by the light stimulation.

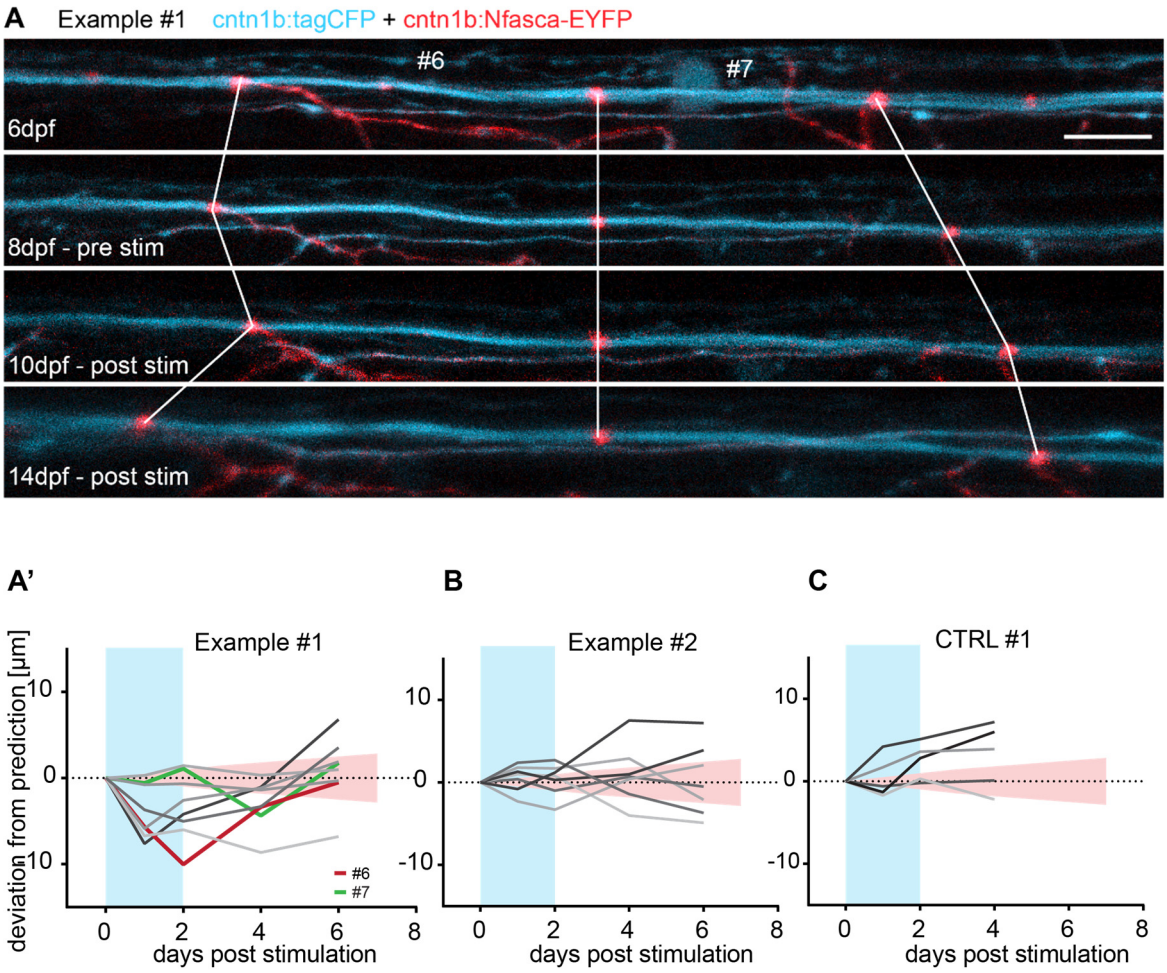

Figure 3.32 Activity induced remodeling of myelin sheath length

(A) Confocal images of a Nfasca-EYFP and tagCFP labeled axon at different timepoints before and after the stimulation. The ChR2-mCherry channel is not shown. Two sheaths, #6 and #7, are shown. While #6 shows remodeling upon optogenetic stimulation, #7 shows normal growth. **(A'-C)** Quantification of sheath length deviations from predicted values**. (A')** Quantification of the axon shown in (A). **(B)** Quantification of another experiment showing smaller effects than the example #1 **(C)** Quantification of a control fish. Also in the control fish, deviations from the predictions could be observed.

Together, I could show that myelin sheaths often show asymmetric growth which cannot be explained by physical barriers like neighboring sheaths or axon collaterals, indicating molecular growth barriers. Indeed, when I correlated pre-myelination Nfasca cluster position with node of Ranvier position I found that the majority of nodes is formed at a position where a cluster had been formed prior to myelination. Furthermore, I collected evidence suggesting that node positioning can remodel upon manipulation of neuronal activity, although I could detect similar effects in the control, ChR2 negative, fish, which could be explained by additional off-target effects caused by the blue light stimulation.

4 DISCUSSION

The aim of my thesis was to investigate mechanisms underlying myelin sheath length regulation and remodeling. I aimed to investigate how myelin sheath length is established during development and how different myelination patterns are formed. I tested for myelin sheath plasticity as this is a prerequisite for activity dependent remodeling. Furthermore, I investigated pre myelination clustering along axons and how this contributes to node of Ranvier positioning.

Some studies, performed in mouse, reported white matter changes or differences in myelination upon manipulations like monocular deprivation or social isolation (Liu et al., 2012; Makinodan et al., 2012; Etxeberria et al., 2016). However, they could not show if existing myelin can actively remodel to adapt to changes in activity. Here, I took advantage of the zebrafish as a model where high temporal resolution imaging can be achieved. Furthermore, I could show how, during development, different myelin sheath lengths and axonal myelination patterns are established and maintained. By a single cell ablation paradigm, I could show, for the first time, that established myelin sheaths can plastically remodel upon partial demyelination.

4.1 Developmental myelin sheath growth

To study how myelin sheath length is regulated, I approached the question from two different perspectives, from the oligodendrocyte point of view and from an axonal point of view.

Myelin sheath length is an important regulator of conduction speed and therefore also nervous system function. By adapting myelin sheath length, conduction velocity can be modulated and precisely timed (Seidl, 2014; Ford et al., 2015). How myelin sheath length is regulated is not fully understood yet, however factors influencing sheath length have been identified, e.g. axon diameter (Murray and Blakemore, 1980; Ibrahim et al., 1995) or regional

differences (Bechler et al., 2015). It has been shown, that single oligodendrocytes can form sheaths of variable length (Murtie et al., 2007; Almeida et al., 2011) and thickness (Hildebrand et al., 1993). I analyzed sheath lengths formed by single oligodendrocytes as well, and also determined the length spread of myelin sheaths formed. The sheaths formed by single cells can span the entire range of lengths measured (Murtie et al., 2007; Almeida et al., 2011). As one cell can form sheaths of all observable lengths, this raises the question, how an oligodendrocyte achieves to establish sheaths of different lengths. To investigate that, I followed myelin segments from their initiation onwards, by which I was able to show that all newly formed myelin segments showed very stereotypic growth dynamics, that can be separated in three distinct growth phases.

First growth phase: In the first 8h after differentiation and sheath initiation, all segments showed a highly uniformly growth with similar growth rates. This high similarity makes it likely, that this growth phase is regulated by oligodendrocyte intrinsic mechanisms without extrinsic influences. If there would be extrinsic cues, every sheath would probably experience slightly different factors, like axon diameter or different expression of surface ligands and hence, every sheath would show different regulation. It has been shown before, that on inert fibers, regional oligodendrocyte-intrinsic differences in sheath length can be detected (Bechler et al., 2015). As oligodendrocytes readily form myelin in culture on inert fibers (Lee et al., 2012a) they might have an oligodendrocyte-intrinsic growth program that continues until external regulation starts.

Second growth phase: The second growth phase starts around 8 hours post initiation (hpi) and lasts until 3-4dpi. In this growth phase the sheath length differences are established by different growth rates of individual sheaths. As one oligodendrocyte forms sheath with different lengths, single sheaths of one cell show different growth rates. The different growth rates could be caused by extrinsic signals that influence the rate with which the sheath grows. Possible mechanism are local vesicle release, axonal activity or the expression of attractive or repulsive cues. During my time-lapse imaging with which I observed the very

early sheath growth, the fish were anesthetized with Tricaine which blocks sodium channels and therefore reduces neuronal activity (Attili and Hughes, 2014), however I could still observe the different growth rates after 8hpi. It is therefore unlikely that the differences are solely caused by axonal activity. However, there might still be some remaining activity that is not Tricaine sensitive that could cause the differences in growth rate. As it has been shown that silencing axons, by blocking synaptic vesicle release, influences sheath length on some axon types (Koudelka et al., 2016) and axonal activity might play a role in the early stabilization of nascent myelin sheaths (Baraban et al., 2018; Krasnow et al., 2018).

Time-lapse imaging of sheaths after differentiation with Tetrodotoxin (TTX), to block neuronal activity, could give insight if the different growth rates are axonal activity dependent. If all sheaths grow with the same dynamics, activity likely plays a role, if they do not it would mean that the different sheath growth rates are independent of axonal activity.

Third growth phase: The third and last growth phase, is a rather passive elongation which is again very uniformly among different sheaths. I could show, by correlating sheath length in this phase with the fish growth, that sheath length elongates to compensate for body growth. As the elongation is again very uniformly and depends on the growth of the fish, I was able to show that myelin segment length in the elongation phase can be quite accurately predicted by the body length increase of the fish. When the fish grow also the axons have to grow in length. As the nodal components are anchored to the cytoskeleton they are probably moved with the growth of the axon and the myelin sheath then follows and elongates with the same rate. For the PNS it has been shown that elongation of the nerve induces myelin elongation (Fernando et al., 2016).

Myelin sheaths seem to have an intrinsic growth phase that starts with sheath initiation and establishes a certain length, then extrinsic signals regulate the growth dynamics and determine if a sheath grows fast or slow, which then also determines the length of a sheath. The model of an oligodendrocyte intrinsic growth phase followed by adaptive regulation has recently been proposed (Bechler et al., 2018).

Sheath growth seems to be independent from the surrounding myelin as the presence or absence of neighboring sheaths did not alter sheath growth dynamics. One possible explanation could be that the length of the sheath and the myelination pattern is already defined. This would mean that the sheaths already slow down growth before they have reached a potential neighboring sheath, hence the presence of a neighboring sheath does not alter the growth. Another possibility could be that a newly formed sheath that meets a neighboring sheath pushes it away and moves the node so it can grow. However, this seems rather unlikely as I only rarely observed sheaths shrinking and never saw sheaths moving along an axon.

Furthermore, sheath growth seems to be independent of oligodendrocyte densities and of the developmental status of the fish as sheath initiated at different timepoints during development show the same growth dynamics and sheath lengths, although the cell density was increased. As the length of sheaths with two neighboring segments did not differ from the length of sheaths with no neighbors, it seems unlikely that sheaths stop growing due to physical barriers. There seems to be something else regulating the sheath length that is independent from physical barriers. A possible explanation could be that the axon regulates the sheath length by different mechanisms, like local vesicle release or expression of surface ligands, which could regulate the rate with which sheaths grow and that eventually determines the length.

A potential model of sheath growth dynamics is depicted in Figure 4.1. The first 8h seem to be oligodendrocyte intrinsic, as all sheaths show the same growth rate. The second growth phase, from 8hpi to 3-4dpi shows very different growth rates that determine the sheath length. The different growth rates could be regulated by the axon as sheath formed by one cell displayed different growth. The last growth phase is a passive elongation phase in which sheath elongate to compensate for body growth.

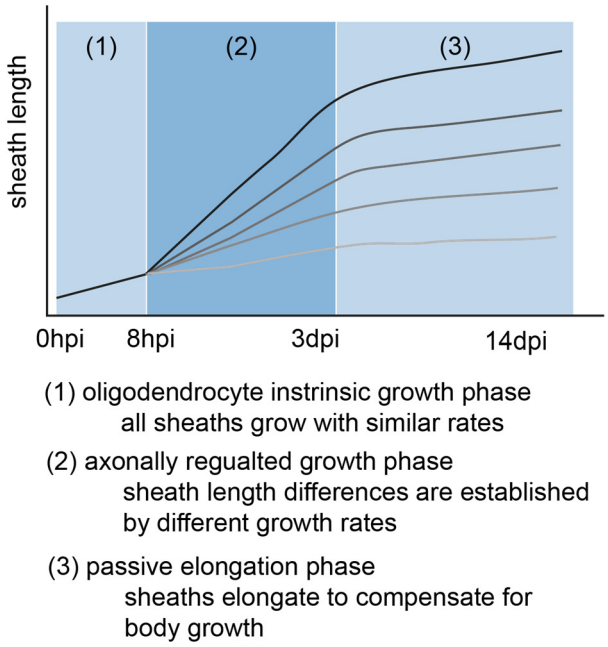

Figure 4.1 Different phases of myelin sheath growth

In the first 8 hours after initiation all sheaths grow with similar dynamics and have roughly the same length. This phase is likely regulated by oligodendrocyte intrinsic mechanisms. After that, until 3-4dpi the sheaths exhibit different growth rates and the length differences between the individual sheaths are established, likely regulated by axonal mechanisms. From 3-4dpi onwards the sheath show only elongation to compensate for body growth. The growth rates are again very similar.

The previous experiments suggested that axonal influences might regulate sheath length by altering sheath growth rate. The next question I approached was, if axonal influences play a role, how are sheaths lengths along one axon distributed?

I analyzed sheath lengths along different axons and found that it is quite variable, however, there are some axons that displayed overall shorter sheaths, while other axons had overall longer ones. This finding also supports the hypothesis of axonal control of sheath lengths, however there must be some more local influences that regulate the exact sheath length. Furthermore, I could not detect any correlation with the diameter, indicating as well a more local regulation for every individual sheath, rather than only physical mechanisms like diameter. But one also has to keep in mind that the diameter was measured with light microscopy and therefore small differences might have been underestimated.

The arrangement of long and short myelin segments along an axon resulted in the formation of specific myelination patterns. When I followed these patterns over time, I could show that

once a pattern is established, it is remarkably stable over time, and that they are a unique feature of every individual axon. Myelination patterns along the same type of axon greatly differed, likely due to each axon establishing the pattern for it to function best, depending on the length and the targets of the axon.

Axons cannot only show full myelination, but also partial myelination patterns were detected in cortical layers in the mouse (Tomassy et al., 2014; Micheva et al., 2016). I could show that also in zebrafish partial myelination patterns exits and by following them over time, I was able to show that they can be maintained for longer periods of time. Similarly, also in mouse cortex partial myelination patterns were observed to be maintained for some time (Hughes et al., 2018) but also ongoing myelination of partially myelinated axons was observed (Hill et al., 2018). Sheaths on these axons are not longer than sheaths on fully myelinated axons, although there would be space for them to grow longer. Hence, something must stop them from growing. Theoretically, it could be a general growth stop regulated intrinsically by the oligodendrocyte or local axonal signals defining permissive and non-permissive areas, resulting in a growth stop. If there is a general growth stop in oligodendrocytes that determines the length one could follow sheath growth of oligodendrocytes where Pten is knocked out, which leads to elevated PIP3 levels which was shown to induce hypermyelination (Goebbels et al., 2012). If the sheath lengths or growth dynamics are not altered this argues for a local regulation of sheath growth stop instead of a general growth stop of the oligodendrocyte.

It was hypothesized, that discontinuous myelination patterns might be involved in higher brain functions (Tomassy et al., 2014). However, single, short ensheathments might not have a strong influence on AP conduction speed, but, due to local clustering and higher densities of voltage gated channels at the heminodes, they might have an influence on the shape of action potentials (Günay et al., 2008; Zhang et al., 2018). The action potential shape, depending if it is wider or more narrow, changes the duration of the depolarization, which might have implications for circuit function as it increases or decreases the chances

of simultaneous arrival of several inputs. If single ensheathments do indeed alter action potential shape could be tested with electrophysiology or computational modeling. Another function of the sparse ensheathment could be to provide local metabolic support, however, this would imply that there is a static, locally increased need for energy.

As mentioned before, when I assessed sheath length along single axons I found that some had overall shorter, other overall longer myelin sheaths. This already indicates an axonal influence on myelin sheath length. However, one factor that is similar among the same type of neuron is the myelination coverage. Especially for CoPAs and RB it was very stereotypic, for the CiDs it was rather divers, but literature suggests also that there are more CiD subtypes (Menelaou et al., 2019) that exhibit different functions (Pujala and Koyama, 2019) and they could exhibit different myelination dynamics.

I also detected a correlation between diameter and myelination, as it has been reported before (Murray and Blakemore, 1980); Almeida et al., 2011). But as RBs have an overall smaller diameter than CoPAs, the myelination differences between these two could therefore also be due to them being different neurons instead of just diameter dependent. For the CiD there is a clear correlation between diameter and myelination.

I also assessed spontaneous axonal activity, as it has been shown before that activity can influence myelination and OPC differentiation (Gibson et al., 2014; Mensch et al., 2015; Koudelka et al., 2016; Mitew et al., 2018). CoPAs showed almost no spontaneous activity, likely be explained by them being integrated in sensory circuits. The CiDs are involved in motor output, and they might be integrated in central pattern generators (CPG) that produce regular patterns of activity (Kimura et al., 2006). Also here, I observed a very diverse pattern for the CiDs, namely that some were highly active while others showed only few Ca^{2+} transients, which can likely also be explained by the existence of different subtypes of CiDs. RB showed some activity, roughly 50% of the analyzed ones showed Ca^{2+} transients, but fewer transients compared to CiDs.

I could not detect any correlation between spontaneous activity and the amount of ensheathment along axons of the same type. The most ensheathed type (CoPAs) were the least active ones. Consistently, it has been shown that blocking vesicle release in CoPAs did not change myelination (Koudelka et al., 2016), arguing for an activity independent regulation of the amount of myelin formed along these axons. As CoPAs are involved in escape responses (Ritter et al., 2001) that have to function from very early onwards the fast myelination of these axons might be regulated independent of activity to secure a fast myelination and functioning of these neurons.

For CiDs I observed high variabilities for both parameters, but as the data was acquired in two independent experiments I could not assess if along CiDs the amount of ensheathment correlates with spontaneous activity. To investigate if myelination along different types of CiDs is activity dependent, and if the activity and myelination status correlates with the different types of CiDs, one could do the experiment of myelin coverage and activity in the same animal and assess both parameters for each neuron.

Together, I was able to describe the growth dynamics of newly generated myelin sheaths with the three different growth phases. Furthermore, I assessed how different myelination patterns are established and maintained.

4.2 Manipulation of myelin sheath length

I aimed to test if established sheaths are able to reinitiate growth again, also long after sheath initiation when they are in their passive elongation phase, as this could be an important regulator to adjust conduction properties. In order to test the ability of sheaths to grow after their active growth phase, I established a laser ablation method, with which I was able to precisely ablate single oligodendrocytes and their respective sheaths. I used two different experimental setups, ablation of single sheaths along fully myelinated axons and demyelination of partially myelinated axons.

With the first paradigm I wanted to test if the neighboring sheaths are able to remodel and if sheath length is plastic and can adapt after manipulations.

I hypothesized two possible remyelination scenarios, either the neighbors reinitiate sheath growth and invade the demyelinated axon or a new sheath is formed to remyelinate it. The first would imply that myelin sheaths are indeed able to remodel and that they sense that the neighboring sheath was ablated, the latter would mean that sheaths are not able to remodel their length upon local demyelination. When I did the experiments, I observed that often a combination of these two events took place. First the neighbors reinitiated fast sheath growth, followed by the formation of a new myelin sheath. I could show, for the first time, that existing myelin sheaths can remodel upon manipulation like ablation of neighboring sheaths. It has now also been shown that in the mouse cortex, myelin sheaths can show length changes during development (Hill et al., 2018; Hughes et al., 2018). The potential ability of existing myelin sheaths to remodel and change in length holds great potential as a mechanism to adaptively modulate conduction properties. As the invasion of the neighboring sheaths occurred before the formation of a new sheath it could be a faster reaction to changes than oligodendrogenesis.

In some cases, the neighboring sheaths did not reinitiate growth again, but the nodes stayed at their initial position. As I sometimes observed axon collaterals, they could explain why some sheaths did not show remodeling due to the collaterals acting as physical growth

barriers. To test if the collaterals account for the cases in which I did not observe remodeling I compared their frequency. In 23.5% (4/17) of the cases I did not observe remodeling and in 28.5% of nodes I observed collaterals, therefore it is likely that the collaterals prevented sheath remodeling in these four cases.

But why do the myelin sheaths reinitiate growth again to cover the demyelinated area? During development sheaths also stop growing without meeting a neighboring sheath. A possible explanation could be, that due to the ablation permissive axon is exposed and diffusion of nodal proteins, potentially the removal of molecular stop signals, may allow for further growth of the myelin sheath. I did not analyze the dynamics of nodal markers after demyelination. Some could stay anchored at the cytoskeleton, and therefore mark the position of the ablated sheath, while others could diffuse to allow sheath growth. It would be interesting, in future experiments to see how different nodal proteins react to demyelination and if they are actively involved in myelin remodeling.

Upon ablation of an oligodendrocyte and following demyelination of the respective axons, a new myelin sheath is formed. There are two possible sources, where the myelin sheaths could come from. The first is, that an oligodendrocyte precursor cell differentiated as a response to the cell ablation of an oligodendrocyte. The other option is, that a mature oligodendrocyte extended a process and remyelinated the axon. During development, differentiating oligodendrocytes only have a 5h time-window to generate new sheaths (Czopka et al., 2013), however, recent evidences suggests that in a demyelinated environment mature oligodendrocytes are capable of extending processes and forming new myelin sheaths (Duncan et al., 2018; Jäkel et al., 2019; Yeung et al., 2019).

EM reconstructions from demyelinated lesions in cats or rhesus monkeys showed oligodendrocytes that were connected to mature thick sheaths as well as thin remyelinated ones, leading to the possibility that mature oligodendrocytes can, under certain circumstances participate in remyelination. The oligodendrocyte participating in remyelination are probably cells that had lost some sheaths by the demyelination (Duncan

et al., 2018). Yeung et al. could show by birth dating of oligodendrocytes in MS lesions, that in shadow plaques no new oligodendrocytes were formed although there was remyelination, arguing that the myelin came from mature oligodendrocytes, however, cells do not necessarily have to divide before differentiation, they could have been already at the lesion site as pre-oligodendrocytes and thereby not detected as newly myelinating oligodendrocytes (Yeung et al., 2019). Another study, comparing human healthy and MS tissue by single nucleus RNA sequencing, showed enhanced myelin gene expression in mature oligodendrocytes, arguing as well for their participation in remyelination in MS lesions (Jäkel et al., 2019).

There is accumulating evidence, that mature oligodendrocyte can, under certain circumstances participate in remyelination. However, in my experiments the damage and inflammation are minimal and most likely to subtle to induce the regrowth of a myelinating process of a mature oligodendrocytes. In my experiments, the newly formed myelin most likely comes from a newly differentiated oligodendrocyte.

Interestingly, I often observed reestablishment of the pre-ablation pattern. One possible mechanism of how this could be achieved is, that parts of the cytoskeleton, where the nodal proteins are anchored, remains at the initial position and guide the sheaths after remyelination to reestablish the functional pattern. As myelin segment length influences conduction speed this could be an important mechanism to re-establish the initial conduction properties.

During developmental growth, the myelin sheaths are getting compacted and cytoplasmic channels are closed (Snaidero et al., 2014). To reinitiate sheath growth cytoplasmic channels would need to be opened to allow transport of myelin components to the growing regions. It has been shown that upon activation of P(3,4,5)P3 in oligodendrocytes, cytoplasmic channels can reopen and myelin sheath growth, here in form of increases in thickness, was observed (Snaidero et al., 2014). Opening of cytoplasmic channels could also be the way of how sheath growth reinitiates upon oligodendrocyte ablation. Local

axonal signaling, due to the demyelination, could induce the opening of cytoplasmic channels to allow for fast sheath growth. This could represent a mechanism of how the axon achieves fast remyelination of the demyelinated axon, by local axon to oligodendrocyte communication, to restore fast AP conduction properties.

With the second ablation paradigm, I demyelinated partially myelinated axons, to see if also here the myelination patterns are reestablished again. By labelling the axon as well in these experiments, I secured that newly formed sheaths are indeed along the same axon and to assess if physical growth barriers like axon collaterals exist. After demyelination I observed, that the ablated myelin sheaths were replaced by new sheaths at similar positions and with a similar length. Possible explanations for this could be that there are, similar to the ablation along fully myelinated axons, nodal molecules that remain at their initial position due to anchorage at the cytoskeleton. It could also well be that extracellular matrix remains at its initial position and guides the newly formed sheath to remyelinate the exact same part of the axon. Another factor could be that the axon has permissive and non-permissive regions for myelination. Upon ablation, the permissive stretch of axon is exposed and is remyelinated again, while the non-permissive regions stay unmyelinated. A mechanism where axons define permissive and non-permissive areas has been recently published. Here axons defined myelinated and unmyelinated regions by expression of Galectin-4 (Díez-Revuelta et al., 2017).

As the slow elongation phase is due to body growth it is predictable and there is no active growth of sheath length after this time, this could either mean that the oligodendrocyte has shut down its growth program or that the sheaths stopped growing due to having reached their final position. As ablation of neighboring sheaths initiates a fast growth again it seems likely that the growth during development ceases due to local regulation at the axon-glia interface instead of a general stop of sheath growth by the oligodendrocyte.

It remains unclear how the remodeling of myelin sheaths upon ablation is mechanistically regulated. I hypothesized two mechanisms how this could be achieved. (1) axon to

oligodendrocyte communication or (2) axon intrinsic positioning of nodes with the myelin sheath passively following (Fig 4.2).

In the first option, the axon would have to locally signal to the neighboring sheaths to grow. Once the new sheath is formed it becomes more complicated as the new sheath is growing while the neighboring sheath is shrinking again. This could only be achieved by very local communication. Recent studies suggest that local calcium signals in young myelin sheaths, partially induced by axonal activity, regulate if the sheaths grow, stop or shrink (Baraban et al., 2018; Krasnow et al., 2018). A similar mechanism could come to play here as well; however, it remains difficult to envision how neighboring sheaths can display opposite dynamics.

The other option, axon intrinsic control of node positioning seems more intuitive and easier to implement, as the axon could move the node and the sheaths would just passively follow. Additionally, complex myelination patterns, as they have been observed in the gerbil auditory system, with sheaths getting shorter closer to the synapse (Ford et al., 2015), could easily be established by axon intrinsic node positioning.

However, these two mechanisms are not mutually exclusive and the truth could be a combination of both.

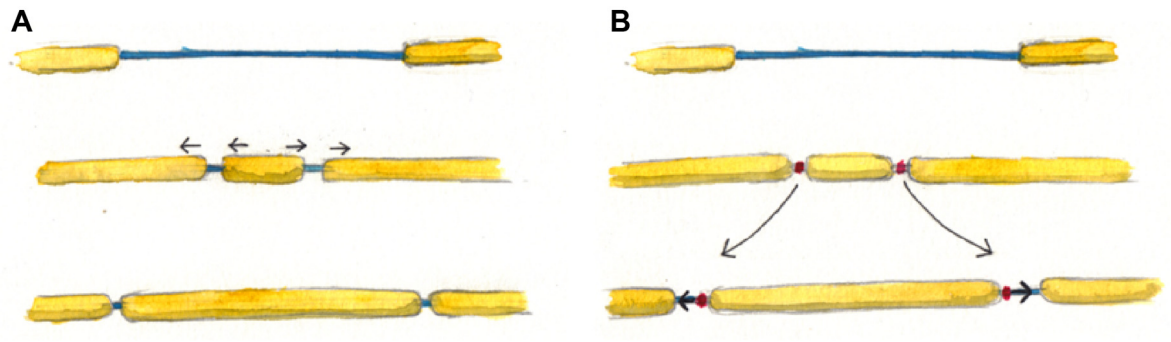

Figure 4.2 Possible mechanism of how myelin sheath remodeling is mechanistically regulated

(A) Axon to oligodendrocyte communication. Local signals regulate that sheaths are growing or shrinking **(B)** Axon intrinsic control of node position. The axon intrinsically regulates node positioning and the myelin sheaths passively follow

4.3 Axonal control of myelin sheath length

In the first two sections of my thesis I collected evidence, that sheath length and the resulting myelination pattern might be determined by extrinsic cues from the axon. This regulation could be managed by anchoring of nodal, but also paranodal proteins, to the cytoskeleton, which is supported by the experiments where I saw re-establishment of pre-ablation patterns.

While imaging, I often observed asymmetric sheath growth, where sheaths were extending into one direction but not in the other, that could not be explained by the presence of physical growth barriers like neighboring sheaths or axon collaterals. As the sheaths where only growing into one direction it seemed as there would be an ‘invisible’ barrier, which could be, instead of a physical barrier, a molecular one.

To investigate if nodal proteins could act as a molecular growth barrier, I used the transmembrane nodal protein Nfasca. Neurofascin 186, the homologous protein in mammals, was shown be involved in node formation, where it is suggested to cluster due to ECM at the node of Ranvier (Susuki et al., 2013).

I observed specific localization dynamics of Nfasca along neurons that were supposed to be myelinated (CoPAs and CiDs were identified to get substantial amount of myelination in the first week of zebrafish development). First of all, Nfasca is a suitable marker to label unmyelinated axon stretches in these neurons, as it reliably localized only to unmyelinated parts and was entirely removed from ensheathed axon segments. Even the formation of very young ensheathments led to the removal of Nfasca from the ensheathed part, securing that the presence of Nfasca signal correlates with the absence of myelin. Second, during development, when parts of the axon stayed unmyelinated, Nfasca clustered along these stretches.

The other localization dynamics I observed, were along RB neurons. RB neurons are rarely ensheathed and if they are, then only by short, often transient myelin segments. Here, unlike

the myelinated axons, when one of the rare ensheathments was formed, Nfasca was surprisingly not excluded from underneath the myelin segment. Along RB axons, although not myelinated, Nfasca did also not form clusters, but it stayed homogeneously distributed. Different localization dynamics of Nfasca, clustering along some but not all axons, might be explained by axon intrinsic differences. First, RB neurons are normally not myelinated, so there is no need to already cluster nodal proteins as there are no nodes to be formed. This would imply that these dynamics should be seen along all unmyelinated neurons. In my thesis, I only focused on RB neurons as largely unmyelinated neurons, but it would be interesting to investigate the differences of Nfasca dynamics along other unmyelinated axons. If there is no clustering this would imply that Nfasca clustering plays a role during myelination and therefore support the hypothesis of axonal mechanisms regulating myelination.

Another difference is, that RB neurons are special, as they only occur in fish and amphibians (Lamborghini, 1987; Williams et al., 2000), and during development they are replaced by DRG neurons. Some studies suggested that RB neurons die early in zebrafish during development (Williams et al., 2000; Svoboda et al., 2001), but we and others (Knafo and Wyart, 2018) observed RB neurons also at later stages. The different dynamics could therefore also be explained by the different evolutionary origin.

At first, around 3dpf, Nfasca was homogeneously distributed, also in CoPA and CiD axons, then clusters did emerge and they became more pronounced when the neuron stayed unmyelinated. I followed these clusters over time and found them to be remarkably stable. They only move due to body growth. Very rarely I observed new clusters being formed or existing clusters disappearing. The high stability, as well as the moving due to body growth, might be explained by cytoskeletal anchoring of these clusters, similar to nodes. Clustering of nodal proteins, like sodium channels or AnkyrinG, have been shown before (Kaplan et al., 1997); (Freeman et al., 2015). *In vitro,* the cluster, or prenode formation depended on AnkyrinG, whereas Neurofascin186 was dispensable (Freeman et al., 2015). It could well

be that this is also the case for the Nfasca clusters I observed *in vivo*. However, as Neurofascin has an AnkyrinG binding motif, the Nfasca clustering could also be due to prior AnkyrinG clustering.

I hypothesized that these Neurofascin clusters could serve as growth barriers during developmental sheath growth, explaining the high probability of asymmetric growth. To test if the clusters serve as growth barriers and therefore determine node position, I imaged unmyelinated axons with clusters and followed them until they got myelinated. I correlated the node position with the pre-myelination cluster position and found that the majority of nodes were formed at position with prior clusters, indicating that sheaths had stopped growing once they reached the clusters. As mentioned before, a mechanism where the axon intrinsically defines the node position could explain how specific myelination patterns along axons (Ford et al., 2015) are implemented. There are some known factors by which axons regulate regions that are to be myelinated or to prevent myelination. JAM2 was shown to prevent somatodendritic myelination (Redmond et al., 2016), and it was has been shown that Galectin-4 expression in neurons labels unmyelinated stretches and prevents their myelination (Díez-Revuelta et al., 2017).

When I followed the axon in these experiments I did not always see clusters forming. Often the axons did show homogeneous distribution and at the next imaging timepoint they were fully myelinated. The clustering and myelination could happen almost simultaneously, making it hard to disentangle them and assess which of them happens first. To circumvent this problem, I aimed to inhibit myelination to investigate if clusters still form in the absence of myelin. When doing so, by the ablation of NTR expressing OPCs with MTZ, I still observed a substantial amount of myelin formed in the beginning. The NTR was expressed under control of olig1 promoter elements and when these cells emerge it takes some time for the NTR to be expressed and to function. The formed myelin might therefore be explained by the OPCs that had already differentiated before the NTR could transform MTZ into the DNA crosslinking agent. Instead of a prevention, myelination was delayed.

Nevertheless, it prolonged the time in which the neuron was unmyelinated, and I could see clusters forming. When the axons were getting myelinated and nodes formed, I assessed the cluster node correlation as well and found similar results. I could see that the majority of nodes had formed at positions with pre-myelination clusters, suggesting that clusters do emerge before myelination and are predictive for node positioning.

If Neurofascin clustering plays an important role in defining node position, it would be interesting to investigate what happens when Nfasca is knocked out. If it has a role in determining node position and stops sheath from growing, in Nfasca KO more sheaths should grow symmetrically and they should also be longer.

Based on the experimental evidence I, hypothesize that the axon determines node of Ranvier position, however, the exact pattern might be refined by the communication of myelin sheaths/oligodendrocytes and the ensheathed axon. The phenomenon of pre-patterning with subsequent refinement of the pattern has already been suggested in other systems, like nicotinic acetylcholine receptor clustering at the motor end plate (Kummer et al., 2006).

If the axon determines the node position, how should the sheaths then know how fast they should grow, as the growth rates determine sheath length differences in the second growth phase? One possible explanation could be, that there are gradients of either permissive or repulsive cues that regulate growth rates locally at the axon-glia interface.

In the last experiment of my thesis I aimed to test for axon intrinsic control of sheath length. To investigate that, I wanted to change an axon intrinsic feature and test for node of Ranvier remodeling. I therefore manipulated activity by optogenetics and hyperactivated a spontaneously very silent neuron and followed node position over time. With pre-stimulation imaging I secured that the sheaths have reached their elongation phase. Upon the optogenetic stimulation I observed that some nodes, and therefore also sheath lengths, remodeled and changed their relative position. Some sheaths showed deviations from their predicted length, indicating activity dependent remodeling. However, I could observe similar

effects in my control experiments, where I did not express Channelrhodopsin. This ‘off-target’ effect might be explained by the stimulation of the fish with bright blue light. I observed increased swimming in the light stimulated fish, which could also indicate an overall increased neuronal activity, making it impossible to disentangle the Channelrhodopsin mediated effect from the general light stimulation effect. Furthermore, it has recently been shown that stimulation with blue light, in contrast to green or red light, alters neuronal gene expression (Tyssowski and Gray, 2019), adding another layer of uncontrolled effects. Hence, we decided, for our future experiments, to switch from Channelrhodopsin to the light activated channel ChrimsonR (Klapoetke et al., 2014). ChrimsonR is activated by red light, and therefore not altering gene expression (Tyssowski and Gray, 2019), and it is more light sensitive than Channelrhodopsin, which should reduce the ‘off-target’ effect by the light stimulation.

Nevertheless, activity induced remodeling could also be caused by axon to oligodendrocyte communication. Local vesicle release or other mechanisms, as a consequence of increased activity, could induce sheath remodeling. One way of testing for that, excluding any glial influence, would be to test if pre-myelination clusters of Nfasca can remodel. As mentioned before, without interference these clusters are remarkably stable, probably due to anchorage to the cytoskeleton. Activity dependent changes in cluster position would therefore imply that the axon intrinsically regulates where these clusters are deposited along the axon and, as the clusters are determinants for nodes, also where nodes of Ranvier will be.

4.4 Hypothetical model of myelin sheath length regulation

Based on the accumulating evidence, I have formulated a hypothetical model of how myelin sheath length and node of Ranvier positioning are axon intrinsically regulated. During early development clusters of Neurofascin formed along unmyelinated axons, and when these axons were getting myelinated, node position correlated with the prior cluster position in most of the cases. This clustering could occur due to axon intrinsic regulation but it could also be induced by other cells like OPCs. In vitro, nodal proteins only cluster upon treatment with oligodendrocyte conditioned medium (Freeman et al., 2015) it is therefore likely, that a secreted factor induces the cluster formation. Similarly, an oligodendrocyte secreted factor could induce the clustering. As I was not able to fully prevent the formation of myelin by the ablation of OPCs I am not able to test if clusters would form *in vivo* in the absence of oligodendrocytes and OPCs.

As I could not prevent myelination with the HDAC inhibitor another strategy could be to use a znf16l mutant fish that shows substantial delay of myelination (Sidik and Talbot, 2015). In these mutants the number of myelinated axons is reduced by a factor of 10 at 5dpf which is around the timepoint where I did my cluster experiment. Hence, it should be possible to observe in these mutants how the clustering dynamics of Nfasca are affected or altered in the absence or substantial reduction of myelination. In the PNS it has been shown that the lack of Schwann cells results in a reduction of clusters of sodium channels and that they show abnormal morphology in terms of width and symmetry (Voas et al., 2009). In culture, on the other hand, similar to the CNS (Kaplan et al., 1997), the absence of Schwann cells prevents cluster formation in dorsal root ganglion neuron cultures (Eshed et al., 2005). In vivo clustering might therefore use different or additional mechanisms compared to clustering of nodal proteins in culture. It could therefore well be that in the zebrafish CNS nodal proteins cluster in the absence of myelin. To conclude, already the pre-myelination clustering of nodal proteins, like sodium channels or Nfasca, in vivo might depend on

several independent mechanisms that are partially axon intrinsic but also depend on glial cells similar to the node assembly mechanisms (Susuki et al., 2013).

If Nfasca clusters act as growth barriers, and myelin sheaths are formed at random positions along the axon, this would also explain the asymmetric growth. Asymmetric growth, as well as growth rate differences, could be regulated by gradients of permissive or repulsive cues. Due to the gradient sheaths would display faster or slower growth rates, that eventually determine the sheath length. On the other hand, the different growth rates could also be regulated by other mechanisms like local vesicle release. Furthermore, Neurofascin does not need to be the master regulator of these processes, it could well be that it´s localization is regulated by other nodal proteins or yet unknown factors. Nevertheless, axonal intrinsic control of sheath length seems to be highly involved in establishing and maintaining axonal myelination patterns.

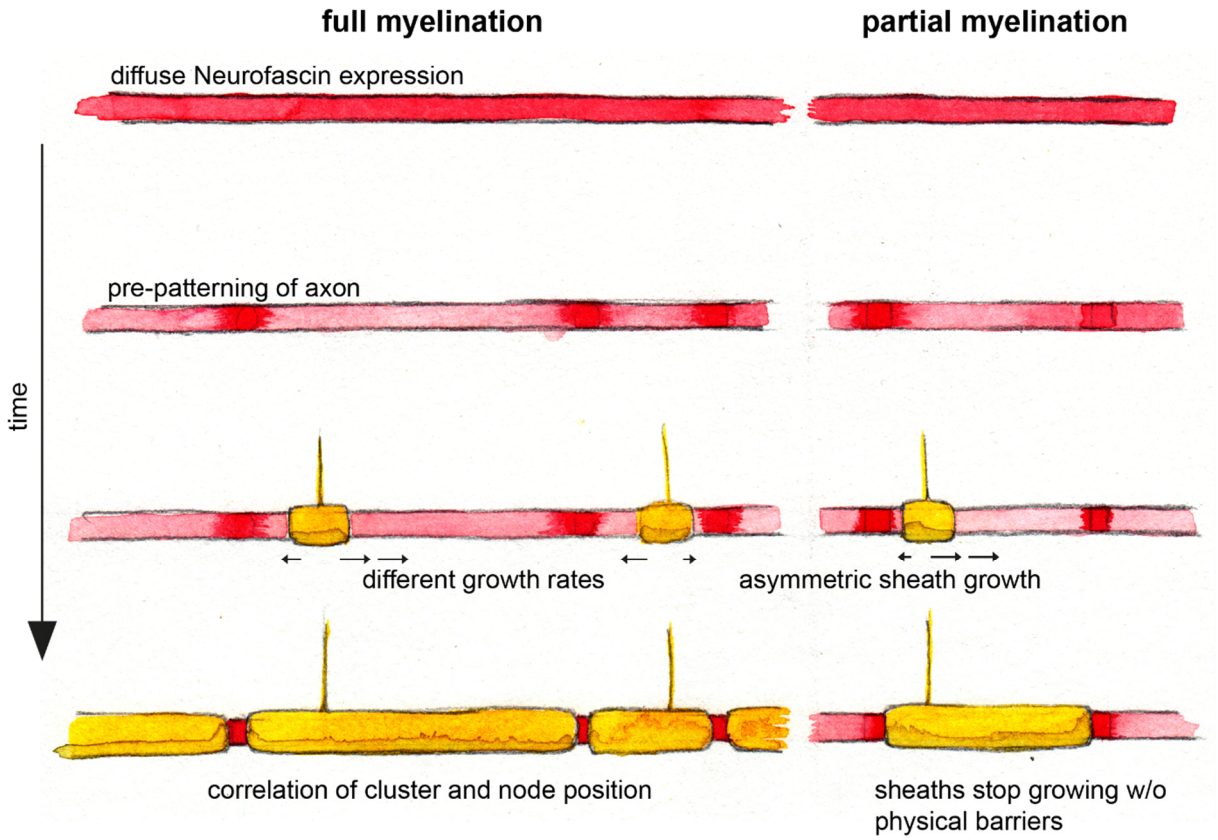

Figure 4.3 Hypothetical model of sheath length regulation by axonal mechanisms along fully and partially myelinated axons

Hypothetical model of how different myelination patterns are established. In the beginning Neurofascin is homogeneously expressed along the axon. During maturation Neurofascin starts forming clusters. Myelin sheaths are formed. As they are formed at random positions along the axon they exhibit asymmetric growth. The sheaths exhibit different growth speeds. After 3-4dpi growth stops even in the absence of physical barriers. Results from my experiments are indicated in the labeling.

Taken together, I could show how different myelin sheath lengths are established and describe their growth dynamics. Furthermore, I was able to show for the first time, that normally very stable myelin sheaths are able to remodel upon manipulation.

I could also accumulate evidence that myelin segment length and node of Ranvier positioning might be axon intrinsically regulated, upon which I formulated a hypothetical model (Fig 4.3) of how this could be achieved and how it fits with my experimental results.

5 References

Almeida, R.G., Czopka, T., Ffrench-Constant, C., and Lyons, D.A. (2011). Individual axons regulate the myelinating potential of single oligodendrocytes in vivo. Development (Cambridge, England) *138*, 4443-4450.

Arancibia-Cárcamo, I.L., Ford, M.C., Cossell, L., Ishida, K., Tohyama, K., and Attwell, D. (2017). Node of Ranvier length as a potential regulator of myelinated axon conduction speed. elife.

Attili, S., and Hughes, S.M. (2014). Anaesthetic tricaine acts preferentially on neural voltage-gated sodium channels and fails to block directly evoked muscle contraction. PloS one *9*, e103751.

Auer, F., Vagionitis, S., and Czopka, T. (2018). Evidence for Myelin Sheath Remodeling in the CNS Revealed by In Vivo Imaging. Current biology : CB *28*, 549-559.e3.

Bakhti, M., Aggarwal, S., and Simons, M. (2014). Myelin architecture: zippering membranes tightly together. Cellular and molecular life sciences : CMLS *71*, 1265-1277.

Baraban, M., Koudelka, S., and Lyons, D.A. (2018). Ca 2+ activity signatures of myelin sheath formation and growth in vivo. Nature neuroscience *21*, 19-23.

Barres, B.A., and Raff, M.C. (1993). Proliferation of oligodendrocyte precursor cells depends on electrical activity in axons. Nature.

Beaulieu, C. (2002). The basis of anisotropic water diffusion in the nervous system - a technical review. NMR in biomedicine *15*, 435-455.

Bechler, M.E., Byrne, L., and Ffrench-Constant, C. (2015). CNS Myelin Sheath Lengths Are an Intrinsic Property of Oligodendrocytes. Current biology : CB *25*, 2411-2416.

Bechler, M.E., Swire, M., and Ffrench-Constant, C. (2018). Intrinsic and adaptive myelination-A sequential mechanism for smart wiring in the brain. Developmental neurobiology *78*, 68-79.

Bekku, Y., Vargová, L., Goto, Y., Vorísek, I., Dmytrenko, L., Narasaki, M., Ohtsuka, A., Fässler, R., Ninomiya, Y., and Syková, E., et al. (2010). Bral1: its role in diffusion barrier formation and conduction velocity in the CNS. The Journal of neuroscience : the official journal of the Society for Neuroscience *30*, 3113-3123.

Bergles, D.E., Roberts, J.D., Somogyi, P., and Jahr, C.E. (2000). Glutamatergic synapses on oligodendrocyte precursor cells in the hippocampus. Nature *405*, 187-191.

Boiko, T., Rasband, M.N., Levinson, S.R., Caldwell, J.H., Mandel, G., Trimmer, J.S., and Matthews, G. (2001). Compact Myelin Dictates the Differential Targeting of Two Sodium Channel Isoforms in the Same Axon. Neuron *30*, 91-104.

Brill, M.H., Waxman, S.G., Moore, J.W., and Joyner, R.W. (1997). Conduction velocity and spike configuration in myelinated fibres: computed dependence on internode distance. Journal of Neurology, Neurosurgery and Psychiatry.

Brinkmann, B.G., Agarwal, A., Sereda, M.W., Garratt, A.N., Müller, T., Wende, H., Stassart, R.M., Nawaz, S., Humml, C., and Velanac, V., et al. (2008). Neuregulin-1/ErbB signaling serves distinct functions in myelination of the peripheral and central nervous system. Neuron *59*, 581-595.

Brivio, V., Faivre-Sarrailh, C., Peles, E., Sherman, D.L., and Brophy, P.J. (2017). Assembly of CNS Nodes of Ranvier in Myelinated Nerves Is Promoted by the Axon Cytoskeleton. Current biology : CB *27*, 1068-1073.

Brösamle, C., and Halpern, M.E. (2002). Characterization of myelination in the developing zebrafish. Glia *39*, 47-57.

Bulina, M.E., Chudakov, D.M., Britanova, O.V., Yanushevich, Y.G., Staroverov, D.B., Chepurnykh, T.V., Merzlyak, E.M., Shkrob, M.A., Lukyanov, S., and Lukyanov, K.A. (2006). A genetically encoded photosensitizer. Nature biotechnology *24*, 95-99.

Bunge, M.B., Bunge, R.P., and Ris, H. (1961). Ultrastuctural Study of Remyelination in an Experimental Lesion in the Adult Cat Spinal Cord. The Journal of cell biology *10*, 67-94.

Caldwell, J.H., Schaller, K.L., Lasher, R.S., Peles, E., and Levinson, S.R. (2000). Sodium channel Na(v)1.6 is localized at nodes of ranvier, dendrites, and synapses. Proceedings of the National Academy of Sciences of the United States of America *97*, 5616-5620.

Charles, P., Hernandez, M.P., Stankoff, B., Aigrot, M.S., Colin, C., Rougon, G., Zalc, B., and Lubetzki, C. (2000). Negative regulation of central nervous system myelination by polysialylated-neural cell adhesion molecule. Proceedings of the National Academy of Sciences of the United States of America *97*, 7585-7590.

Curado, S., Anderson, R.M., Jungblut, B., Mumm, J., Schroeter, E., and Stainier, D.Y.R. (2007). Conditional targeted cell ablation in zebrafish: a new tool for regeneration studies. Developmental dynamics : an official publication of the American Association of Anatomists *236*, 1025-1035.

Curado, S., Stainier, D.Y.R., and Anderson, R.M. (2008). Nitroreductase-mediated cell/tissue ablation in zebrafish: a spatially and temporally controlled ablation method with applications in developmental and regeneration studies. Nature protocols *3*, 948-954.

Czopka, T., Ffrench-Constant, C., and Lyons, D.A. (2013). Individual oligodendrocytes have only a few hours in which to generate new myelin sheaths in vivo. Developmental cell *25*, 599-609.

Dawson, M.R.L., Levine, J.M., and Reynolds, R. (2000). NG2-expressing cells in the central nervous system: Are they oligodendroglial progenitors? Journal of neuroscience research, 471-479.

Díez-Revuelta, N., Higuero, A.M., Velasco, S., Peñas-de-la-Iglesia, M., Gabius, H.-J., and Abad-Rodríguez, J. (2017). Neurons define non-myelinated axon segments by the regulation of galectin-4-containing axon membrane domains. Scientific reports *7*, 12246.

Douglass, A.D., Kraves, S., Deisseroth, K., Schier, A.F., and Engert, F. (2008). Escape behavior elicited by single, channelrhodopsin-2-evoked spikes in zebrafish somatosensory neurons. Current biology : CB *18*, 1133-1137.

Duncan, I.D., Radcliff, A.B., Heidari, M., Kidd, G., August, B.K., and Wierenga, L.A. (2018). The adult oligodendrocyte can participate in remyelination. Proc Natl Acad Sci USA *115*, E11807-E11816.

Early, J.J., Cole, K.L.H., Williamson, J.M., Swire, M., Kamadurai, H., Muskavitch, M., and Lyons, D.A. (2018). An automated high-resolution in vivo screen in zebrafish to identify chemical regulators of myelination. elife.

Emery, B. (2010). Regulation of oligodendrocyte differentiation and myelination. Science (New York, N.Y.) *330*, 779-782.

Emery, B., Agalliu, D., Cahoy, J.D., Watkins, T.A., Dugas, J.C., Mulinyawe, S.B., Ibrahim, A., Ligon, K.L., Rowitch, D.H., and Barres, B.A. (2009). Myelin gene regulatory factor is a critical transcriptional regulator required for CNS myelination. Cell *138*, 172-185.

Eshed, Y., Feinberg, K., Poliak, S., Sabanay, H., Sarig-Nadir, O., Spiegel, I., Bermingham, J.R., and Peles, E. (2005). Gliomedin mediates Schwann cell-axon interaction and the molecular assembly of the nodes of Ranvier. Neuron *47*, 215-229.

Etxeberria, A., Hokanson, K.C., Dao, D.Q., Mayoral, S.R., Mei, F., Redmond, S.A., Ullian, E.M., and Chan, J.R. (2016). Dynamic Modulation of Myelination in Response to Visual Stimuli Alters Optic Nerve Conduction Velocity. The Journal of neuroscience : the official journal of the Society for Neuroscience *36*, 6937-6948.

Faivre-Sarrailh, C., and Devaux, J.J. (2013). Neuro-glial interactions at the nodes of Ranvier: implication in health and diseases. Frontiers in cellular neuroscience *7*, 196.

Fernando, R.N., Cotter, L., Perrin-Tricaud, C., Berthelot, J., Bartolami, S., Pereira, J.A., Gonzalez, S., Suter, U., and Tricaud, N. (2016). Optimal myelin elongation relies on YAP activation by axonal growth and inhibition by Crb3/Hippo pathway. Nature communications *7*, 12186.

Fields, R.D. (2008). White matter in learning, cognition and psychiatric disorders. Trends in neurosciences *31*, 361-370.

Fields, R.D. (2015). A new mechanism of nervous system plasticity: activity-dependent myelination. Nature reviews. Neuroscience *16*, 756-767.

Ford, M.C., Alexandrova, O., Cossell, L., Stange-Marten, A., Sinclair, J., Kopp-Scheinpflug, C., Pecka, M., Attwell, D., and Grothe, B. (2015). Tuning of Ranvier node and internode properties in myelinated axons to adjust action potential timing. Nature communications *6*, 8073.

Franklin, R.J.M., and Ffrench-Constant, C. (2008). Remyelination in the CNS: from biology to therapy. Nature reviews. Neuroscience *9*, 839-855.

Freeman, S.A., Desmazières, A., Fricker, D., Lubetzki, C., and Sol-Foulon, N. (2016). Mechanisms of sodium channel clustering and its influence on axonal impulse conduction. Cellular and molecular life sciences : CMLS *73*, 723-735.

Freeman, S.A., Desmazières, A., Simonnet, J., Gatta, M., Pfeiffer, F., Aigrot, M.S., Rappeneau, Q., Guerreiro, S., Michel, P.P., and Yanagawa, Y., et al. (2015). Acceleration of conduction velocity linked to clustering of nodal components precedes myelination. Proceedings of the National Academy of Sciences of the United States of America *112*, E321-8.

Fünfschilling, U., Supplie, L.M., Mahad, D., Boretius, S., Saab, A.S., Edgar, J., Brinkmann, B.G., Kassmann, C.M., Tzvetanova, I.D., and Möbius, W., et al. (2012). Glycolytic oligodendrocytes maintain myelin and long-term axonal integrity. Nature *485*, 517-521.

Garratt, A.N., Britsch, S., and Birchmeier, C. (2000). Neuregulin, a factor with many functions in the life of a Schwann cell. BioEssays : news and reviews in molecular, cellular and developmental biology.

Ghosh, A., Sherman, D.L., and Brophy, P.J. (2018). The Axonal Cytoskeleton and the Assembly of Nodes of Ranvier. The Neuroscientist : a review journal bringing neurobiology, neurology and psychiatry *24*, 104-110.

Gibson, E.M., Purger, D., Mount, C.W., Goldstein, A.K., Lin, G.L., Wood, L.S., Inema, I., Miller, S.E., Bieri, G., and Zuchero, J.B., et al. (2014). Neuronal activity promotes oligodendrogenesis and adaptive myelination in the mammalian brain. Science (New York, N.Y.) *344*, 1252304.

Goebbels, S., Oltrogge, J.H., Wolfer, S., Wieser, G.L., Nientiedt, T., Pieper, A., Ruhwedel, T., Groszer, M., Sereda, M.W., and Nave, K.-A. (2012). Genetic disruption of Pten in a novel mouse model of tomaculous neuropathy. EMBO molecular medicine *4*, 486-499.

Günay, C., Edgerton, J.R., and Jaeger, D. (2008). Channel density distributions explain spiking variability in the globus pallidus: a combined physiology and computer simulation database approach. The Journal of neuroscience : the official journal of the Society for Neuroscience *28*, 7476-7491.

Harauz, G., Ladizhansky, V., and Boggs, J.M. (2009). Structural polymorphism and multifunctionality of myelin basic protein. Biochemistry *48*, 8094-8104.

Hildebrand, C., Remahl, S., Persson, H., and Bjartmar, C. (1993). Myelinated Nerve Fibers in the CNS. Progress in Neurobiology, 319-384.

Hill, R.A., Li, A.M., and Grutzendler, J. (2018). Lifelong cortical myelin plasticity and age-related degeneration in the live mammalian brain. Nature neuroscience *21*, 683-695.

Hines, J.H., Ravanelli, A.M., Schwindt, R., Scott, E.K., and Appel, B. (2015). Neuronal activity biases axon selection for myelination in vivo. Nature neuroscience *18*, 683-689.

Hughes, E.G., Kang, S.H., Fukaya, M., and Bergles, D.E. (2013). Oligodendrocyte progenitors balance growth with self-repulsion to achieve homeostasis in the adult brain. Nature neuroscience *16*, 668-676.

Hughes, E.G., Orthmann-Murphy, J.L., Langseth, A.J., and Bergles, D.E. (2018). Myelin remodeling through experience-dependent oligodendrogenesis in the adult somatosensory cortex. Nature neuroscience *21*, 696-706.

Hursh, J.B. (1939). Conduction velocity and diameter of nerve fibers. Am J Physiol Legacy Content, 131-139.

Ibrahim, M., Butt, A.M., and Berry, M. (1995). Relationship between myelin sheath diameter and internodal length in axons of the anterior medullary velum of the adult rat. Journal of the Neurological Sciences *133*, 119-127.

Itoh, K., Stevens, B., Schachner, M., and Fields, R.D. (1995). Regulated Expression of the Neural Cell Adhesion Molecule L1 by Specific Patterns of Neural Impulses. Science *270*, 1369-1372.

Jäkel, S., Agirre, E., Mendanha Falcão, A., Bruggen, D., Wai Lee, K., Knuesel, I., Malhotra, D., Ffrench-Constant, C., Williams, A., and Castelo-Branco, G. (2019). Altered human oligodendrocyte heterogeneity in multiple sclerosis. Nature, 543-547.

Jenkins, S.M., and Bennett, V. (2002). Developing nodes of Ranvier are defined by ankyrin-G clustering and are independent of paranodal axoglial adhesion. Proceedings of the National Academy of Sciences of the United States of America *99*, 2303-2308.

Kaller, M.S., Lazari, A., Blanco-Duque, C., Sampaio-Baptista, C., and Johansen-Berg, H. (2017). Myelin plasticity and behaviour-connecting the dots. Current opinion in neurobiology *47*, 86-92.

Kaplan, M.R., Cho, M.-H., Ullian, E.M., Isom, L.L., Levinson, S.R., and Barres, B.A. (2001). Differential Control of Clustering of the Sodium Channels Nav1.2 and Nav1.6 at Developing CNS Nodes of Ranvier. Neuron.

Kaplan, M.R., Meyer-Franke, A., Lambert, S., Bennett, V., Duncan, I.D., Levinson, S.R., and Barres, B.A. (1997). Induction of sodium channel clustering by oligodendrocytes. Nature *386*, 724-728.

Karttunen, M.J., Czopka, T., Goedhart, M., Early, J.J., and Lyons, D.A. (2017). Regeneration of myelin sheaths of normal length and thickness in the zebrafish CNS correlates with growth of axons in caliber. PloS one *12*, e0178058.

Kessaris, N., Fogarty, M., Iannarelli, P., Grist, M., Wegner, M., and Richardson, W.D. (2006). Competing waves of oligodendrocytes in the forebrain and postnatal elimination of an embryonic lineage. Nature neuroscience *9*, 173-179.

Kimura, Y., Okamura, Y., and Higashijima, S.-i. (2006). alx, a zebrafish homolog of Chx10, marks ipsilateral descending excitatory interneurons that participate in the regulation of spinal locomotor circuits. The Journal of neuroscience : the official journal of the Society for Neuroscience *26*, 5684-5697.

Kirby, B.B., Takada, N., Latimer, A.J., Shin, J., Carney, T.J., Kelsh, R.N., and Appel, B. (2006). In vivo time-lapse imaging shows dynamic oligodendrocyte progenitor behavior during zebrafish development. Nature neuroscience *9*, 1506-1511.

Klapoetke, N.C., Murata, Y., Kim, S.S., Pulver, S.R., Birdsey-Benson, A., Cho, Y.K., Morimoto, T.K., Chuong, A.S., Carpenter, E.J., and Tian, Z., et al. (2014). Independent optical excitation of distinct neural populations. Nature methods *11*, 338-346.

Knafo, S., and Wyart, C. (2018). Active mechanosensory feedback during locomotion in the zebrafish spinal cord. Current opinion in neurobiology *52*, 48-53.

Komada, M., and Soriano, P. (2002). BetaIV-spectrin regulates sodium channel clustering through ankyrin-G at axon initial segments and nodes of Ranvier. The Journal of cell biology *156*, 337-348.

Koudelka, S., Voas, M.G., Almeida, R.G., Baraban, M., Soetaert, J., Meyer, M.P., Talbot, W.S., and Lyons, D.A. (2016). Individual Neuronal Subtypes Exhibit Diversity in CNS Myelination Mediated by Synaptic Vesicle Release. Current biology : CB *26*, 1447-1455.

Krasnow, A.M., Ford, M.C., Valdivia, L.E., Wilson, S.W., and Attwell, D. (2018). Regulation of developing myelin sheath elongation by oligodendrocyte calcium transients in vivo. Nature neuroscience *21*, 24-28.

Krityakiarana, W., Espinosa-Jeffrey, A., Ghiani, C.A., Zhao, P.M., Topaldjikian, N., Gomez-Pinilla, F., Yamaguchi, M., Kotchabhakdi, N., and Vellis, J. de (2010). Voluntary exercise increases oligodendrogenesis in spinal cord. The International journal of neuroscience *120*, 280-290.

Kummer, T.T., Misgeld, T., and Sanes, J.R. (2006). Assembly of the postsynaptic membrane at the neuromuscular junction: paradigm lost. Current opinion in neurobiology *16*, 74-82.

Kwan, K.M., Fujimoto, E., Grabher, C., Mangum, B.D., Hardy, M.E., Campbell, D.S., Parant, J.M., Yost, H.J., Kanki, J.P., and Chien, C.-B. (2007). The Tol2kit: a multisite gateway-based construction kit for Tol2 transposon transgenesis constructs. Developmental dynamics : an official publication of the American Association of Anatomists *236*, 3088-3099.

Lamborghini, J. (1987). Disappearance of Rohon-Beard neurons from the spinal cord of larval Xenopus laevis. J. Comp. Neurol., 47-55.

Lee, S., Leach, M.K., Redmond, S.A., Chong, S.Y.C., Mellon, S.H., Tuck, S.J., Feng, Z.-Q., Corey, J.M., and Chan, J.R. (2012a). A culture system to study oligodendrocyte myelination processes using engineered nanofibers. Nature methods *9*, 917-922.

Lee, Y., Morrison, B.M., Li, Y., Lengacher, S., Farah, M.H., Hoffman, P.N., Liu, Y., Tsingalia, A., Jin, L., and Zhang, P.-W., et al. (2012b). Oligodendroglia metabolically support axons and contribute to neurodegeneration. Nature *487*, 443-448.

Liu, J., Dietz, K., DeLoyht, J.M., Pedre, X., Kelkar, D., Kaur, J., Vialou, V., Lobo, M.K., Dietz, D.M., and Nestler, E.J., et al. (2012). Impaired adult myelination in the prefrontal cortex of socially isolated mice. Nature neuroscience *15*, 1621-1623.

Liu, P., Du, J.-L., and He, C. (2013). Developmental pruning of early-stage myelin segments during CNS myelination in vivo. Cell research *23*, 962-964.

Makinodan, M., Rosen, K.M., Ito, S., and Corfas, G. (2012). A critical period for social experience-dependent oligodendrocyte maturation and myelination. Science (New York, N.Y.) *337*, 1357-1360.

Mangin, J.-M., Li, P., Scafidi, J., and Gallo, V. (2012). Experience-dependent regulation of NG2 progenitors in the developing barrel cortex. Nature neuroscience *15*, 1192-1194.

McKenzie, I.A., Ohayon, D., Li, H., Faria, J.P. de, Emery, B., Tohyama, K., and Richardson, W.D. (2014). Motor skill learning requires active central myelination. Science (New York, N.Y.) *346*, 318-322.

Menelaou, E., Kishore, S., and McLean, D.L. (2019). Distinct Spinal V2a and V0d Microcircuits Distribute Locomotor Control in Larval Zebrafish.

Mensch, S. (2015). Investigating axon-oligodendrocyte interactions during myelinated axon formation in vivo.

Mensch, S., Baraban, M., Almeida, R., Czopka, T., Ausborn, J., El Manira, A., and Lyons, D.A. (2015). Synaptic vesicle release regulates myelin sheath number of individual oligodendrocytes in vivo. Nature neuroscience *18*, 628-630.

Micheva, K.D., Wolman, D., Mensh, B.D., Pax, E., Buchanan, J., Smith, S.J., and Bock, D.D. (2016). A large fraction of neocortical myelin ensheathes axons of local inhibitory neurons. elife.

Miller, D.J., Duka, T., Stimpson, C.D., Schapiro, S.J., Baze, W.B., McArthur, M.J., Fobbs, A.J., Sousa, A.M.M., Sestan, N., and Wildman, D.E., et al. (2012). Prolonged myelination in human neocortical evolution. Proceedings of the National Academy of Sciences of the United States of America *109*, 16480-16485.

Miller, R.H. (2002). Regulation of oligodendrocyte development in the vertebrate CNS. Progress in Neurobiology *67*, 451-467.

Mitew, S., Gobius, I., Fenlon, L.R., McDougall, S.J., Hawkes, D., Xing, Y.L., Bujalka, H., Gundlach, A.L., Richards, L.J., and Kilpatrick, T.J., et al. (2018). Pharmacogenetic stimulation of neuronal activity increases myelination in an axon-specific manner. Nature communications *9*, 306.

Morrison, B.M., Lee, Y., and Rothstein, J.D. (2013). Oligodendroglia: metabolic supporters of axons. Trends in cell biology *23*, 644-651.

Murray, J.A., and Blakemore, W.F. (1980). The relationship between internodal length and fibre diameter in the spinal cord of the cat. Journal of the Neurological Sciences *45*, 29-41.

Murtie, J.C., Macklin, W.B., and Corfas, G. (2007). Morphometric analysis of oligodendrocytes in the adult mouse frontal cortex. Journal of neuroscience research *85*, 2080-2086.

Nave, K.-A. (2010). Myelination and the trophic support of long axons. Nature reviews. Neuroscience *11*, 275-283.

Pajevic, S., Basser, P.J., and Fields, R.D. (2014). Role of myelin plasticity in oscillations and synchrony of neuronal activity. Neuroscience *276*, 135-147.

Peles, E., and Salzer, J.L. (2000). Molecular domains of myelinated axons. Current Opin in Neurobiol.

Pérez-Cerdá, F., Sánchez-Gómez, M.V., and Matute, C. (2015). Pío del Río Hortega and the discovery of the oligodendrocytes. Frontiers in neuroanatomy *9*, 92.

Pierre, K., and Pellerin, L. (2005). Monocarboxylate transporters in the central nervous system: distribution, regulation and function. Journal of neurochemistry *94*, 1-14.

Pietri, T., Manalo, E., Ryan, J., Saint-Amant, L., and Washbourne, P. (2009). Glutamate drives the touch response through a rostral loop in the spinal cord of zebrafish embryos. Developmental neurobiology *69*, 780-795.

Piscopo, D.M., Weible, A.P., Rothbart, M.K., Posner, M.I., and Niell, C.M. (2018). Changes in white matter in mice resulting from low-frequency brain stimulation. Proceedings of the National Academy of Sciences of the United States of America *115*, E6339-E6346.

Poliak, S., Gollan, L., Salomon, D., Berglund, E.O., Ohara, R., Ranscht, B., and Peles, E. (2001). Localization of Caspr2 in Myelinated Nerves Depends on Axon–Glia Interactions and the Generation of Barriers along the Axon. J. Neurosci. *21*, 7568-7575.

Poliak, S., and Peles, E. (2003). The local differentiation of myelinated axons at nodes of Ranvier. Nature reviews. Neuroscience *4*, 968-980.

Pujala, A., and Koyama, M. (2019). Chronology-based architecture of descending circuits that underlie the development of locomotor repertoire after birth. elife.

Rasband, M.N., and Peles, E. (2015). The Nodes of Ranvier: Molecular Assembly and Maintenance. Cold Spring Harbor perspectives in biology *8*, a020495.

Redmond, S.A., Mei, F., Eshed-Eisenbach, Y., Osso, L.A., Leshkowitz, D., Shen, Y.-A.A., Kay, J.N., Aurrand-Lions, M., Lyons, D.A., and Peles, E., et al. (2016). Somatodendritic Expression of JAM2 Inhibits Oligodendrocyte Myelination. Neuron *91*, 824-836.

Remahl, S., and Hildebrand, C. (1982). Changing relation between onset of myelination and axon diameter range in developing feline white matter. Journal of the Neurological Sciences *54*, 33-45.

Rinholm, J.E., Hamilton, N.B., Kessaris, N., Richardson, W.D., Bergersen, L.H., and Attwell, D. (2011). Regulation of oligodendrocyte development and myelination by glucose and lactate. The Journal of neuroscience : the official journal of the Society for Neuroscience *31*, 538-548.

Rios, J.C., Rubin, M., St. Martin, M., Downey, R.T., Einheber, S., Rosenbluth, J., Levinson, S.R., Bhat, M.A., and Salzer, J.L. (2003). Paranodal Interactions Regulate Expression of Sodium Channel Subtypes and Provide a Diffusion Barrier for the Node of Ranvier. J. Neurosci.

Ritter, D.A., Bhatt, D.H., and Fetcho, J.R. (2001). In Vivo Imaging of Zebrafish Reveals Differences in the Spinal Networks for Escape and Swimming Movements. J. Neurosci., 8956-8965.

Rosenbluth, J. (1999). A brief history of myelinated nerve fibers: one hundred and fifty years of controversy. Journal of Neurocytology, 251-262.

RS Smith and ZJ Koles (1970). Myelinated nerve fibers: computed effect of myelin thickness on conduction velocity. American Journal of Physiology.

Salzer, J.L. (2003). Polarized Domains of Myelinated Axons. Neuron *40*, 297-318.

Schain, A.J., Hill, R.A., and Grutzendler, J. (2014). Label-free in vivo imaging of myelinated axons in health and disease with spectral confocal reflectance microscopy. Nature medicine *20*, 443-449.

Scholz, J., Klein, M.C., Behrens, T.E.J., and Johansen-Berg, H. (2009). Training induces changes in white-matter architecture. Nature neuroscience *12*, 1370-1371.

Schoonheim, P.J., Arrenberg, A.B., Del Bene, F., and Baier, H. (2010). Optogenetic localization and genetic perturbation of saccade-generating neurons in zebrafish. The Journal of neuroscience : the official journal of the Society for Neuroscience *30*, 7111-7120.

Seidl, A.H. (2014). Regulation of conduction time along axons. Neuroscience *276*, 126-134.

Shen, S., Li, J., and Casaccia-Bonnefil, P. (2005). Histone modifications affect timing of oligodendrocyte progenitor differentiation in the developing rat brain. The Journal of cell biology *169*, 577-589.

Sherman, D.L., and Brophy, P.J. (2005). Mechanisms of axon ensheathment and myelin growth. Nature reviews. Neuroscience *6*, 683-690.

Sidik, H., and Talbot, W.S. (2015). A zinc finger protein that regulates oligodendrocyte specification, migration and myelination in zebrafish. Development (Cambridge, England) *142*, 4119-4128.

Sierra, A., Castro, F. de, Del Río-Hortega, J., Rafael Iglesias-Rozas, J., Garrosa, M., and Kettenmann, H. (2016). The "Big-Bang" for modern glial biology: Translation and comments on Pío del Río-Hortega 1919 series of papers on microglia. Glia *64*, 1801-1840.

Simon, C., Götz, M., and Dimou, L. (2011). Progenitors in the adult cerebral cortex: cell cycle properties and regulation by physiological stimuli and injury. Glia *59*, 869-881.

Simons, M., and Nave, K.-A. (2015). Oligodendrocytes: Myelination and Axonal Support. Cold Spring Harbor perspectives in biology *8*, a020479.

Snaidero, N., Möbius, W., Czopka, T., Hekking, L.H.P., Mathisen, C., Verkleij, D., Goebbels, S., Edgar, J., Merkler, D., and Lyons, D.A., et al. (2014). Myelin membrane wrapping of CNS axons by PI(3,4,5)P3-dependent polarized growth at the inner tongue. Cell *156*, 277-290.

Snaidero, N., and Simons, M. (2014). Myelination at a glance. Journal of cell science *127*, 2999-3004.

Snaidero, N., Velte, C., Myllykoski, M., Raasakka, A., Ignatev, A., Werner, H.B., Erwig, M.S., Möbius, W., Kursula, P., and Nave, K.-A., et al. (2017). Antagonistic Functions of MBP and CNP Establish Cytosolic Channels in CNS Myelin. Cell reports *18*, 314-323.

Stathopoulos, P., Alexopoulos, H., and Dalakas, M.C. (2015). Autoimmune antigenic targets at the node of Ranvier in demyelinating disorders. Nature reviews. Neurology, 143-156.

Sun, T., Pringle, N.P., Hardy, A.P., Richardson, W.D., and Smith, H.K. (1998). Pax6 Influences the Time and Site of Origin of Glial Precursors in the Ventral Neural Tube. Molecular and Cellular Neuroscience.

Susuki, K., Chang, K.-J., Zollinger, D.R., Liu, Y., Ogawa, Y., Eshed-Eisenbach, Y., Dours-Zimmermann, M.T., Oses-Prieto, J.A., Burlingame, A.L., and Seidenbecher, C.I., et al. (2013). Three mechanisms assemble central nervous system nodes of Ranvier. Neuron *78*, 469-482.

Svoboda, K.R., Linares, A.E., and Ribera, A.B. (2001). Activity regulates neuronal cell death. Development (Cambridge, England).

Takada, N., and Appel, B. (2010). Identification of genes expressed by zebrafish oligodendrocytes using a differential microarray screen. Developmental dynamics : an official publication of the American Association of Anatomists *239*, 2041-2047.

Takeuchi, H., Sekiguchi, A., Taki, Y., Yokoyama, S., Yomogida, Y., Komuro, N., Yamanouchi, T., Suzuki, S., and Kawashima, R. (2010). Training of working memory impacts structural connectivity. The Journal of neuroscience : the official journal of the Society for Neuroscience *30*, 3297-3303.

Teh, C., Chudakov, D.M., Poon, K.-L., Mamedov, I.Z., Sek, J.-Y., Shidlovsky, K., Lukyanov, S., and Korzh, V. (2010). Optogenetic in vivo cell manipulation in KillerRed-expressing zebrafish transgenics. BMC developmental biology *10*, 110.

Thiele, T.R., Donovan, J.C., and Baier, H. (2014). Descending Control of Swim Posture by a Midbrain Nucleus in Zebrafish. Neuron.

Tomassy, G.S., Berger, D.R., Chen, H.-H., Kasthuri, N., Hayworth, K.J., Vercelli, A., Seung, H.S., Lichtman, J.W., and Arlotta, P. (2014). Distinct profiles of myelin distribution along single axons of pyramidal neurons in the neocortex. Science (New York, N.Y.) *344*, 319-324.

Tyssowski, K.M., and Gray, J.M. (2019). Blue light induces neuronal-activity-regulated gene expression in the absence of optogenetic proteins.

Virchow, R. (1856). Gesammelte Abhandlungen zur wissenschaftlichen Medizin (Frankfurt: Meidinger).

Voas, M.G., Glenn, T.D., Raphael, A.R., and Talbot, W.S. (2009). Schwann Cells Inhibit Ectopic Clustering of Axonal Sodium Channels. Journal of Neuroscience *29*, 14408-14414.

Wang, S., Sdrulla, A.D., diSibio, G., Bush, G., Nofziger, D., Hicks, C., Weinmaster, G., and Barres, B.A. (1998). Notch Receptor Activation Inhibits Oligodendrocyte Differentiation. Neuron *21*, 63-75.

Williams, J.A., Barrios, A., Gatchalian, C., Rubin, L., Wilson, S.W., and Holder, N. (2000). Programmed cell death in zebrafish rohon beard neurons is influenced by TrkC1/NT-3 signaling. Developmental biology *226*, 220-230.

Xiao, L., Ohayon, D., McKenzie, I.A., Sinclair-Wilson, A., Wright, J.L., Fudge, A.D., Emery, B., Li, H., and Richardson, W.D. (2016). Rapid production of new oligodendrocytes is required in the earliest stages of motor-skill learning. Nature neuroscience *19*, 1210-1217.

Yeung, M.S.Y., Djelloul, M., Steiner, E., Bernard, S., Salehpour, M., Possnert, G., Brundin, L., and Frisén, J. (2019). Dynamics of oligodendrocyte generation in multiple sclerosis. Nature *566*, 538-542.

Young, K.M., Psachoulia, K., Tripathi, R.B., Dunn, S.-J., Cossell, L., Attwell, D., Tohyama, K., and Richardson, W.D. (2013). Oligodendrocyte dynamics in the healthy adult CNS: evidence for myelin remodeling. Neuron *77*, 873-885.

Zalc, B., Goujet, D., and Colman, D. (2008). The origin of the myelination program in vertebrates. Current biology : CB *18*, R511-2.

Zatorre, R.J., Fields, R.D., and Johansen-Berg, H. (2012). Plasticity in gray and white: neuroimaging changes in brain structure during learning. Nature neuroscience *15*, 528-536.

Zhang, W., Fan, B., Agarwal, D., Li, T., and Yu, Y. (2018). Axonal sodium and potassium conductance density determines spiking dynamical properties of regular- and fast-spiking neurons. Nonlinear Dyn *311*, 1290.

6 PUBLICATIONS

Auer F., Vagionitis S. and Czopka T. (2018) Evidence for Myelin Sheath Remodeling in the CNS Revealed by In Vivo Imaging *Curr Biol*, 28(4): 549–559

Czopka T. and **Auer F**. (2017) New Approaches to Analyse Axon-Oligodendrocyte Communication in vivo *Neuroforum* 23(4): A175–A181

Fenske S., Pröbstle R., **Auer F**., Hassan S., Marks V., Pauza D., Biel M., Wahl-Schott C. (2016) Comprehensive multilevel *in vivo* and *in vitro* analysis of heart rate fluctuations in mice by ECG telemetry and electrophysiology *Nat. Protocols, 11*(1): 61-86

Fenske, S., Krause S. C., Hassan S. I., Becirovic E., **Auer F.**, Bernard R., Kupatt C., Lange P., Ziegler T.,Wotjak C. T., Zhang H., Hammelmann V., Paparizos C., Biel M. and Wahl-Schott C. A. (2013). Sick sinus syndrome in HCN1-deficient mice. *Circulation* 128(24): 2585-2594.

7 EIDESTATTLICHE VERSICHERUNG

Hiermit versichere ich an Eides statt, dass ich die vorliegende Dissertation ‚Investigating mechanisms of myelin sheath length regulation and plasticity' selbstständig angefertigt habe, mich außer der angegebenen keiner weiteren Hilfsmittel bedient und alle Erkenntnisse, die aus dem Schrifttum ganz oder annähernd übernommen sind, als solche kenntlich gemacht und nach ihrer Herkunft unter Bezeichnung der Fundstelle einzeln nachgewiesen habe.

I hereby confirm that the dissertation ‚Investigating mechanisms of myelin sheath length regulation and plasticity' is the result of my own work and that I have only used sources or materials listed and specified in the dissertation.

München, den 18.09.2019 Franziska Auer

Unterschrift

8 DECLARATION OF AUTHOR CONTRIBUTION

Experimental design: FA, TC

Setup design/assembly: FA, TC

Conducting experiments: FA, SV

Analysis of experiments: FA

Visualizing the results of experiments: FA

Supervision, project administration: TC

Thesis writing: FA

Date, place

Signature Franziska Auer

Signature Stavros Vagionitis

Signature Dr. Tim Czopka